Dissertation presented to the Instituto Tecnológico de Aeronáutica, in partial fulfillment of the requirements for the Degree of Master of Science in the Program of Aeronautics and Mechanical Engineering, Materials and Manufacturing Processes Area.

**André Hemerly Maia**

# IMPACTS ON THE SURFACE INTEGRITY OF TITANIUM MILLING WITH MINIMUM QUANTITY LUBRICATION AND FLOOD OF COOLANT

Dissertation approved in its final version by the signatories below:

Prof. Dr. Jefferson de Oliveira Gomes
Advisor

Prof. Dr. Luiz Carlos Sandoval Góes
Prorector of Graduate Studies and Research

Campo Montenegro
São José dos Campos, SP – Brasil
2015

## BIBLIOGRAPHIC REFERENCE

MAIA, André Hemerly. **Impacts on the surface integrity of titanium milling with minimum quantity lubrication and flood of coolant**. 2015. 120f. Dissertation of Master of Science in Manufacturing Technology – Instituto Tecnológico de Aeronáutica, São José dos Campos.

## CESSION OF RIGHTS

AUTHOR'S NAME: André Hemerly Maia
PUBLICATION TITLE: Impacts on the surface integrity of titanium milling with minimum quantity lubrication and flood of coolant.
PUBLICATION KIND/YEAR: Dissertation / 2015

_____
André Hemerly Maia
Praça Marechal do Ar Eduardo Gomes, 50, Vila das Acácias
CEP: 12228-900, São José dos Campos - SP

# IMPACTS ON THE SURFACE INTEGRITY OF TITANIUM MILLING WITH MINIMUM QUANTITY LUBRICATION AND FLOOD OF COOLANT

**André Hemerly Maia**

Thesis Committee Composition:

| | | | |
|---|---|---|---|
| Prof. Drª. | Maria Margareth da Silva | Chairperson | - ITA |
| Prof. Dr. | Jefferson de Oliveira Gomes | Advisor | - ITA |
| Prof. Dr. | Anderson Vicente Borille | | - ITA |
| Dr. | Edson Costa Santos | | - ISI LASER |

**ITA**

# *Agradecimentos*

Aos meus pais, Maria e Ageu, pela compreensão e afeto, apoio em todas as ocasiões, e pelo exemplo de persistência.

A Elisa, com amor, pela paciência em meio às turbulências e companheirismo nos momentos de felicidade. Por todo o carinho.

Ao meu irmão Henrique, Tia Dalva, Tio Azildo e Tia Enilda, pelos memoráveis momentos em família e pelo exemplo de educação.

Ao Prof. Jefferson pela confiança, suporte, orientação e conselhos para o desenvolvimento desse trabalho.

Ao Prof. Borille pelos valiosos conselhos.

Aos amigos Guilherme, Luiz, André Lima, André D'Oliveira, pela descontração e boas risadas que mostram que os problemas não são assim tão grandes.

Ao Ronnie da Bahia pela enorme (lá ele) paciência, camaradagem e coorientação do trabalho.

Aos companheiros do Centro de Competência em Manufatura e do ITA, Rafael Hiroshi, Milena, Patrícia, Samir, Enivaldo, Lucas, Nico, Ever, Rafael Mundim, Janete, Prof. André Antunes, Donizete, Gilberto, e todos que de alguma forma contribuíram: meu sincero obrigado.

Aos colegas do SENAI Joinville, Alexsandro Rabello, André Zanatta, Edson Santos, Fernando Kasten, pela disponibilidade e contribuição nas etapas experimentais.

Ao Leandro Almeida, da PANalytical, pelas explicações e sugestões durante a etapa experimental.

A empresa Sandvik Coromant pelo apoio técnico e material, imprescindíveis para a execução desse trabalho.

Ao CNPq pelo apoio financeiro concedido.

*"It is sometimes a mistake to climb; it is always a mistake never even to make the attempt. If you do not climb you will not fall. This is true. But is it that bad to fall, that hard to fall?"*

(Neil Gaiman)

# Resumo

Titânio e suas ligas são considerados materiais de alto desempenho devido à combinação de propriedades tais como resistência mecânica, baixo peso específico, e resistência mecânica a temperatura elevada. Essas mesmas propriedades resultam em péssima usinabilidade e altas temperaturas que podem produzir tensões residuais trativas e danos superficiais. Tais características, em especial tensões residuais, impactam diretamente na vida em fadiga, que constitui o principal modo de falha na indústria aeronáutica. Portanto grandes volumes de fluido refrigerante são necessários para evitar danos superficiais, representando até 30% dos custos totais de usinagem. Entre as alternativas para reduzir o consumo de fluidos de corte, a técnica de mínima quantidade de lubrificante (MQL) tem sido investigada para operações de torneamento e furação, em termos de desgaste de ferramenta e integridade de superfície. Contudo existe uma lacuna em relação ao fresamento e impactos nas características de integridade de superfície, sendo esse o foco do trabalho. Em uma primeira etapa, forças de usinagem foram investigadas, assim como morfologia e características associadas ao mecanismo de formação do cavaco. Então a qualidade superficial foi avaliada em termos de tensões residuais superficiais, rugosidade e dureza ao longo da profundidade, comparando o método de MQL com a técnica de inundação. Forças de usinagem foram menores para as condições com MQL (aproximadamente 10% menores em comparação com inundação), sendo resultado das maiores temperaturas desenvolvidas no corte e consequente redução da resistência do material. Cavacos segmentados foram obtidos em todas as condições de usinagem. O aspecto da superfície livre do cavaco, segmentos descontínuos, e trincas são evidências de que um mecanismo de propagação de trincas está envolvido na formação do cavaco. Em termos de integridade de superfície, resultados indicam que MQL não afeta a rugosidade da superfície, contudo tensões residuais são menos compressivas. Considerando a faixa de parâmetros que foram testados, a profundidade de corte radial não teve influência nas tensões residuais. Condições que desenvolveram maiores forças de usinagem resultaram em tensões menos compressivas, potencialmente causadas pela maior carga térmica devido ao nível de deformação plástica. Nas condições de acabamento, usinagem com MQL tem a tendência de reduzir a dureza na camada superficial, enquanto com inundação ocorre o efeito contrário como resultado de encruamento. Em operações de semi-acabamento, MQL produziu aumento de dureza, enquanto inundação resultou em um pico subsuperficial.

# Abstract

Titanium and its alloys are considered high performance materials because of the combination of properties such as mechanical strength, low density and strength up to high temperatures. The same properties also result in poor machinability and high temperatures that may produce tensile residual stresses and surface damage. These characteristics, in special residual stresses, impact directly on fatigue life, the main failure mode in aeronautical industry and corresponding to 60% of failures. Thus large amounts of coolant are required in machining operations to avoid surface damage, which may represent up to 30% of the total machining costs. Among the alternatives for reducing the coolant consumption, minimum quantity lubrication (MQL) has been evaluated for drilling and turning both in terms of tool wear and surface integrity. However there is a gap in regard of milling operations and the impacts on surface integrity parameters, and this is the focus of the present study. On a first phase, the machining forces were investigated, as well as chip morphology and characteristics related to its formation mechanism. Then the workpiece quality was evaluated in terms of surface residual stresses, roughness and hardness beneath the machined surface, comparing the MQL method to conventional cooling with flood of coolant. Machining forces were found to be lower for MQL conditions (10% lower as compared to flood cut), and this is believed to be a result of thermal softening of the material. Segmented chips were observed for all the cutting conditions. The aspect of the free surface of the chip, discontinuous segments, and cracks are evidence that a crack propagation mechanism is involved in chip formation. In terms of surface integrity parameters, results indicate that MQL does not affect the surface roughness, but residual stresses are less compressive than when using flood of coolant. Considering the range of parameters that were tested, radial depth of cut had no influence on residual stresses. Conditions which developed higher machining forces and consequently mechanical load resulted in less compressive residual stresses, potentially caused by the increased thermal load due to plastic strain. The hardness beneath the surface was affected by the lubri-cooling method in the finishing operations. Flood cut induced higher levels of cold work, while in MQL machining the thermal softening compensates the increase in surface hardness, and the final state is rather similar to the bulk value. In the case of semi-finishing conditions, machining with MQL increased the surface hardness. Flood cut, on the other side, produced a subsurface hardness peak (from 300 to 600 μm beneath surface, approximately).

# List of Figures

# List of Tables

# List of Abbreviations

| | |
|---|---|
| CCM | *Centro de Competência em Manufatura* |
| CFRP | Carbon fiber reinforced polymer |
| CP titanium | Commercially pure titanium |
| CSC | Crossed slits collimator |
| EDM | Electrical discharge machining |
| EDS | Energy-dispersive X-ray spectroscopy |
| EP additives | Extreme pressure additives |
| ITA | *Instituto Tecnológico de Aeronáutica* |
| LN2 | Liquid nitrogen |
| MQC | Minimum quantity cooling |
| MQL | Minimum quantity lubrication |
| MRR | Material removal rate |
| NDM | Near dry machining |
| PCD | Polycrystalline diamond |
| PPC | Parallel plate collimator |
| PVD | Physical vapor deposition |
| SEM | Scanning electron microscopy |
| SI | Surface integrity |
| XRD | X-ray diffraction |

# Contents

# 1 Introduction

The demand for lighter aircrafts is justified by the consequent decrease in fuel consumption. The most straightforward way to achieve this objective is by simply reducing the density of the materials that are used. According to general guidelines of a Lockheed study, cited by PETERS *et al.* (2003), reducing the density by 10% also results in 10% weight savings. The same effect can be obtained by increasing the material strength by 35%. Although based on military aircraft, this brings attention to the fact that the easiest way to reduce the total weight is by applying lighter materials. To achieve this objective, the aerospace industry is likely to invest higher orders of magnitude than automotive industry, having in mind all the product lifecycle and the high performance requirements. This is shown in the Table 1.1 below.

**Table 1.1.** Tolerable extra costs for weight reductions of 1 kg or 1% of the structural weight

| Industry | T€/ kg | T€/ wt % |
|----------|--------|----------|
| Automobile | 0.01 | 0.1 |
| Regional aircraft | 0.5 | 100 |
| Large aircraft | 1 | 1000 |
| Space | 10 | 10000 |

Adapted from: (PETERS *et al.*, 2003).

Considering the later generation of commercial aircrafts, the prior information is fully verified. Both Boeing and Airbus have been making increased use of composite materials and titanium alloys due to the resultant weight savings. As represented in Figure 1.1, when compared to the last generation of aircrafts, the Boeing 787 Dreamliner and also Airbus A350XWB airframes use almost three times more composite materials (specially carbon fiber reinforced polymer - CFRP) than its predecessors. In the case of titanium, the use has grown by around two times, associated with CFRP. Once their coefficients of thermal expansion closely match, and titanium passivated layer is chemically very stable, titanium alloys are the preferred material for combined application with CFRP. The most common alloy since the later 1960's is Ti-6Al-4V (PETERS *et al.*, 2003; HALE, 2006; ZANIN, 2012).
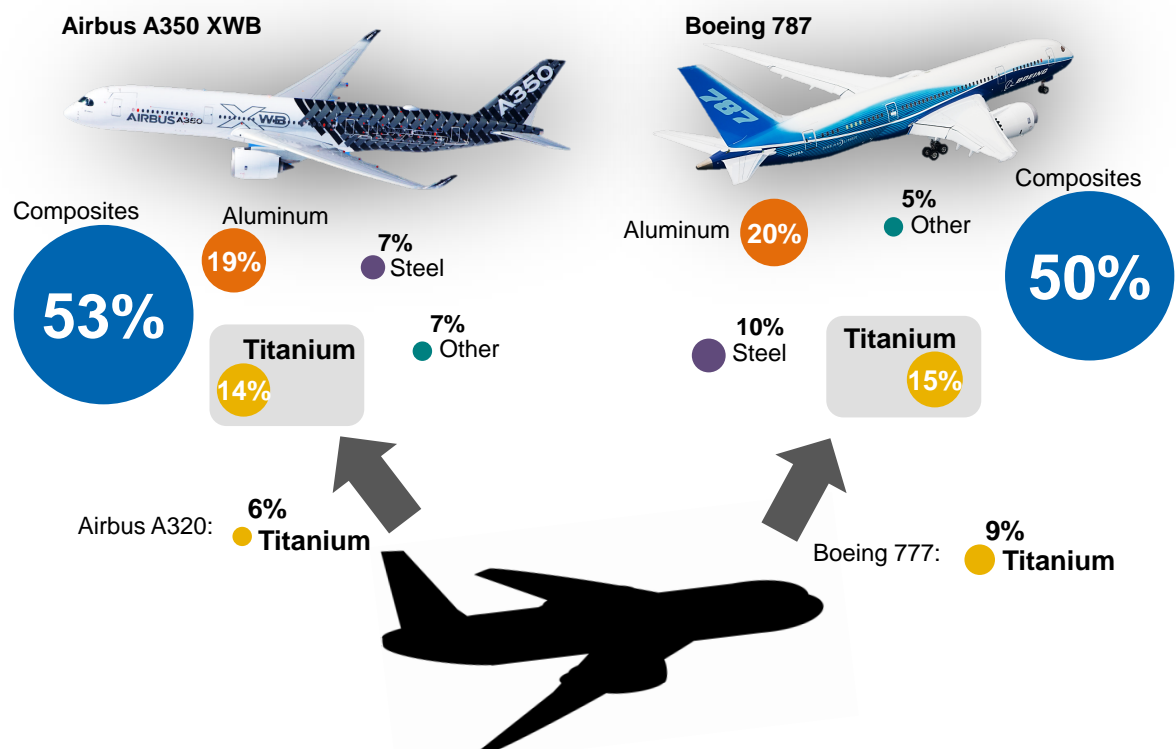
**Figure 1.1.** Material usage in the new generation of commercial airplanes from Airbus and Boeing, as compared to the older generations. Airbus A350XWB shown on the left side; Boeing 787 Dreamliner on the right. Adapted from: (HALE, 2006; ZANIN, 2012)

Titanium's outstanding specific strength is another property that motivates its application in aerospace market. Although some high grade steels possess superior mechanical strength, the low density of titanium alloys – around 40% lower than that of steel - make them a better option for weight optimization. An example of this is the landing gear of Boeing 777, whose most of the parts are made of the titanium alloy Ti-10V-2Fe-3Al with tensile strength of 1193 MPa. Compared to the high strength low alloy steel 4340M, at 1930 MPa, it represented weight savings of over 580 kg (BOYER, 2010). In regard of aluminum parts, on the other side, titanium is a substitute when there are space restrictions, like in the landing gear beam of some aircrafts and other structural parts (BOYER, 1996).

Unfortunately, the same properties that make titanium a very attractive material can also represent a challenge in regard of the manufacturing processes. The high mechanical strength demands a large amount of energy for processing the wrought product into the finished component. Associated with the low modulus of elasticity, it promotes a large elastic recovery that can result in dimensional inaccuracy and regenerative vibrations in machining. Furthermore, even the transformation of the mineral into slabs, billets and other raw materials

is very energy consuming, thus making it expensive when compared to steel and aluminum alloys. This motivates the use of "near-net-shape" processing techniques for reducing the waste of material (KAHLES *et al.*, 1985; DONACHIE, 2000; LEYENS; PETERS, 2003).

Nevertheless, machining stills the primary finishing process for titanium aerospace parts. The geometrical precision and surface quality that can be obtained by this way are hardly achieved by other methods. Considering specifically the airframe production, end milling and drilling are amongst the most important machining operations; for aeroengines, turning and drilling are the major operations. The drawback is that machining also generates a large amount of heat, which is concentrated in the tool tip and small areas of the workpiece. Once again, this is due to the mechanical and thermal properties of titanium. The results are high tool wear rate and the possibility of damaging the surface, both in the mechanical and metallurgical senses (KAHLES *et al.*, 1985; EZUGWU, WANG, 1997).

Several machining alternatives try to overcome the related problems and improve the machinability of titanium and heat resistant alloys. Comprising from tool materials and coatings to lubri-coolant techniques, there is the possibility of lowering the production costs, although it has to be studied from case to case. Cryogenic cooling with liquid nitrogen (LN2), for instance, has shown a great potential for improving tool life (KLOCKE *et al.*, 2013). On the other side, industrial implementation is restricted by the high installation and operating costs. Another option is minimum quantity lubrication (MQL), in which a spray of compressed air and lubricant (in the form of small droplets) is directed to the machined area. It has the potential of decreasing the friction between tool and workpiece, achieving tool life that is comparable to conventional flood cut while reducing cutting fluid costs. For aluminum parts its industrial use is already spread, while for titanium machining there is the need for more researches (RAHIM; SASAHARA, 2011). It is estimated that the economic gain arising from the elimination of the cutting fluid can represent up to 20~30% of machining costs of difficult-to-machine materials (SHOKRANI; DHOKIA; NEWMAN, 2012).

Regardless of the lubri-coolant technique that is used, machining introduces modifications on the properties of the surface layer. These surface properties are related to some specific phenomena, which can reflect in the functional performance of the material. To better understand these connections, a branch of science called surface science has been developed, and linked to it, the concept of surface integrity (SI). The SI refers to the *inherent or enhanced condition of a surface produced in machining or other surface generation operation* (FIELD; KAHLES, 1964; cited by ASTAKHOV, 2010). Properties like residual stresses, hardness, roughness and microstructural alterations may have remarkable impact on

fatigue strength, one of the most demanded requirements for aerospace structural parts (SASAHARA, 2005; SUN; GUO, 2009). Since the late 1970's, the subject has been studied by KOSTER *et al.* (1970) at Metcut Research Associates. Still, up to nowadays those features are seldom considered during the design phase, and also rarely taken into account as a machining specification. It is identified thus an opportunity to improve the product quality by the interaction between design and manufacturing stages of the product lifecycle, as represented in Figure 1.2.
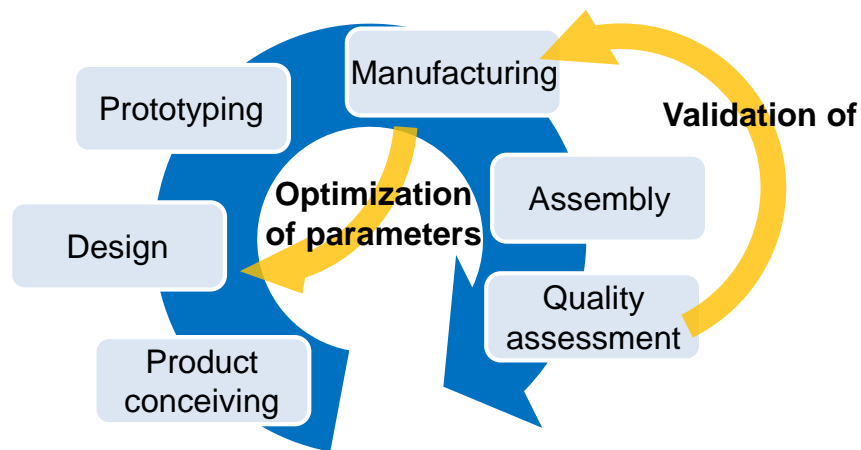


**Figure 1.2.** Interaction of phases in the product life cycle: investigation of the properties generated during manufacturing provides possibilities of improved design.

The cycle is closed when investigating the percentage of fatigue failures in aerospace applications. As can be seen in Figure 1.3, it represents a much larger percentage of failures than in conventional engineering industry (CAMPBELL; LAHEY, 1984; BROOKS; CHOUDHURY, 2002; FINDLAY; HARRISON, 2002). Maximizing the fatigue strength is thus essential and, as shown before, this can be achieved by means of the manufacturing process, specially machining. Alternatively, it can be assumed that increasing the fatigue strength allows the part to be redesigned with smaller weight and dimensions. This fully meets the demands for lighter and environmentally friendly aircrafts with lower fuel consumption.

**General industry**

**Aeronautical industry**
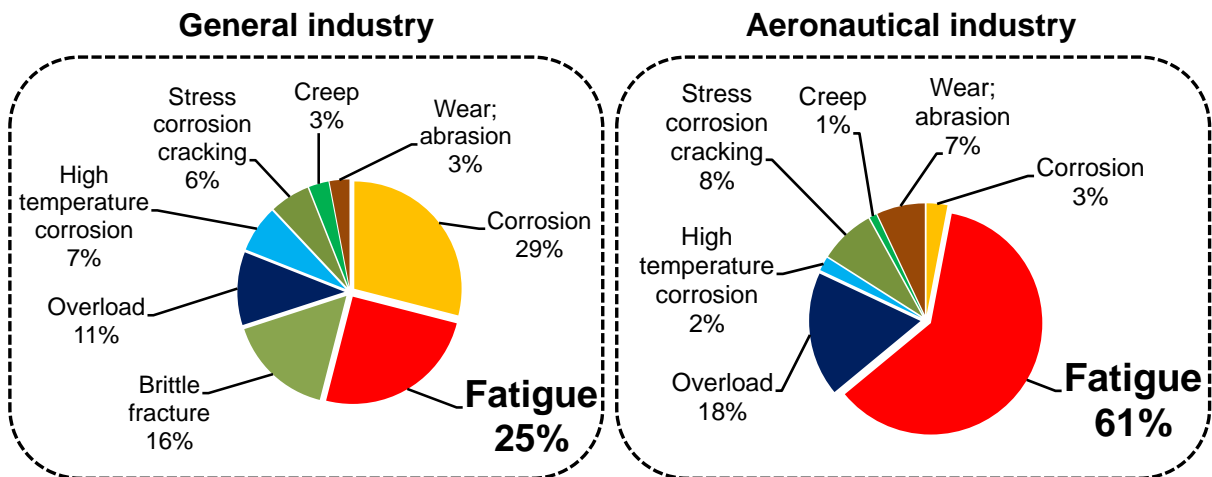
**Figure 1.3.** Comparison of the frequency of failure mechanisms for the general industry and aircraft components. Adapted from: (CAMPBELL; LAHEY, 1984; BROOKS; CHOUDHURY, 2002; FINDLAY; HARRISON, 2002)

Summarizing, it is possible to present the relevance of the theme in two ways:

**Industrial relevance**: potential gains both in weight saving and fatigue life through the improvement of surface properties.

**Scientific relevance**: analysis of the impact of milling parameters and lubri-cooling techniques on the surface integrity and its heterogeneity.

The present dissertation is an initial approximation to the challenge of further integrating the manufacturing and design phases, in the presented context. The effects of machining conditions over surface integrity of titanium alloy Ti-6Al-4V were assessed, as well as the effect of MQL when compared to flood cut. Simple blocks of material were used, once the focus is the evaluation of surface characteristics. In a future research, this information is likely to be applied in the manufacturing of demonstrator workpieces, analog to aerospace parts in terms of geometry. Fatigue testing could provide data to be compared to the surface integrity, thus closing the gap.

# 2 Objectives

## 2.1 General

To investigate the surface integrity produced by the milling process of Ti-6Al-4V in regard of flood and MQL lubri-coolant techniques.

## 2.2 Specific

- To analyze the chip morphology in search for evidences about its formation process (pages 81-86);
- To develop a cutting force map concerning the most important cutting parameters in end milling (pages 87-89);
- To compare the cutting forces in flood cut condition to minimum quantity lubrication (pages 87-89);
- To assess the surface integrity generated by finishing and semi finishing machining, in terms of residual stresses, hardness beneath the machined surface and topography (pages 89-101);
- To analyze the impact of an alternative lubri-cooling technique (MQL) on the surface integrity in terms of residual stresses, roughness, and hardness profile along the depth (pages 89-101).

# 3 Literature review

## 3.1 Titanium and titanium alloys

Titanium and its alloys have a particular combination of mechanical strength, density, corrosion resistance, and stability up to significant temperatures. Compared to other engineering materials, there is a specific range that makes titanium usage an interesting option, and sometimes even a requirement. Some alloys may have tensile strength that is comparable to martensitic stainless steels or superalloys, with 60% of theirs density. Commercial titanium alloys can be used at temperatures around 550ºC, and most environments do not represent a threat in terms of corrosion. It is not a rare metal: rather than this, it is the fourth most abundant structural metal in the Earth's crust. The challenge is that it is seldom found in high concentrations, and the purification process to obtain the pure metal is the main responsible making it an expensive material (DONACHIE, 2000). The Table 3.1 provides further information regarding the comparison of titanium to other engineering materials.

**Table 3.1.** Comparison of properties of titanium and common engineering materials.

| | Ti | Fe | Ni | Al |
|---|---|---|---|---|
| Melting temperature [°C] | 1670 | 1538 | 1455 | 660 |
| Allotropic transformation [°C] | $\beta \rightarrow \alpha$; 882 | $\gamma \rightarrow \alpha$; 912 | - | - |
| Crystal structure | bcc → hcp | fcc → bcc | - | - |
| Room temperature E [GPa] | 115 | 215 | 200 | 72 |
| Yield stress level [MPa] | 1000 | 1000 | 1000 | 500 |
| Density [g/cm$^3$] | 4.5 | 7.9 | 8.9 | 2.7 |
| Comparative **corrosion** resistance | ⬆⬆ (green) | ⬇ (red) | ~ | ⬆ (green) |
| Comparative reactivity with **oxygen** | Very high | Low | Low | High |
| Comparative price of **metal** | ⬆⬆ (red) | ⬇ (green) | ⬆ (red) | ~ |

Adapted from: (LÜTJERING; WILLIAMS, 2007)

Among the mineral sources, rutile ($TiO_2$) and ilmenite ($FeTiO_3$) are the most commonly used for obtaining titanium sponge by the Kroll process. It starts with a pre cleaning and enrichment step resulting in slag concentrate, which is reacted with chlorine to produce titanium tetrachloride ($TiCl_4$). In a reactor, liquid magnesium is used to reduce $TiCl_4$ to titanium sponge and magnesium chloride. Although alternative methods are believed to be less expensive, the Kroll process is still the only one suitable for industrial scale production (LEYENS; PETERS, 2003).

The titanium sponge is then mechanically densified to create an electrode for the melting process, with the possibility of also using scrap material. At this point, alloying elements can be added to induce the desired characteristics. A vacuum arc furnace consumes the electrode and produces the ingot. For further purification of the material, the melting process is performed at least twice. Billets, bars, plates, sheets and other mill products can be obtained from the ingots by forming techniques. However, further manufacturing processes yet have to be applied to achieve the final geometry of the product (LEYENS; PETERS, 2003).

Titanium has two allotropic forms, meaning that it can crystalize in two distinct structures depending on the temperature. At room temperature, titanium crystallizes in a hexagonal close packed structure (hcp) known as α-phase. Achieving 882°C (transus temperature) and above the β-phase with body-centered cubic (bcc) structure becomes stable. This duality of crystal structures - and the possibility of stabilizing them – allows the control and manipulation of the microstructure in order to obtain a large variety of properties. Both lattices are shown in Figure 3.1 (DONACHIE, 2000).

Regarding plastic deformation, the phases have remarkably different mechanical behaviors that can be inferred from the crystal structure itself. The hcp structure has restricted slip systems, a product of its compact planes and compact directions. The most densely packed plane consists in the base of the hexagonal prism of the unit cell, denominated as basal plane. It is depicted in Figure 3.1, as well as two other important planes. Combined with three densely packed directions, it results in only three slip systems (LEYENS; PETERS, 2003).
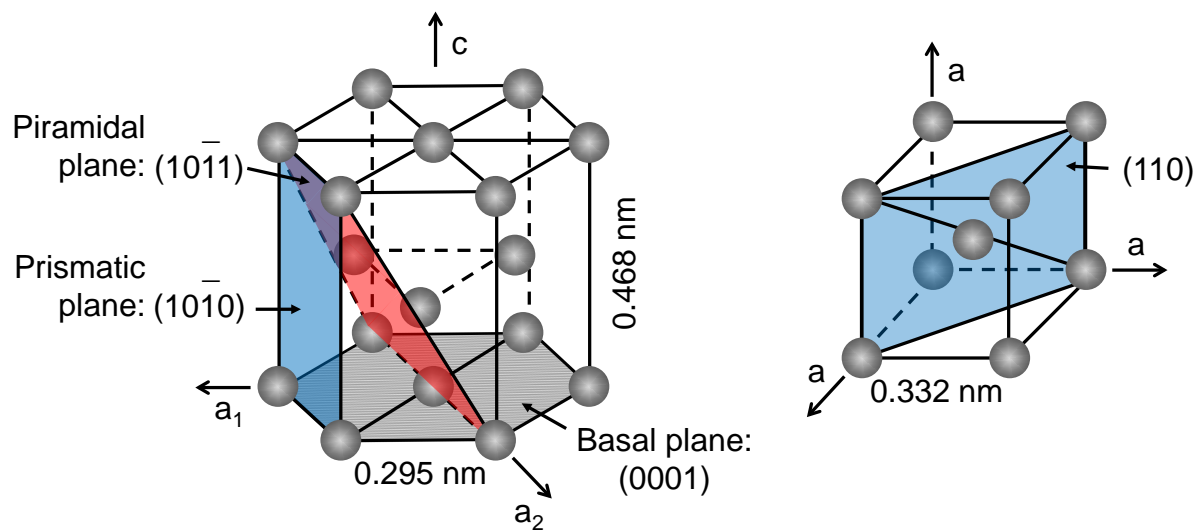
**Figure 3.1.** Crystal structure of hcp α and bcc β phase. Adapted: (LEYENS; PETERS, 2003).

It is important to notice that the lattice parameters of α titanium are a=0.295 nm and c=0.468 nm, resulting in a c/a ratio of 1.587. Comparing to an ideal close packed hexagonal lattice, in which c/a=1.633, this difference means that the prism planes are more spaced, and the atoms in it are closer. Thus the packing density of the prism planes increases, favoring slip on these planes, relative to the basal planes. Both prism and basal planes have three slip systems, however only two are independent of each other, resulting in only four independent slip systems. On the other side, the body-centered cubic lattice combines six densely packed planes – {110} - with two preferential directions each, <111>, therefore resulting in twelve slip systems. This means that β-titanium has many more options for the movement of dislocations, and is more susceptible to plastic deformation than α-titanium. The ductility that is observed in pure titanium at room temperatures is induced by twinning modes. However increasing concentrations of solute atoms in α-titanium suppress this mechanism (LEYENS; PETERS, 2003; LÜTJERING; WILLIAMS, 2007).

Another essential point to understand the characteristics of the different alloys is the diffusion in each phase. At 500°C, the self-diffusion coefficient of α-titanium is one order of magnitude smaller than that of β-titanium. This is directly related to the atomic packing in the unit cells, because a more compact lattice represents more restrictions for movement of the atoms (and the hcp structure is more densely packed than bcc). Therefore, alloys containing mostly α phase have superior creep resistance as a result of the limited volume diffusion (LEYENS; PETERS, 2003; LÜTJERING; WILLIAMS, 2007)

### 3.1.1  Classification of alloys and microstructures

Alloying elements may be added to titanium in order to stabilize α or β phases, and in some cases this is made simultaneously. By properly controlling the volume fractions of each phase and the morphology of the microstructure, materials can be developed to fulfill specific requirements. Figure 3.2 presents the common alloying elements and their effects related to α and β phases. The classification of titanium alloys normally considers three main categories: α, α+β and β alloys.
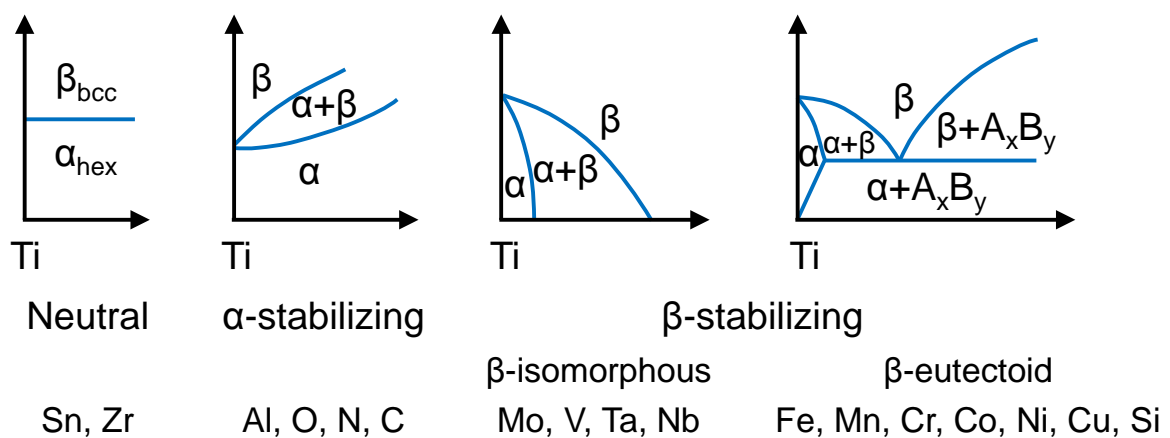


**Figure 3.2.** Influence of alloying elements on phase diagram of Ti alloys (schematically). Adapted from: (LÜTJERING; WILLIAMS, 2007)

Commercially pure (CP) titanium, α alloys and near-α alloys may all be included in the first group. Here, the microstructure is entirely composed by the phase with hcp arrangement, and this contributes to the excellent weldability. These alloys cannot be heat treated for strength improvement unless under very specific cooling conditions. Furthermore, once the main stabilizer element is aluminum, they tend to have lower density (LÜTJERING; WILLIAMS, 2007).

CP titanium grades are preferred where corrosion resistance, rather than mechanical strength, is the primary requirement. In cases where outstanding corrosion resistance is required palladium may be added (ASTM grades 7 and 11). Introducing small quantities of oxygen, which acts as an interstitial, greatly improves mechanical strength, but also degrades ductility. In practice, all technical grades contain some percentage of oxygen to increase the mechanical strength. In general, the annealed 300 series stainless steels have similar

properties, thus weight saving must be a strong motivation in the considered application (BOYER, 1996; DONACHIE, 2000).

Alpha and near-alpha alloys present higher mechanical strength. In the first case, this is greatly due to the presence of aluminum and neutral elements as substitutional atoms. Ti-5Al-2.5Sn is one of the oldest alloys, with large acceptance in low temperature applications such as pressure vessels for hydrogen storage. Because of stress corrosion problems and precipitation of intermetallic compounds, aluminum content is limited to a maximum of 6% for all conventional alloys. Near-alpha titanium contains limited quantities of β-stabilizers, responsible for the increased mechanical strength – some amount of β is retained after heating and cooling (less than about 10% vol, according to LÜTJERING and WILLIAMS (2007)). However, they tend to behave like conventional α alloys because of the large volume of α phase, and thus present good creep resistance (BOYER, 1996; DONACHIE, 2000).

When both α and β stabilizers are added to titanium, a microstructure with two coexisting phases is developed, composing a category called α+β alloys. The combination of properties that is obtained makes this group of alloys the most common ones. Among them, Ti-6Al-4V itself corresponded once to more than 55% of the USA titanium market (in 1998), and even today this can be considered the most used alloy (LÜTJERING; WILLIAMS, 2007). It presents an exceptional good balance of mechanical strength, ductility, fatigue and fracture properties up to temperatures around 300°C.

A pseudo-binary diagram of Ti-6Al x V system is shown in Figure 3.3, the transus temperature close to 1000°C because of the α stabilizers. In the annealed condition, its yield strength is about 850 MPa, but solution treating and aging can improve this to 1000 MPa. Another factor for the success of Ti-6Al-4V is the extensive production experience and reliability, which is especially valuable regarding the aerospace industry. Other examples of α+β alloys are Ti-6-6-2 (Ti-6Al-6V-2Sn), developed primarily for high strength; Ti-6-2-4-6 (Ti-6Al-2Sn-4Zr-6Mo), with focus on high strength and toughness; and Ti-6-2-2-2-2 (Ti-6Al-2Sn-2Zr-2Mo-2Cr), for application in gas turbine engines at temperatures up to 400°C (DONACHIE, 2000; LEYENS; PETERS, 2003).
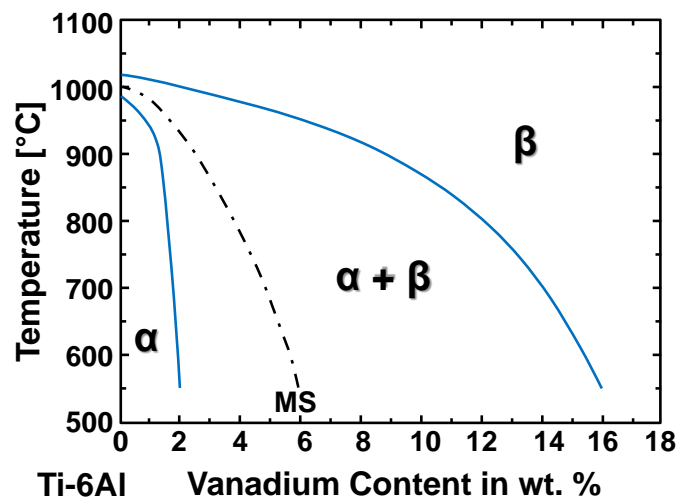
**Figure 3.3.** Pseudo-binary phase diagram of Ti-6Al x V, with variable vanadium content. MS is the martensitic transformation start temperature. Adapted from: (LEYENS; PETERS 2003).

The final category, β alloys, actually comprises metastable β alloys located in the α+β field. Quantities of β stabilizer elements are enough to avoid the martensitic transformation upon fast cooling. References in the literature state that martensitic structures found sometimes in β alloys are strain induced during the polishing step. After removing the affected layer by electrolytic polishing, no martensite is likely to be visualized. Beta alloys are capable of developing the highest levels of mechanical strength. After fast cooling from the β field and further aging at 500°C to 600°C, fine particles are homogeneously precipitated. This increases the yield strength to around 1200 MPa (tensile strength up to 1400 MPa). The use of this group of alloys is restricted by the high density as a result of adding heavy alloying elements, weak oxidation resistance and poor weldability (LÜTJERING; WILLIAMS, 2007).

The microstructure of titanium alloys is composed of equiaxed or lamellar morphologies. Equiaxed grains are a result of recrystallization of α phase and benefit ductility, fatigue strength, as well as superplastic characteristics. In general it is associated to a high level of cold work within the α-β field on prior process (forging) that introduces significant stored energy, in other words, dislocations. Heat treating at relatively low temperatures then allows complete recrystallization. Another possibility is to cool the material at very low rates, starting from temperatures below the β-transus, so that only equiaxed grains are formed (LÜTJERING; WILLIAMS, 2007).

Lamellar structures originate from α phase nucleation at prior β grain boundaries. Characteristics are improved fracture toughness and superior resistance to creep and fatigue

crack growth. This is explained by the ability of this structure to deflect propagating cracks along differently oriented lamella, thus consuming more energy. Fully lamellar microstructures are result of cooling from above the β-transus temperature, and depending on the cooling rate either fine or coarse grains can be formed. Rapid quenching may induce a martensitic transformation producing very fine needle-like microstructure. However it does not result in large distortion of the lattice, thus the hardening effect is only moderate (DONACHIE, 2000; LEYENS; PETERS, 2003).

It is possible to treat the alloy to obtain a bimodal microstructure, with both equiaxed and lamellar morphologies, in order to obtain a balanced profile of properties. This is made by solution heat treatment bellow the β-transus temperature (inside the α+β field) in order to obtain equiaxed grains in a lamellar α+β matrix. Table 3.2 displays general trends for selected properties in regard of each microstructure. Following, Figure 3.4 shows examples of both coarse and fine microstructures of titanium alloys.

**Table 3.2.** Influence of microstructure morphology on selected properties of titanium alloys.

| Fine | Coarse | Property | Lamellar | Equiaxed |
|:---:|:---:|:---:|:---:|:---:|
| ↑ | ↓ | Yield / ultimate strength | ↓ | ↑ |
| ↑ | ↓ | Ductility | ↓ | ↑ |
| ↓ | ↑ | Fracture toughness | ↑ | ↓ |
| ↑ | ↓ | Fatigue strength (crack initiation) | ↓ | ↑ |
| ↓ | ↑ | Creep strength | ↑ | ↓ |
| ↑ | ↓ | Superplasticity | ↓ | ↑ |

Adapted from: (DONACHIE, 2000; LEYENS; PETERS, 2003)
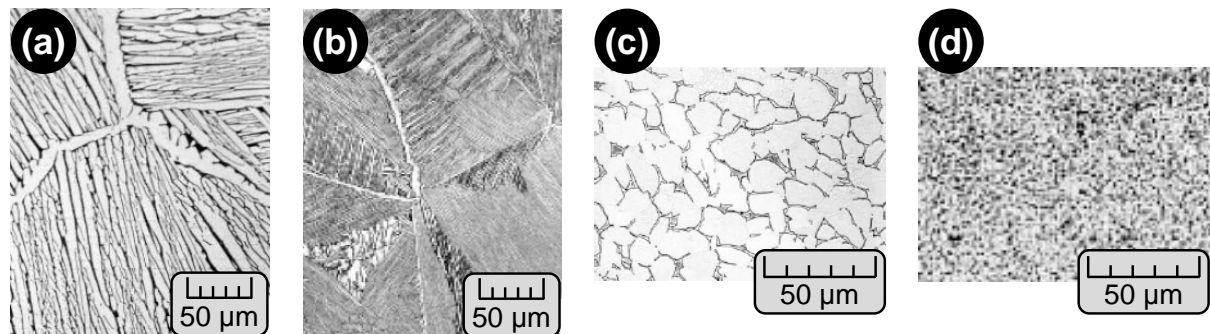


**Figure 3.4.** Typical microstructures of titanium alloys: (a) coarse lamellar; (b) fine lamellar; (c) coarse equiaxed; (d) fine equiaxed. Adapted from: (LÜTJERING; WILLIAMS, 2007).

### 3.1.2 Aerospace applications

The major requirements for the aerospace industry are the specific strength and heat resistance, fatigue strength, crack resistance, and chemical resistance. Processing characteristics also have great importance in the decision of which material will be selected for a specific application. In comparison with steels and aluminum alloys, titanium alloys achieve higher levels of specific characteristics, especially fatigue strength. The main limitation for its spread usage is the high cost related to both the raw products and processing to obtain the final shape and properties (MOISEYEV, 2005).

Titanium alloys are applied in the wing frames, fasteners, pylons, hydraulic cylinders, landing gear beams, engine bulkheads of military aircrafts, stabilizer structure, among others. Some of these examples are shown in Figure 3.5. With the intense use of composites in the new generation of commercial aircrafts (around 50% of the total weight), titanium is the preferred material for parts in contact with them. The first reason is because there is high galvanic potential between aluminum and graphite, and in the presence of moisture the aluminum would be corroded away. In addition, the coefficient of thermal expansion of titanium is much lower than that of aluminum, and closer to that of graphite. Considering the temperature range of fuselage structure, this may result in very high loading (BOYER, 2010).
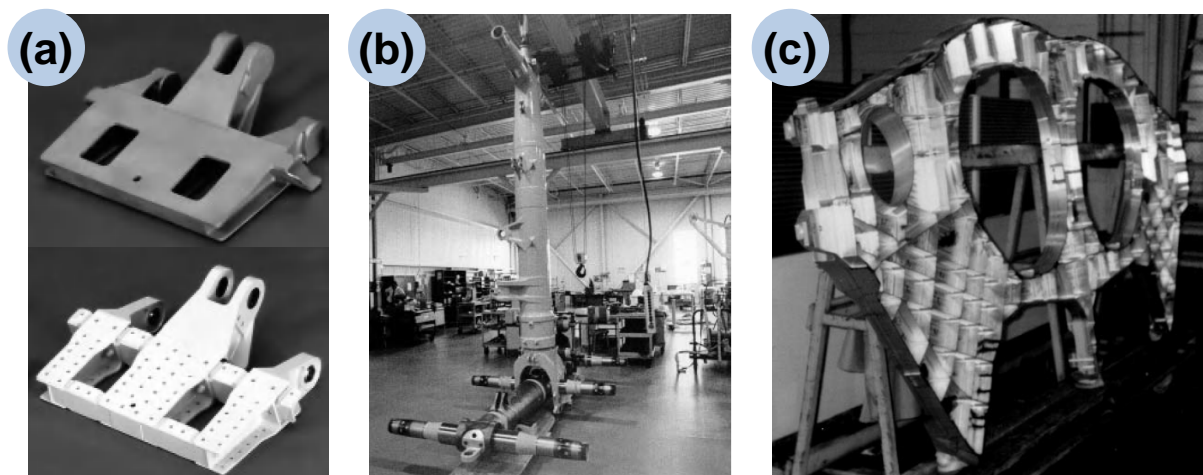


**Figure 3.5.** Examples of aircraft structural applications of titanium: (a) Cast (up) and assembled (below) variant of a spoiler fitting; (b) landing gear of Boeing 777, whose main beam and most of the components are made in titanium; (c) engine bulkhead of a military aircraft. Adapted from: (LEYENS; PETERS, 2003; LÜTJERING; WILLIAMS, 2007)

According to M'SAOUBI *et al.* (2008) the efficiency of aeroengines is directly related to the static and dynamic masses. Over the life of an aeroengine, it is estimated that each kilogram weight reduction means around US\$ 150,000 savings in fuel cost (EZUGWU, 2005). This fosters not only the increase in titanium usage, but also the development of new alloys that can withstand extreme operational temperatures. Perhaps the most significant example of this is the development of titanium aluminides ($\gamma$-TiAl), especially alloys based on the TiAl and Ti3Al intermetallic compounds. They present low density, high mechanical strength at elevated temperatures, high resistance to oxidation, and high creep strength. The disadvantages are the low ductility and fracture toughness at room temperature. These characteristics make $\gamma$-TiAl alloys notorious difficult-to-cut materials (TRETYACHENKO, 2006; KLOCKE *et al.*, 2013).

Current application of titanium alloys in aeroengines is mainly directed to the compressor blades, stators, blisks, fan blades, plug and nozzle etc. Figure 3.6 displays some examples.
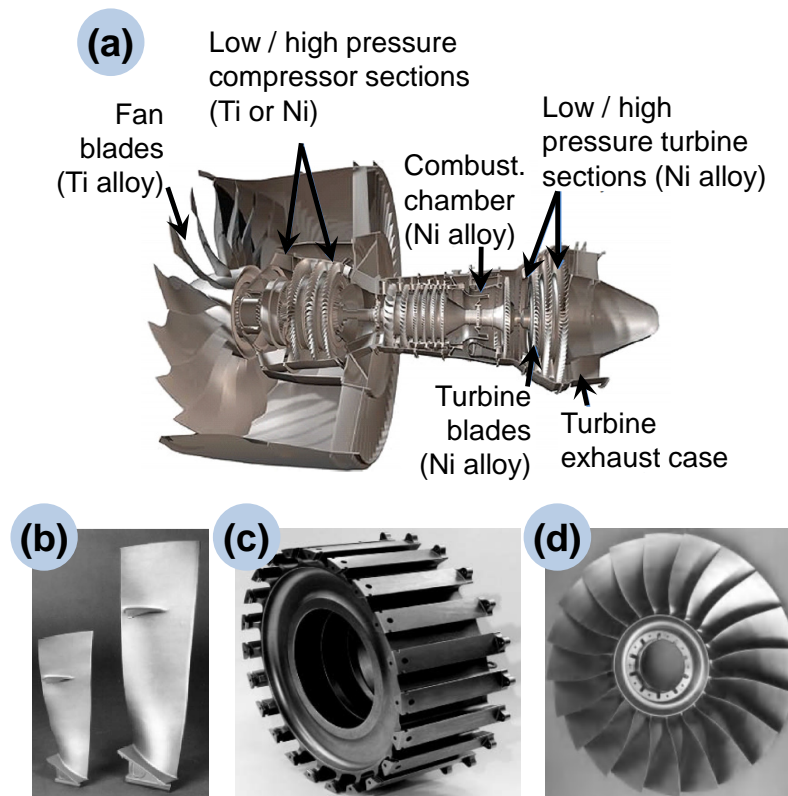


**Figure 3.6.** (a) Schematic view of a commercial aeroengine presenting the main parts where titanium and nickel alloys are applied; (b) forged and recrystallized fan blades of Ti-6Al-4V (length of the larger blade about 1 m); (c) Ti forged and machined fan disk; (d) example of an integrally bladed disk, or "blisk", design. Adapted from: (ULUTAN; OZEL, 2011; LEYENS; PETERS, 2003; LÜTJERING; WILLIAMS, 2007)

### 3.1.3 Manufacturing processes

Several machining processes are involved in the manufacturing of aerospace parts. Although near net shaping methods are capable of reducing fabrication steps, in most of the cases the final geometry and quality of the component can only be achieved by a machining process. For aeroengine parts, the most common processes are turning and drilling, while for airframe production end milling and drilling are the major operations. Compressor blades and blisks (bladed disks) strongly rely on 5-axis milling, where the simultaneous movement along five axes is needed to create the geometry (EZUGWU; WANG, 1997; SOUZA, 2006).

Typically, the component is machined to near finish dimensions in the solution treated condition. Then age hardening increases its strength to maximum levels, and finally it is finish machined to achieve the desired geometry and characteristics (EZUGWU, 2005).

## 3.2 Machining

In the context of manufacturing technology, machining is one of the oldest techniques that are used to produce the desired shape of components. Since the end of the 19th century metal cutting operations have been studied, resulting in theories about the phenomena that are involved in the generation of chips. Even today there is discussion about the mechanisms involved in chip formation. This is greatly due to the variety of materials, cutting tools, machining parameters and process kinemactics that are used. Even for the simplest case of orthogonal cut, no single model is able to represent the chip formation mechanism for both brittle and ductile materials (ASTAKHOV, 2006; KLOCKE, 2011).

The concept of the shear plane was developed in the 1900s, representing the boundary between the workpiece and the chip. It is the plane along which all the shear deformation is assumed to occur, a simplified assumption that is physically impossible. Yet it allowed Merchant to develop his "card model", in which the material deforms as a series of thin elements like a set of cards. Based on this assumption, equations for the strain, strain rate and machining forces were obtained (ASTAKHOV, 2006; KLOCKE, 2011; ALTINTAS, 2012).

Despite its historical significance, it is suggested that the shear plane model presents several drawbacks that affect the precision of predictions. According to ASTHAKOV (2005), some of them are:

- Sudden change of velocity of the material becoming the chip would require infinite acceleration;

- Infinite strain if it is considered that all deformation occurs at the shear plane;

- Strain velocity and strain rate calculation should consider the velocity of the chip in relation to the tool, rather than absolute velocities;

- Not applicable to brittle materials, in which plastic deformation is restricted;

- Power and energy consumption should be inferred with consideration of both the developed stresses and strains, which determine the energy that is spent in deformation of the work material.

Contemporary view of chip formation in metal cutting understands that this mechanism is entirely connected to material behavior. Additionally, the same material may behave in different ways depending on the loading conditions. Brittle materials originate discontinuous chips, separated from the workpiece by rapid crack propagation. Depending on the position and orientation of the resultant force a bending moment may arise, contributing to the achievement of a stress state that breaks the chip. Otherwise, material is fractured purely in compression, forming small fragments and dust (more common when using negative tools). Shear deformation is not possible or at least restricted in both situations because of the brittle nature of the material (ASTAKHOV; SHVETS, 1998; KLOCKE, 2011).

In the case of ductile materials, the same consideration of the bending moment as a major contribution may be assumed. According to this model, shear occurs along a curved surface rather than a plane because of the superposition of pure shear stress and bending stresses as shown in Figure 3.7 (a). First contact of the tool with the workpiece introduces stresses and a bending moment because the resultant force P is not aligned with the centerline of the material being cut. The chip is only generated when the bending action SxL interacts and creates a stress state that is enough to produce a crack, at the borders of line 1-1. The bending moment action also explains the curly geometry of chips without any consideration of cutting fluids (ASTAKHOV; SHVETS, 1998, 2004).

In practice, however, several micrographs made after quick stop testing do not clearly show a curved aspect of the shear zone. What can be seen in Figure 3.7 (b) and in most of the cases is a zone of finite width with intense shear deformation and a straight aspect called primary shear zone, A in Figure 3.7 (c). This figure shows a conceptual view of chip

formation mechanism, based on the shear plane model, but also introducing features that are observed in experiments (KLOCKE, 2011).

It is possible that the bending moment hypothesis complements this model. Additional experimental work is needed to validate it.
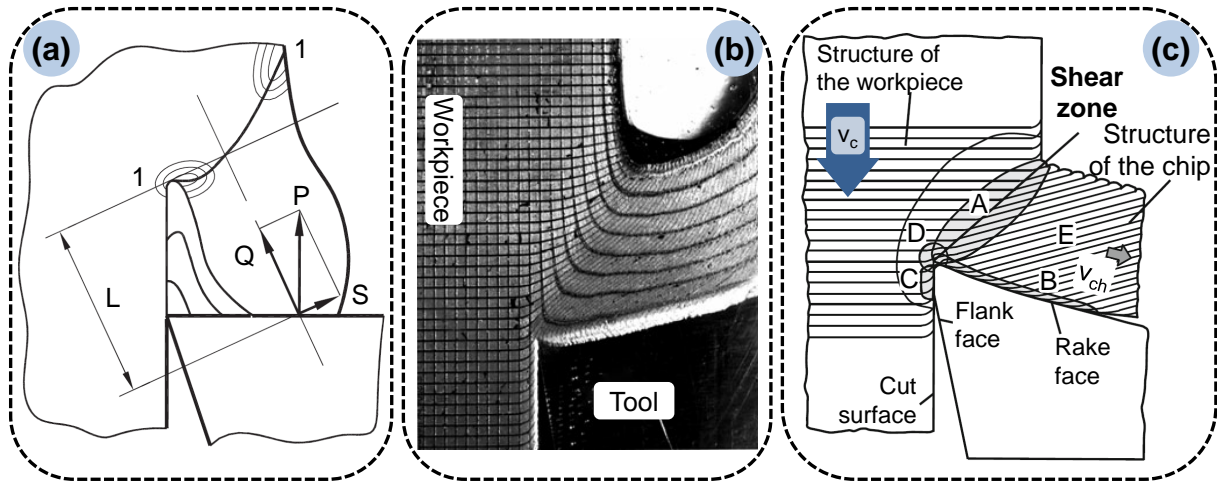


**Figure 3.7.** Models of the chip formation mechanism. (a) The bending moment hypothesis, proposed by ASTAKHOV and SHVETS (1998, 2004). (b) Image of a quick stop test, with a grade engraved in the material. (c) Modern view of the shear plane model, in which several zones can be identified: A, B and C are the primary, secondary and tertiary shear zone, respectively. D is the stagnation zone, where the material flow speed is close to zero, and E is the chip itself. Adapted from: (KLOCKE, 2011)

When shear deformation progresses with tool penetration, the chip also slides over the rake face of the tool, originating the secondary shear zone. High compressive pressure is developed, and the deformation of the material in this region resembles a viscous flow process with an extremely high degree of deformation. Detachment of the chip first occurs in front of the cutting tool, and is designated as a continuous chip (KLOCKE, 2011).

Two other chip types are segmented and lamellar, or saw-toothed, chips. The first one is formed when the deformability of the material (shear strength) is exceeded and detachment occurs. Segments fuse with each other right after it, resulting in long chips. Lamellar chips are common in the case of materials that combine low thermal conductivity, significant strain hardening, and high ductility. Its mechanism will be discussed later, as it is the rule when machining titanium alloys (KLOCKE, 2011).

The mechanisms of chip formation are valid for every machining process with definite cutting edge, since the concept behind material removal is the same. On the other side, there are significant differences in terms of chip morphology, cutting forces, process temperature, and the resultant geometry. Studies developed for orthogonal cut and turning operations are not directly applicable to milling. Its nature subjects the tool to interrupted cut and therefore impact loads, creating harsh operational conditions (KAHLES *et al.*, 1985).

Even the microgeometry of the tool, i.e. the cutting edge radius and the shape of chip breaker, and tool wear may have strong influence on some parameters like cutting forces and residual stresses (SCHWACH; GUO, 2006). This can be accounted as another challenge for modeling machining processes. As an alternative, empirical models are frequently used, like the Kienzle equation for cutting forces, equation (1) (KIENZLE, 1952; cited by GOMES, 2001). Main disadvantage is that for each different combination of tool and material, new constants must be obtained.

$$F_C\!\!\Big/\!\!b = k_{C1.1} \cdot h^{(1-mc)} \tag{1}$$

The term $k_{C1.1}$ is the specific cutting force, representing the load that must be applied to remove a chip with unitary cross section $b \times h = 1 \times 1$ mm², and mc is a term depending on the material and tool. Once the uncut chip thickness h is elevated to the power (1-mc), the cutting force is non-linear with it.

Depending on the complexity of the part to be milled, several processes may be applied to achieve the final shape. Turbine blades for example are rough milled mostly as wall geometry. The final surface is machined by simultaneous movement of five axes and ball end milling tools in order to produce the tridimensional profile. Structural parts are somewhat simpler as they can be imagined as a group of walls and floors. Then peripheral and face milling are the generating processes, respectively. Figure 3.8 depicts some of the possible milling operations.
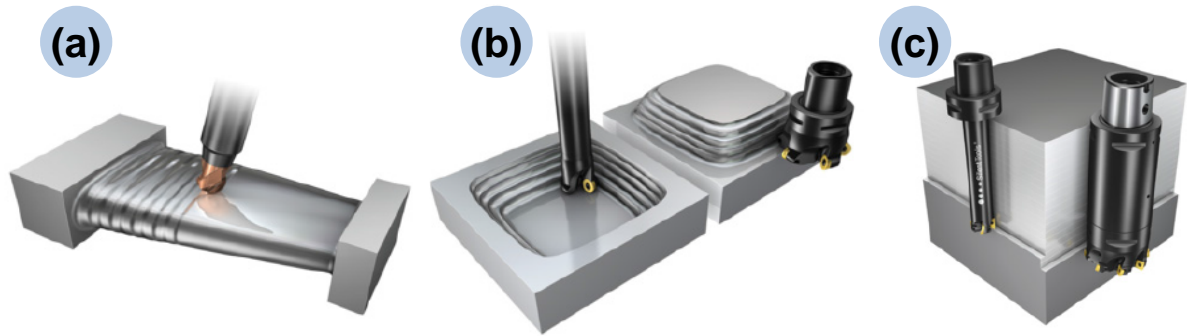
**Figure 3.8.** Several milling operations. (a) 5-axis milling of a turbine blade; (b) rough milling of a pocket / rough contour milling; (c) deep shoulder milling.

As stated before, the chip generation process and several other aspects of machining are dependent on the material that is being cut. Therefore, the next section is dedicated to discussing some details of the machining process of titanium and its alloys.

### 3.2.1 Machining of titanium and its alloys

Titanium and its alloys are classified as hard to cut materials, together with nickel based and some iron based alloys (e.g. austenitic stainless steel). They require higher cutting energy than low-strength alloys like plain carbon steel or aluminum. M'SAOUBI *et al.* (2008) affirm that, once machining is the purposeful fracture of a determined layer of material, it is reasonable to consider both the strength and the strain at fracture. The product of these properties is capable of providing an approximate idea of the difficulty to machine the material. It is also reasonable to evaluate the product considering properties at elevated temperatures, once heat is produced in machining.

Perhaps the most challenging issue in the context of titanium machining is the heat concentration close to the cutting edge of the tool. EZUGWU and WANG (1997) state that up to 80% of the heat generated is transferred into the tool because of the low thermal conductivity of titanium (about 1/6 that of steels), which does not enable heat ejection through the chips. It also leads to heat concentration in the cutting zone, similar to the behavior of austenitic stainless steels (OUTEIRO; UMBRELLO, M'SAOUBI, 2006). In production terms, this means that cutting speeds are very low even when compared to hardened steels, seldom exceeding 70 m/min (COROMANT, 2002).

The workpiece is also substantially heated, and both the tool and the machined part experience steep temperature gradients. REISSIG *et al.* (2004) developed a method for

evaluating the temperature gradient in the machined surface of titanium. It was obtained by means of a correlation with the maximum vanadium concentration in β-grains. Figure 3.9 depicts that temperatures as high as 1000°C are developed in drilling, achieving much lower and stable values after a depth of 25 μm. Such environment is favorable to diffusion, chemical reactivity and plastic deformation. Despite its chemical inertness at room temperatures, titanium becomes highly reactive beyond 500°C, and even the hardest tools are deteriorated because of chemical wear (KAHLES *et al.,* 1985).
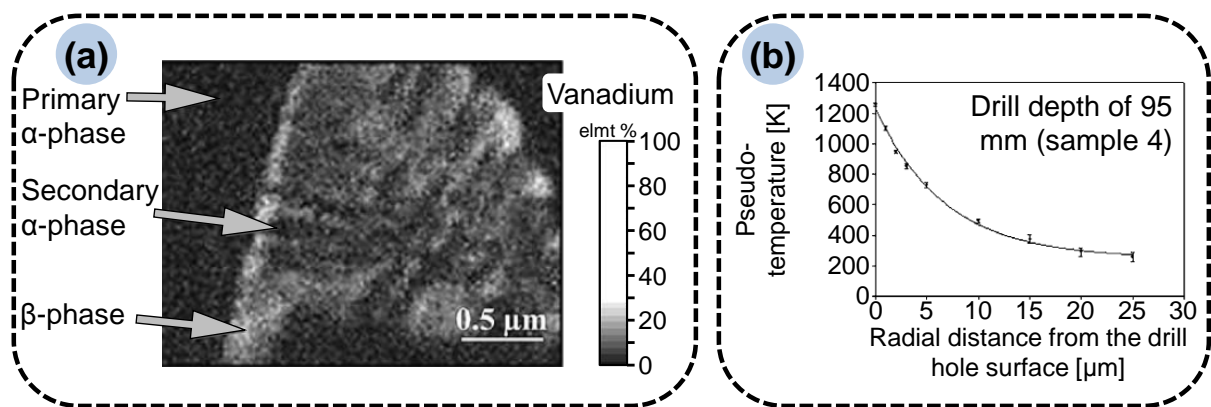


**Figure 3.9.** (a) Vanadium elemental mapping of a transformed β-grain, with the highest concentration near the grain boundaries and decreasing towards the grain center. (b) Radial gradient of the pseudo-temperature in drilling. Adapted from: (REISSIG *et al.*, 2004).

Even at light cutting conditions, diffusion between the tool and the workpiece is likely to occur. In carbide tools the bonding element (cobalt) may diffuse to the workpiece, resulting in weakened support of the carbide particles. This effect is combined with the strength reduction due to temperature rise. Further machining leads to attrition, the removal of grains of tool material by the adherent chip or workpiece, shown in Figure 3.10. Nevertheless, attrition is not restricted to carbide tools, and is reported to be a major contributor to the flank wear, no matter the tool material. Analysis of the chips allows the identification of tool particles adhered to them. More evidence of attrition is provided by uneven flank face, as an effect of the grains being torn away (DEARNLEY; GREARSON, 1986; JAWAID; SHARIF; KOKSAL, 2000).
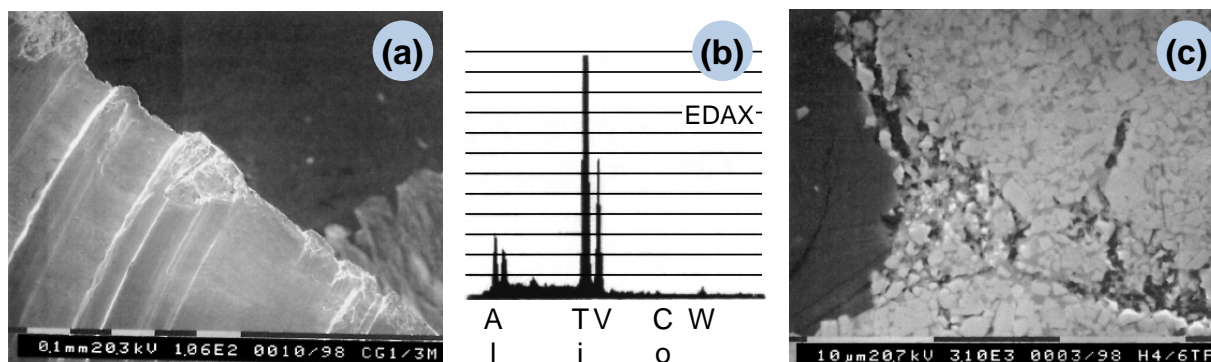
**Figure 3.10.** (a) Adhesion of workpiece material on the tool; (b) EDAX analysis of the workpiece showing the presence of W, which is evidence of diffusion. (c) Section view of the tool: because of the diffusion of the binder (Co), carbide particles are torn out, in a mechanism named as attrition. Adapted from: (JAWAID; SHARIF; KOKSAL, 2000).

In addition, the increase in the temperature at the region that is being cut does not result in significant softening. As mentioned before, titanium maintains its mechanical strength up to moderate / high temperatures (500°C). Intermittent processes such as milling expose the cutting edges to variable thermal and mechanical loading. Thermal cracks result from the cyclic heating and cooling at the cutting edge (JAWAID; SHARIF; KOKSAL, 2000).

Another failure mechanism that is frequent in regard of titanium alloys is adhesion. The high pressures at the cutting edge may cause titanium to develop a strong bond with the cutting tool. Coatings are used many times to avoid adhesion, but once delamination occurs rapidly when machining hard to cut materials, it cannot be fully prevented. The adhered particles are removed on the next cuts, in some cases also pulling out parts of the tool and leading to chipping. Frequently, tool material can also be found of the chips and workpiece (JAWAID; SHARIF; KOKSAL, 2000; ZHANG *et al.*, 2010; DA SILVA *et al.*, 2013).

Experiments with coated tools did not produce satisfactory results in some cases. Several references indicate that coatings are rapidly delaminated from the substrate, after only very few cuts (DEARNLEY; GREARSON, 1986; JAWAID; SHARIF; KOKSAL, 2000; COROMANT, 2002; GHANI *et al.*, 2013). In drilling, however, SHARIF and RAHIM (2007) have shown evidence that a TiAlN-PVD coating over a cemented carbide substrate can be effective, providing much longer tool life. For moderate cutting speed (45 m/min), the increase was nearly five times. A possible explanation is the formation of a micro-thin oxide layer of $Al_2O_3$ that provides thermal insulation to the tool.

Other coatings, like TiN and TiCN, are also industrially used. According to cutting conditions that are used, distinct performances can be observed. The decision upon whether to use or not coated tools requires analysis of each case (KAHLES *et al.,* 1985).

Machining operations of titanium produce segmented chips (also named "saw-tooth" chips, "serrated" chips), even at relatively low cutting speeds. The main theory, supported by several authors for the conventional range of machining parameters, is the thermoplastic instability leading to adiabatic shear banding. For heat resistant alloys in general, the low thermal conductivity and high mechanical strength at high temperatures are favorable to its occurrence (MOLINARI; MUSQUAR; SUTTER, 2002). In its essence, this phenomenon results from a change in the orientation of the shear plane to another in which deformation is more favorable. ASTAKHOV (2006) presents the cycle involved in the formation of this chip morphology, shown in the Figure 3.11.
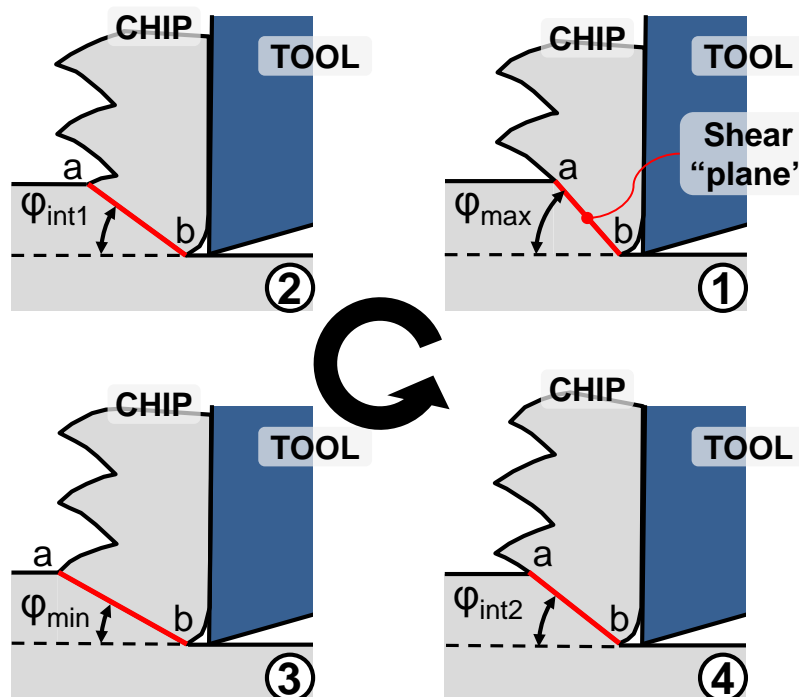


**Figure 3.11.** System consideration of the model of chip formation of the saw-toothed continuous fragmentary chip. Adapted from: (ASTAKHOV, 2006)

In the first step, the formation of chip starts with shear deformation along the surface of the maximum combined stress, indicated by "ab". It is located at an angle $\varphi_{max}$ with respect to the cutting speed. During the cutting action, both strain hardening and heat generation derived from plastic deformation have impact on changing the orientation of the shear surface

(plane), the first effect being more significant. This is shown in the second phase and the angle $\varphi_{int1}$ decreases until it achieves the minimum value, in the third step. At this point, the thermal softening effect (due to heat generation in plastic deformation) overcomes work hardening. The unstable condition is established, and the process accelerates itself, leading to the formation of an adiabatic shear band (KOMANDURI; HOU, 2002; KOMANDURI; VON TURKOVICH, 1981). As a result of this, the angle $\varphi$ starts to increase again, and eventually the stress and temperature conditions will be favorable to the beginning of a new cycle - when $\varphi_{int2}$ achieves its maximum (ASTAKHOV, 2006; KLOCKE, 2011).

This segmentation mechanism is directly related to the contact length between the tool and the chip. In the cyclic process described above, only a restricted volume of material is deformed. Instead of a secondary shear zone that extends to a significant part of the rake surface, just the segment that is being formed is subjected to most of the cutting load.

It can be seen that most of the challenges regarding titanium machining are related to the high temperatures that are developed. Thus it is natural to search for methods that are capable of lowering the temperatures in machining. As will be exposed later, several lubri-cooling techniques act in this sense, and have been a topic of great interest.

### 3.2.2 Lubri-cooling techniques

Cutting fluid application is the most representative and widely used method for the improvement of the tribological conditions in machining. The basic functions of the fluids are to remove the heat that is generated by plastic deformation and shearing, as well as to lubricate the contact interfaces. By suppressing thermal expansion of the workpiece and the conditions that promote rapid tool wear, the productivity and part quality can be both improved. In specific cases, such as drilling and machining of cavities, carrying away the chips also becomes an important function of metalworking fluids (ASTAKHOV, 2006; KLOCKE, 2011; SHOKRANI; DHOKIA; NEWMAN, 2012).

Cutting fluids are often regarded as supporting media that are necessary but not important. It is estimated that they are responsible for 17% of the total manufacturing costs. Tools, in comparison, account for no more than 8% of total costs, as can be stated in the graphs of Figure 3.12, from a German automotive industry (NASIR, 1998; ASTAKHOV, 2006). KLOCKE and EISENBLÄTTER (1997) presented a similar statistic in which tool costs represent approximately 2 to 4%, in comparison to 7 to 17% of cooling lubrication system. BRINKSMEIER *et al.* (1999) state that, with this cost composition, it seems

incomprehensible that most of innovation and research activities have focus on tools. The comparison becomes even more absurd when hard to cut materials are considered, where cutting fluids may be responsible for 20% to 30% (PUSAVEC *et al.,* 2010). Health and environmental issues impose further challenges, therefore several techniques have been studied to improve the cutting process, as well as reduce fluid usage.

**Structure of manufacturing costs**

Machine tool costs
38.3%

General costs
28.5%

Tool costs
7.5%

Staff costs
8.8%

**Costs of coolant application 16.9%**
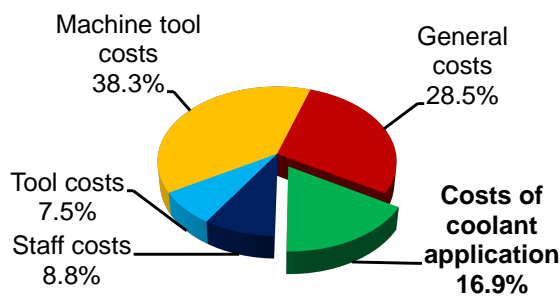
**Structure of coolant cost**

Cleaning
3.7%

Electricity
2.9%

Other
4.2%

Laboratory equipment
5.2%

Service
10.7%

Staff
14.3%

Depreciation and waste disposal
59.0%
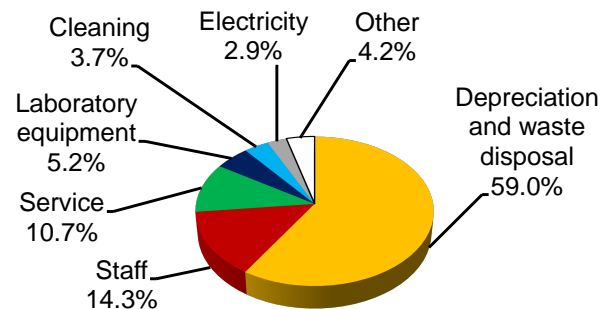
**Figure 3.12.** Cost structure of a German automotive industry; and structure of costs related to coolants Adapted from: (NASIR, 1998; ASTAKHOV, 2006)

The conventional method of application, known as flood cut, consists of a jet of fluid directed to the cutting zone. In the case of hard to cut materials, it is generally suggested that copious volumes of coolant should be supplied to provide heat removal. There is a large variety of fluids that are commercially available, ranging from water soluble to straight oils (ASTAKHOV, 2006).

A great number of hypotheses have been developed about the mechanisms by which metalworking fluid improves cutting. Nevertheless, they do not allow the clear understand of what is really happening at the contact interfaces. Two paramount questions are still open: (1) the way in which cutting fluids can penetrate into the contact interfaces; (2) whether the cutting fluids act as coolants, lubricants or both (ASTAKHOV, 2006; KLOCKE, 2011).

It is worth making a remark about the hypothesis that cutting fluids act by penetrating in between the cutting tool and the chip, as boundary lubricants. Comparison of the specific tool load and the contact pressure of leak-proof flanges shows that the first one presents much higher values. This simple parallel allows one to conclude that the high pressure developed in the tool-chip interface precludes any fluid access to the rake face. Theories related to capillarity effect, fluid access through microvoids etc. are shown to lack physical basis when the machining boundary conditions are considered (ASTAKHOV, 2008).

It is possible, however, that extreme pressure (EP) additives exert some influence in the tool-chip interface. Lubrication engineering frequently uses EP additives such as MoS2 (molybdenum disulphide) in order to achieve stable films, for example, in the gear teeth contact or bearings (STACHOWIAK; BATCHELOR, 2000).

Therefore, the main possible influences of cutting fluids in the cutting process are:

- Lubricating the chip and tool interface out of the flow zone;
- Lubricating the tool and workpiece interface;
- Removing heat from the tool and workpiece;
- Improve chip breaking through directing the fluid jet.

Despite the described challenges, flood cut is probably the most widespread lubri-cooling technique. In some cases, it is essential for improvement of tool life and workpiece quality. Several research branches are focused on alternatives to flood cut, and the decision upon one or another requires an extensive evaluation of the process.

An alternative for drastically reducing the cutting temperature and tool wear is supplying the cutting fluid under high pressure (p > 80 bar). Literature references report an increase in tool life by a factor of 2.3 (VB = 0.3 mm) when applying cutting fluid at a pressure of 140 bar, in comparison to conventional supply at 6 bar (KLOCKE, 2011). By directing the fluid jet to the gap between tool and chip, smaller and fractured chips could be obtained. On another study, results show that for the same cutting time the maximum flank wear was reduced by almost 45% when supplying cutting fluid under a pressure of 150 bar, as depicted in Figure 3.13. At the same time, contact area decreased, while cutting force and consequently specific tool load increased (KLOCKE *et al.*, 2012). Encouraging results were also obtained by SILVA *et al.*, in the high speed range. At 175 m/min, application of cutting fluid at 203 bar increased life of polycrystalline diamond (PCD) tools by a factor of more than 20 as compared to conventional cooling (DA SILVA, 2013). The trend for high pressure cooling is the increase of mechanical load, and reduction of thermal load.
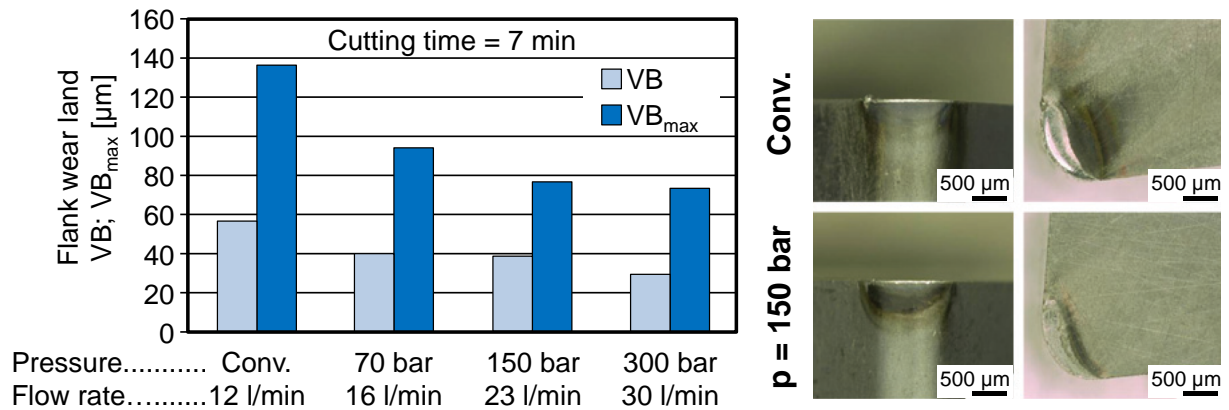
**Figure 3.13.** Dependency of tool wear and chip forms on the lubricoolant supply pressure in longitudinal external turning of Ti-6Al-4V. Cutting speed $v_c = 60$ m/min; depth of cut $a_p = 1$ mm; feed f = 0.2 mm. (KLOCKE *et al.*, 2012)

It is important to note that high pressure systems are very energy consuming. The equipment described by DA SILVA *et al.* (2013), for example, has a power of 22.4 kW, while the machine tool itself has a motor drive of 11 kW. This must be considered in the economic analysis.

Even more impressive results regarding tool life are obtained through the use of cryogenic cooling. This technique makes use of a fluid at extremely low temperature, i.e. liquid nitrogen (LN2) at -196°C. Literature results show that maximum flank wear may be reduced by 61% when turning titanium aluminides, in comparison to conventional cooling. High pressure coolant supply at 300 bar and 42 l/min reduced maximum flank wear by 41%, and MQL with vegetable oil with an air-oil flow of 70 l/min, by 7% (KLOCKE *et al.*, 2013). Once again, the major disadvantage is related to the costs of the system.

Rather than from the described methods, minimum quantity lubrication (MQL) seeks economic gains by drastically reducing the amount of fluid that is used. It is also called near dry machining (NDM) because only fine droplets of lubricant are delivered precisely at the cutting zone. Oil is conveyed by compressed air that acts as the transport medium, producing an aerosol. Its function is to reduce friction at the interfaces between tool, workpiece and chip. Often the quantity that is used is so small that no residue covers the workpiece after machining, and thus the term NDM. Environmental and health benefits are also obtained with MQL, once fluid disposal is simplified and the operator does not need to handle hazardous fluids (ASTAKHOV, 2006; KLOCKE, 2011; SOUZA, 2014).

Cooling effect is only of secondary importance in MQL. This is a consequence of the low thermal capacity of oil and air and the small quantities that are applied. When an emulsion is used in place of oil, lubricating effect is much lower, and the technique is also referred as minimum quantity cooling (MQC) (KLOCKE, 2011). The effect may be maximized by applying air at low temperatures. When end milling Ti-6Al-4V with an external MQL system, air at 17°C and flow of 88 l/min, YUAN *et al.* (2011) obtained approximately two times the tool life of wet cut condition. Cooled air at -15°C and 280 l/min was able to increase tool life up to 5.5 times (compared to wet cut) as shown in Figure 3.14. It must be noted that this considers the use of two different equipments simultaneously: MQL, plus cooling air system. Even with the encouraging results, the method seems fairly practical and economically reasonable.
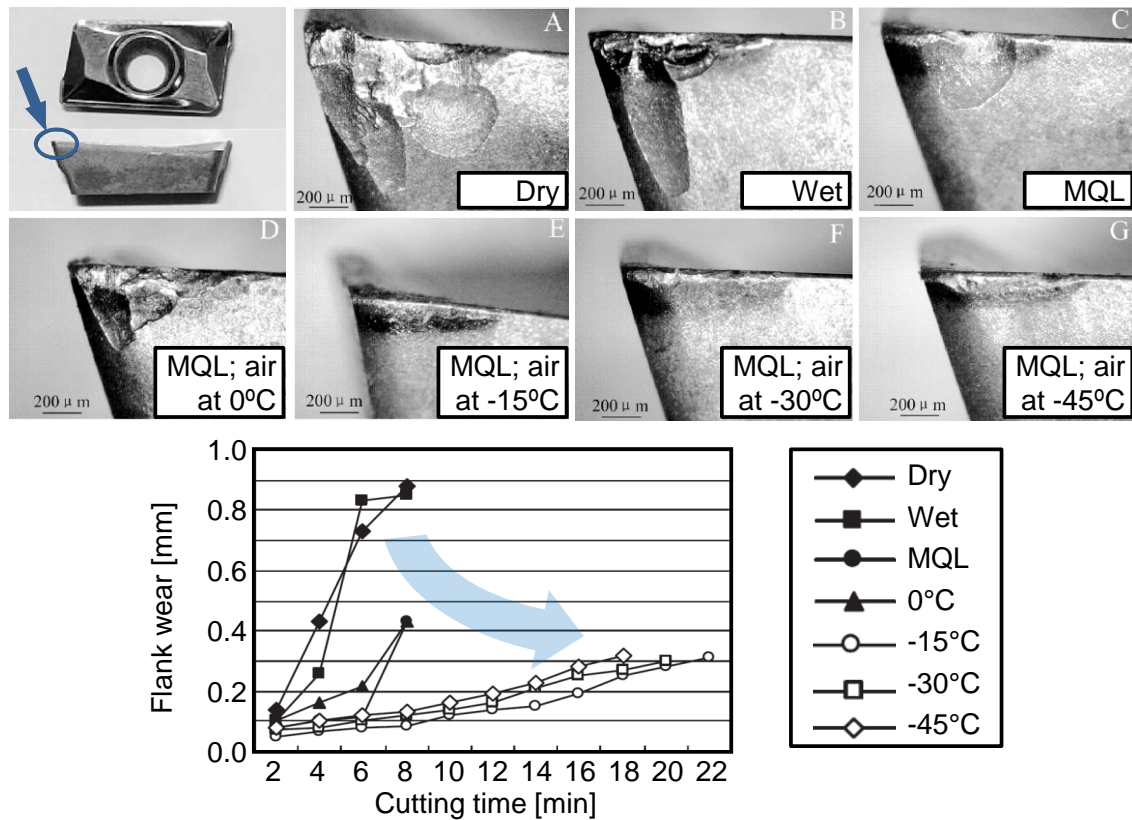


**Figure 3.14.** Tool wear after milling titanium alloy Ti-6Al-4V for 8 min, and evolution of flank wear with cutting time. $v_c = 62.8$ m/min; $a_p = 1.0$ mm; $a_e = 8.0$ mm; f = 0.075 mm/rev. Adapted from: (YUAN *et al.*, 2011).

Even for hard-to-machine materials like titanium, encouraging results in MQL drilling have been reported. Comparison of flank wear, corner wear, thrust force, torque and

temperatures shows that even external application of the mist is capable of producing results similar to the ones of flood cut. This is an indication that thermal load is not heavily increased, despite the low amount of applied fluid. Data from the tests is shown in Figure 3.15. Experiments further demonstrate that palm oil has a better lubricating effect (RAHIM; SASAHARA, 2011).
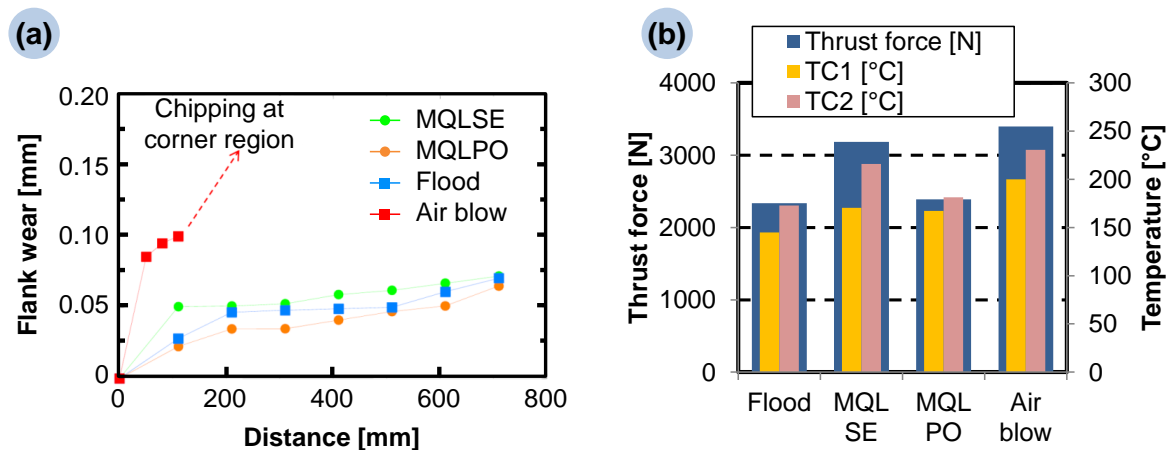


**Figure 3.15.** Comparison of tool wear, thrust force and temperatures in Ti-6Al-4V drilling with synthetic ester lubricant mist (MQLSE), palm oil mist (MQLPO), flood of coolant, and air blow. TC correspond to thermocouples positioned at approximately 1.25 mm from the hole wall. Adapted from: (RAHIM; SASAHARA, 2011)

Several MQL systems are commercially available, and besides the particularities of each one, the principle is the same. The MQL medium can be supplied through independent nozzles or by means of the machine tool spindle and internal ducts inside the tool. In addition, the aerosol may be produced externally or directly in front of the tool, the system being classified as 1-channel or 2-channel respectively. The main advantage of 2-channel systems is that once the aerosol does not have to be conducted through long ducts, coalescence of lubricant drops is avoided. As depicted in Figure 3.16, there are then four possibilities.
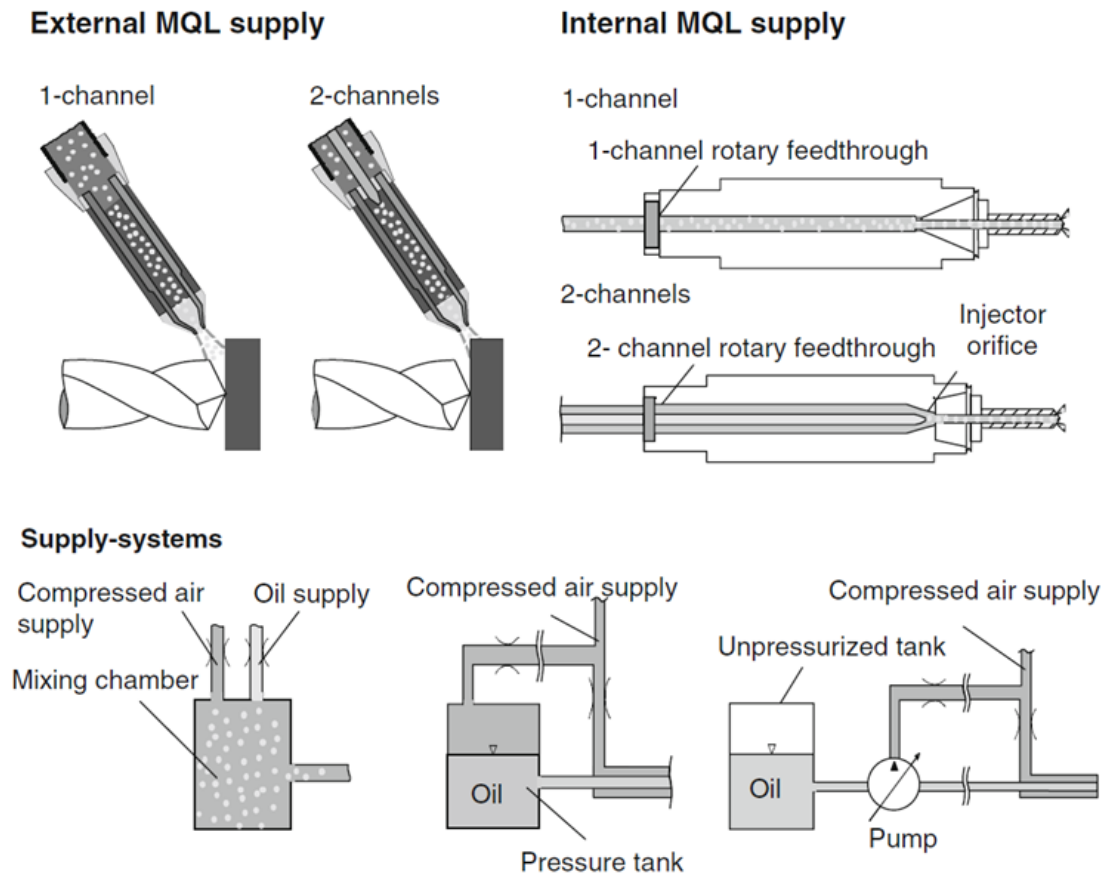
**Figure 3.16.** MQL supply systems. From: (KLOCKE, 2011)

External supply is advantageous from the point of view that no modification is necessary in the machine tool, and such a system often is inexpensive. However, the external nozzle may not be able to provide proper mist at the cutting zone – for example in deep hole drilling. The internal system delivers the aerosol exactly at the cutting zone, but it requires tools and internal channels with specific features (no right angles, cavities, sharp corners, low roughness etc.) (ASTAKHOV, 2008; TAI *et al.*, 2014).

An economic analysis developed by SOUZA (2014) compares dry machining to MQL and flood cut (both using an emulsion of vegetable oil and water), for cast iron milling. The estimated costs using MQL along one year are 36% lower than for flood cut. It is important to note that each combination of machining process, part geometry, material and cutting fluid will influence the cost structure.

Selection of the lubri-cooling technique and cutting fluid is dependent on many aspects. In some cases, it is crucial to take into account mechanical and metallurgical properties that are related to functional performance of the component. Aerospace structural parts are into this group as surface characteristics are especially important for fatigue life. As

will be shown later, systems like cryogenic cooling also provide better surface properties. Whether the cost associated with their use is economically worthwhile must be decided on a case-by-case basis.

## 3.3   Surface integrity

For many engineering applications, the functional performance will be closely related to properties of the surface of the material. Wear, fatigue strength, toughness and electric properties are some of the examples in which specific features are desired at the outer layers. In fact, a number of physical and chemical phenomena are related to characteristics that are intrinsic to the surface and subsurface of the material. Additionally the several surfaces of a particular part could be associated to different functions and therefore distinct properties. In this context, the concept of surface integrity arises: "*the inherent or enhanced condition of a surface produced in a machining or other surface generation operation*" (FIELD; KAHLES, 1964; cited by ASTAKHOV, 2010).

According to ASTAKHOV (2010), the term surface engineering may be defined as the concomitant design of surface and substrate as a functionally graded system to achieve a cost-effective performance enhancement of which neither is capable on its own. Once this is a function oriented effort, the boundary conditions regarding the requirements must be well established. The objective is to manipulate technologies in order to generate optimal surface properties for specific applications in the most cost-effective manner. In this context, main branches of activities can be defined as shown in Figure 3.17(a).

Real surfaces of solids are far from being smooth and perfect. Rather than this, they present a specific topography and micro layers related to the manufacturing process, temperature action and oxide formation. Most of the manufacturing processes produce a work hardened layer as a result of the mechanical interaction, but thermal loads may also introduce permanent deformation (BRINKSMEIER *et al.*, 1982). Above it there is an amorphous or microcrystalline structure, called "Beilby" layer, as well as oxides resultant from contact with oxygen, adsorbed gases and water vapour. They are shown schematically in Figure 3.17(b) (ASTAKHOV, 2010).
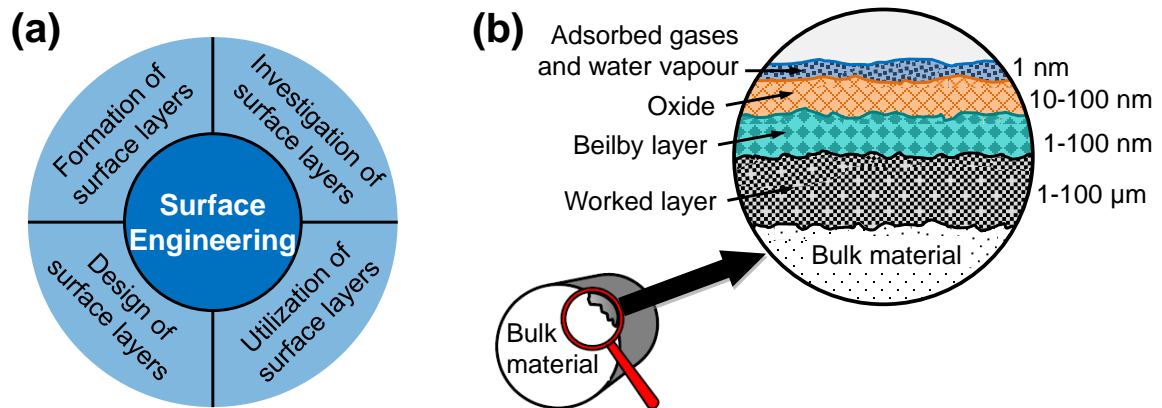
**Figure 3.17.** (a) Main branches (areas) of surface engineering. (b) Real solid surface and layers. Adapted from: (ASTAKHOV, 2010)

Surface engineering is a function oriented subject, and regarding aerospace industry, it has been shown that the most important design parameter is the fatigue life. Thus it can be inferred that the function to be carried out by aerospace structural parts is to withstand cyclic loads. A high degree of safety must be associated, but at the same time light parts are demanded to fulfill economical requirements. The search for these three concomitant objectives led the aerospace industry to be among the first to consider the surface integrity of their pieces ASTAKHOV (2010).

KOSTER *et al.* (1970) were the first group of researches to explore these links. One of the greatest achievements was the verification of alterations in the outer layers of machined titanium parts, such as plastic deformation, microcracking, phase transformation, work hardening and hardness modifications, residual stresses etc. These surface aspects were evaluated for several machining operations and conditions, and further faced with fatigue life experiments. The results contributed to the recognition of surface integrity as a key factor in product quality and service behavior (KOSTER *et al.*, 1970; KAHLES *et al.*, 1985).

In the manufacturing chain of a component, several operations are performed in order to obtain the desired geometry. In its essence, this is made by generating surfaces that define the material boundaries. For material removing processes, the physical interaction produces characteristics that are different from the bulk. The next sections present further information connecting the fatigue life to surface parameters, and then to the machining operations that create them.

### 3.3.1   Influence of surface integrity on fatigue life

The former studies by KAHLES *et al.* (1985) demonstrated the impact of several machining operations and cutting conditions on the fatigue life. Evaluating the endurance limit for high cycle fatigue, it was stated that gentle grinding was able to increase the load capacity of the component by almost four times when compared to abusive grinding. This difference was smaller when comparing gentle and abusive milling but still significant. It is an indication that proper selection of the cutting parameters can result in improved properties and performance.

During cyclic loading, crack initiation usually occurs at the surface of the workpiece associated to stress concentrators, where the actuating stress is maximized. Technical materials contain imperfections like roughness, pores, inclusions, notches, as well as a microstructure of various crystallographic orientations, morphology and boundary structures. All those features may act as stress raisers. After the onset of crack, the discontinuity of the surfaces further raises the level of local stresses, increasing crack length. On most of the cases, the regime of crack propagation prevails, and is the most relevant for fatigue life assessment. At this phase, other properties are considered relevant, like the residual stress state and the ductility, which in general is at least partially consumed during manufacturing (KRUPP, 2007).

Probably the most direct impact of machining is on the surface topography, and it has to be considered from two standpoints: process control and functional performance. Traditionally, the roughness parameters have been extensively used as an index of the variations in the process due to tool wear, machine tool vibrations etc., instead of a measurement for inferring the performance of the component (PETROPOULOS; PANDAZARAS; DAVIM, 2010). This approach is used in many tribology applications, but other functional requirements may be related to the geometrical state of the surface, as can be seen in Table 3.3.

Surface roughness is associated to stress concentration and localized plastic strain field when micronotches are introduced by machining. This zone of plasticity is manifested as a slip band. Literature references suggest that microcracks are initiated at those persistent slip bands, and thus it is reasonable to establish the relationship between roughness and fatigue life (NOVOVIC *et al.*, 2004).

**Table 3.3.** Physical / functional significance of several surface topography parameters. Two asterisks indicate a pronounced influence.

| Functional properties | $R_a$, $R_q$ | $R_a$, $R_{pm}$ | $R_t$, $R_z$ | $R_{sk}$ | $R_{ku}$ | $R_{sm}$ | $R_{DelA}$ | $W_a$ |
|---|---|---|---|---|---|---|---|---|
| Contact stiffness | * | | ** | * | * | ** | * | * |
| Fatigue strength | * | * | ** | | * | | ** | |
| Thermal conductivity | * | ** | | | | ** | * | * |
| Friction and wear | * | | ** | ** | ** | * | ** | * |
| Mechanical sealing | * | | ** | ** | | | ** | ** |
| Fatigue corrosion | * | * | | * | | * | * | |
| Assembly tolerances | * | | ** | | | | * | * |

From: (PETROPOULOS; PANDAZARAS; DAVIM, 2010)

However, this argument cannot be generalized. NOVOVIC *et al.* (2004) also presented examples indicating that depending on the material the effect of surface roughness could be very distinctive. In regard of steels, it is suggested that even fine grinding (with gentle parameters) reduce the fatigue strength when compared to polished samples. EL-HELIEBY and ROWE (1980) came to the conclusion that this may be true for fully annealed samples, but when residual stresses are present the effect of roughness is not relevant.

MATSUMOTO, HASHIMOTO and LAHOTI (1999) reported the same trend comparing the fatigue life of AISI 52100 steel samples finished by grinding and hard turning. Experimental evidence also supports that fatigue strength of titanium and nickel alloys was insensitive to roughness as well (KOSTER *et al.*, 1970; TAYLOR; CLANCY, 2007).

Further studies endorse that workpieces where surface roughness is lower do not necessarily present higher fatigue life. Single point tools are reported to greatly increase the strength to cyclic loads of Ti-6Al-4V as compared to ground or ground and polished samples, despite presenting deeper grooves. Experimental data is shown in Table 3.4, comparing several characteristics of the workpieces, and the fatigue life obtained for Krouse bending specimens. This can only be explained when evaluating the residual stresses that are present. On the other side, samples with machining marks oriented parallel to the stress axis were capable of withstand at least 100% more cycles than samples with transversal marks (LEVERANT *et al.*, 1979).

**Table 3.4.** Results of a study evaluating the influence of both roughness and residual stresses on fatigue life. G: grinding; GP: grinding and polishing; SPT1: shaped with single point tool condition 1; SPT2: shaped with single point tool condition 2; SPT1-P: shaped with single point tool condition 1, parallel to stress axis.

|  | G | GP | SPT1 | SPT2 | SPT1-P |
|---|---|---|---|---|---|
| Depth of machining groove that initiated crack [μm] | 0.7-1.3 | 1.1-2.4 | 2.3-3.3 | 4.4-4.6 | 2.3-3.3 |
| Root radius of machining groove that initiated crack [μm] | 1.8-5.1 | 1.8-3.3 | 51-75 | 102-228 | 51-75 |
| Surface residual stress [MPa] | -97 | -504 | -490 | -524 | -490 |
| Cycles to failure – stress range of 0.7 | 6,700 | 6,800 | 10,500 | 13,900 | **22,000** |
| Cycles to failure – stress range of 0.5 | 34,600 | 27,600 | 122,000 | 124,000 | **528,000** |
| Cycles to failure – stress range of 0.3 | 180,000 | 476,900 | Run-out | Run-out | **Run-out** |

Adapted from: (LEVERANT *et al.*, 1979).

Regardless of roughness influence on fatigue strength, data correlation should be done with caution. Consideration of an isolated factor may lead to misinterpretation of the physical phenomenon taking place. Therefore it is important to embrace all the relevant surface integrity parameters in such an analysis.

As already mentioned, residual stress is a very significant parameter influencing fatigue life. It is usually defined as the stress that remains in mechanical parts that are not subjected to any outside stresses (loads). In a broad sense, result from heterogeneous plastic deformation of the material, and it is the result of the metallurgical and mechanical history of the part. Residual stresses are possibly the main parameter associated to fatigue of structural components. Added to the stresses due to external loads, the total level may be increased or decreased (TOTTEN; HOWES; INOUE, 2002).

Compressive residual stresses are capable of greatly improving the fatigue life of the component. This is due to the strong influence on the crack propagation mechanism. Actually, residual stresses are considered to have a strong significance for fatigue life only during crack propagation, whereas its influence on crack initiation is negligible (WAGNER; BIGONEY, 2003; KRUPP, 2007). Once residual stress acts as a pre load in the material, when it assumes a compressive character the stress intensity factor is reduced (MITSUBAYASHI; MIYATA; AIHARA, 1994).

Referring to the Table 3.4, the compressive residual stress level led to higher fatigue life of samples SPT1, SPT2 and SPT1-P. The same is not true for GP, however, but probably this was due to the very shallow layer of highly compressive residual stress induced by polishing. In other words, after just a few microns the value of residual stress is much lower in magnitude, comparable to G (LEVERANT *et al.*, 1979).

Studying the fatigue behavior of shot peened steel, MITSUBAYASHI, MIYATA and AIHARA (1994) evaluated the crack length growth rate. It was observed to be substantially reduced when the crack achieves the depth of highly compressive residual stress, as shown in Figure 3.18. The same figure also demonstrates the result obtained from a mathematical model developed by the authors. Once a reasonable correlation was found, the model was applied in order to estimate the fatigue life of several residual stress profiles. According to the presented results, the magnitude of the residual stress is the most affecting parameter in fatigue life.
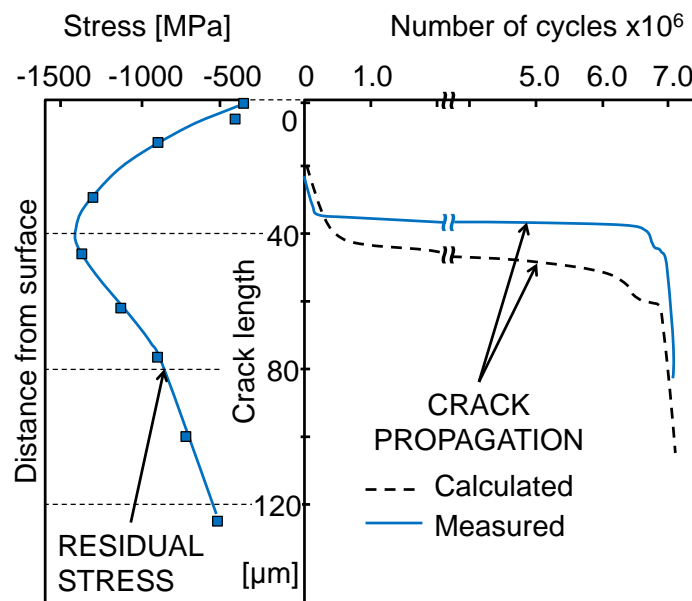


**Figure 3.18.** Crack propagation along the depth and comparison to residual stress profile. It can be seen that at the region of maximum compressive residual stress the rate of crack length increase in relation to the number of cycles is very low. Adapted from: (MITSUBAYASHI; MIYATA; AIHARA, 1994)

Many studies on the surface integrity of materials after machining also present data about the hardness along the depth and the microstructure. In most of the cases this data is obtained to maintain coherence with literature rather than to establish correlations with

functional performance. Few studies evaluate the influence of each property alone. Thus it is hard to confirm whether those properties are important to fatigue strength or not.

In a general view, it is considered that higher surface hardness leads to a retardation of crack initiation for smooth surfaces owing to the increase in strength. The same may not be true for rough surfaces, once in some cases there is no crack initiation phase. Because of the low residual ductility, it is considered that a higher hardness level imparts negatively in the propagation phase. Thus two opposite trends actuate at the distinct phases (WAGNER, 1999; LEYENS; PETERS, 2003).

Results presented by several literature references, on the other side, frequently indicate a correlation that is stronger with residual stress itself. Bending fatigue tests of titanium samples cold worked by swaging to a 50% reduction in area presented the same behavior as conventionally forged samples (forging at 1241 K in the $\alpha$-$\beta$ phase field, annealing for 1 h at 1227 K, water quenched, and then aged at 977 K for 2h). Evaluation was made in terms of crack length growth rate, allowing one to conclude that cold work do not influence fatigue life at all. Hardness, in turn, is a measurement of the residual ductility of the material, reduced by cold work (LEVERANT *et al.*, 1979). Similar results were reported also by WEBER and HERTZBERG (1973).

Different conclusions were achieved by SASAHARA (2005), for 0.45%C steel in rotating bending fatigue test. Results show that samples with higher surface hardness (around 25% more than the bulk) generally had greater life, even with residual stresses close to zero. Mean values of the experimental results are plotted in the graph of Figure 3.19. The crack length growth was not measured, but from the viewpoint of the fracture mechanics exposed before, these results are related to a retarded crack initiation due to the higher hardness. It should be noted that analysis only considered mean values of the fatigue life, despite the large variation of the results.
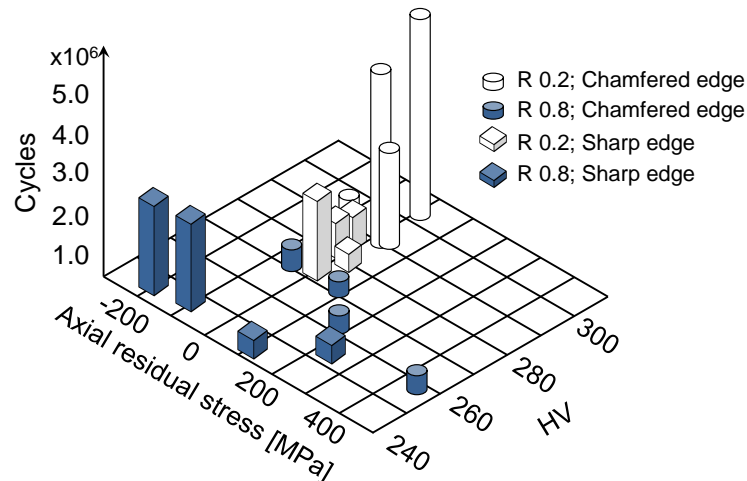
**Figure 3.19.** Mean value of fatigue life for workpieces with different surface hardness and residual stresses. Adapted from: (SASAHARA, 2005).

As can be seen, assessing the correlation between hardness and fatigue life is not straightforward. Considering that it is a measure of the level of cold working of the material then it is related to the mechanical load during the machining process. It may be the case that hardness should actually be understood as complementary data to understand the development of the residual stresses rather than an isolated parameter. A similar view is shared by BUSSU and IRVING (2003), observing that "*published data on the influence of pre strain and prior deformation on fatigue crack growth rates are invariably associated with presence of residual stress fields as well as the deformation field*". In their investigation, aluminum samples produced from plates that were friction stir welded and then stress relieved (by 2% stretching) presented the same behavior as the parent material in terms of crack growth behavior. Despite this, the hardness profiles were considerably different, and it is concluded that crack growth rate is unlikely to be influenced by the introduced strain.

Further studies regarding surface treatments and fatigue life, such as the remarkable investigation performed by WAGNER (2003) and also by PIPPAN (1991), inevitably consider both the level of cold work (and therefore the hardness profile) and residual stresses. These properties are essentially linked in their development.

Some materials are more susceptible to develop microstructural characteristics influencing fatigue life than others. Steels can be cited as an example. In manufacturing processes with high heat input, like grinding and electrical discharge machining (EDM), a transformed layer termed as "white layer" might be formed. In the literature, the term is used as a generic phrase referring to very hard surface layers formed mostly in ferrous materials

under a variety of conditions, which appear white under the microscope. White layers are highly undesirable because in most of the cases it is composed of untempered martensite, with very brittle nature (THIELE; MELKOTE, 1999; GHANEM *et al.*, 2002; SIPOS; LÓPEZ; TRUCCO, 2008).

Fatigue life of titanium alloys is related to the morphology of the microstructure, both in terms of grain size, shape and volume fractions. During machining operations grains next to the generated surface are greatly deformed. In some cases the volume fraction of α and β phases might change, but generation of brittle phases is not common (CHE-HARON, 2001; SUN; GUO, 2009; ROTELLA *et al.*, 2014). The point is that for the range of thermal and mechanical loads developed in machining, there is no strong connection between microstructural changes and fatigue life. Loss of ductility because of work hardening is considered the main microstructural problem, but as shown before, cold work does not have strong influence on fatigue life. Correlations with residual stresses frequently are much more significant and taken as the source of changes in fatigue life behavior (ULUTAN; OZEL, 2011).

Knowledge on the characteristics of α and β structures provides insight in this topic. As exposed before, α phase is hexagonal and such a crystal structure is restricted in terms of dislocation movement and hence plastic deformation. When a manufacturing process such as machining imposes permanent deformation along a definite direction, this strain is preferentially taken by several grains (THOMAS; TURNER; JACKSON, 2010). If this is the case, it is reasonable to assume that the residual stress state will also be heterogeneous, with significant differences from one grain to another. Consequently, some parts (grains) of the material may be much more susceptible to crack initiation and propagation because of both residual stresses and the exhausted ductility of the material.

If theory motivates the metallurgical evaluation of the material's surface layer, on the other side few experiments try to establish correlations to functional performance. In other words, the significance of hardness and microstructural alterations due to machining on the fatigue life is not properly understood. Another point is that other characteristics, such as residual stresses, seems to have a much more remarkable effect, and this relative importance is unknown.

### 3.3.2 Impact of machining on the surface integrity

At some level, all machining processes affect the surface characteristics described previously. The difference between them is that each one has its own signature, since it removes the material by a specific mechanism. Even in regard of a determined process kinematics, final characteristics vary in a certain spectrum because of the conditions of application. Cutting parameters, lubrication, tool wear and cutting edge geometry are some examples of these conditions. Hence prediction of detailed information about surface integrity based on other prior tests is hardly possible in practice. Only general trends may be established, because the results obtained with one process and tool may not be directly valid for another setup (RECH; HAMDI; VALETTE, 2008).

Discussion of the mechanisms that modify the state (integrity) of the surface becomes clearer when considering two categories of properties (PETROPOULOS; PANDAZARAS; DAVIM, 2010):

- Geometrical aspects, referring to the topography and roughness;
- Metallurgical, mechanical, physical-chemical and crystallographic characteristics, like hardness, residual stresses, plastic deformation and work hardening, texture, chemical stability and others. Once the main characteristics related to fatigue life are residual stresses, hardness and microstructure of the material, they will be further discussed, following topography.

In the literature, it is common to assign the geometrical description of a surface as its "texture" or "topography". It may lead to some confusion, once the term texture is also used in the metallurgy context referring to an aggregate whose grains are oriented, to a greater or lesser degree, about some particular direction or directions. Therefore the term topography will be uniquely adopted here when referring to the geometric characteristics of a surface (CULLITY, 1954; PETROPOULOS; PANDAZARAS; DAVIM, 2010).

The basic topography is idealized as the result from the movement of a sharp edge tool, successively removing material from the workpiece. Considering the usual range of cutting conditions, it is possible to write equations for the theoretical roughness parameters. In the case of up and down peripheral milling (PETROPOULOS; PANDAZARAS; DAVIM, 2010; WYEN; JAEGER; WEGENER, 2013):

$$Rz_t = \frac{f_z^2}{8 \cdot \left(\frac{1}{2} \cdot d \pm \frac{f_z \cdot n}{\pi}\right)} \approx \frac{f_z^2}{(4 \cdot d)} \qquad (2)$$

$$Ra_t \approx 0.064 \cdot \frac{f_z^2}{d} \qquad (3)$$

Equation (2) represents the maximum peak to valley amplitude, Rz, as a function of feed per tooth, $f_z$, tool diameter, d, and spindle rotation, n. For up milling (+) has to be used, whereas (-) is used for down milling operations. For $f_z$ in millimeters per tooth and $d$ in millimeters, the roughness will also be given in millimeters. Equation (3) is a simplification to calculate the average roughness (WYEN; JAEGER; WEGENER, 2013).

In spite of the mathematical approximate formulas for calculating roughness parameters, experimental results are often very distinct. WYEN, JAEGER and WEGENER (2013) evaluated equations that included the influence of the cutting edge roundness, but without any significant improvement. In fact, their experimental data has shown no increase in average surface roughness ($R_a$) with the cutting edge radius, while mathematical models predicted a strong direct relation. It is suggested that tool vibration, material adhesion and workpiece properties are associated with the deviations of theoretical models.

In terms of the lubri-cooling method, EZUGWU *et al.* (2007) assessed the surface roughness in turning of Ti-6Al-4V with PCD (polycrystalline diamond) tools and high pressure coolant supply. It extended tool life when compared to conventional flood cut without causing abrasion of the surface during the machining process. However it is not possible to confirm a tendency for the surface roughness because data is mostly dispersed.

ROTELLA *et al.* (2014) evaluated the machining of Ti-6Al-4V using MQL, cryogenic cooling, and dry cut. The use of other lubri-cooling techniques was not able to significantly alter the roughness at some specified cutting condition at all, in turning operation. Despite the affirmation that results were found to be largely and consistently superior when describing cryogenic cooling, the graphs do not show remarkable differences. For clarification of such relations, it is believed that statistical analyses should be performed.

In contrast, KLOCKE *et al.* (2013) analyzed the turning process of gamma titanium aluminides with several lubri-cooling methods. The tendency that is observed in the results is that high pressure tends to slightly increase surface roughness in relation to conventional wet cut. Cryogenic cooling presented the lower values of roughness, followed by MQL, and then high pressure supply. Dry cut was responsible for the higher values.

With cooling air at low temperatures being applied together with a MQL system, lower roughness was achieved by an intermediate temperature, at -15°C. Conventional flood cooling and MQL solely were very similar, while dry cut produced higher roughness in face milling (YUAN *et al.*, 2011).

RAHIM and SASAHARA (2011b) presented consistent results either, but only comparing two types of oils for MQL drilling of Ti-6Al-4V. According to their discussion, the use of palm oil improved the lubrication and reduced friction at the tool-workpiece interface, in comparison to synthetic ester. Therefore the roughness was lower because of the reduced adhesion, reflecting one of the benefits of providing proper lubrication during machining.

Machining affects mechanical and metallurgical surface properties by a combination of mechanical and thermal effects. At the extremes, there are examples of purely mechanical processes, like abrasive jet machining, and also thermal operations such as electro discharge machining (EDM). Turning, milling, drilling and other processes with definite cutting edges combine both effects (GRZESIK; KRUSZYNSKI; RUSZAJ, 2010). Although the material removal is made by the penetration of the tool, which is essentially a mechanical action, part of the energy is converted into heat and thus acts as thermal load. In the case of titanium and other heat resistant alloys this effect is more pronounced, leading to temperatures up to 1000°C. Figure 3.20 depicts temperature distributions of titanium compared to steel during machining.
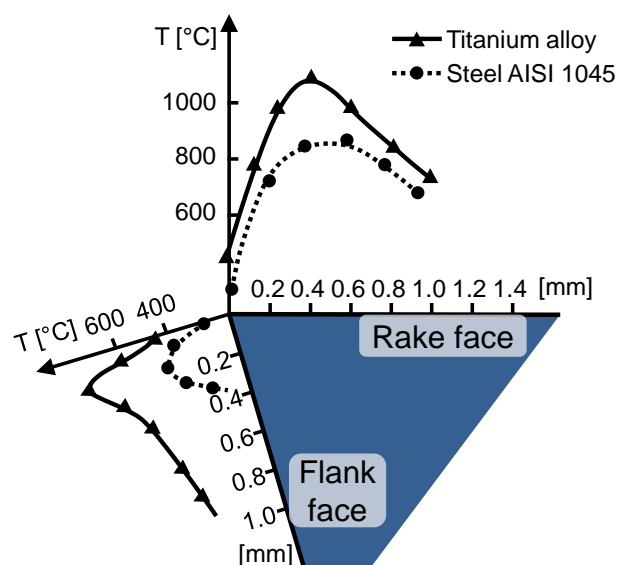


**Figure 3.20.** Comparison of temperature distributions in orthogonal machining of titanium and AISI 1045 steel (ASTAKHOV, 2006).

The mechanical effect is caused by forces acting on the material and generating plastic deformation. In the case of machining, deformation is non-uniform and associated to predominantly compressive residual stresses (TOTTEN; HOWES; INOUE, 2002). Once there is plastic strain, it can be inferred that the hardness will be higher at the surface, where strain is supposed to be maximum. Then decreasing along the depth until the value of the bulk material is achieved. The microstructure near the surface will be deformed accordingly, in the same direction of the cutting tool (ULUTAN; OZEL, 2011).

Thermal load is related to deformation by the volume expansion of the material due to temperature. It often creates thermal gradients and then heterogeneous volume expansion, associated with high strain levels. Depending on the direction of the gradient, compressive or tensile residual stresses may be developed (BRINKSMEIER *et al.*, 1982). For example, during quenching heat flows to the outside of the workpiece. The surface contracts more than the bulk which resists the surface deformation. Depending on the temperature gradient, the strain that is induced at the surface may exceed the yield point of the material. At this moment, the surface material develops tensile plastic stresses. When the room temperature is achieved, the situation is the inverse, and surface material is pulled by the bulk that has contracted.

Abusive grinding (high feed / high depth of cut conditions), on the other side, introduces a large amount of heat that largely increases the temperature of the surface layer. Again, thermal expansion is so large that causes it to deform plastically, partially followed by the subsurface. At room temperature, the surface tries to contract, resisted by the subsurface. This means that tensile residual stresses are introduced (BRINKSMEIER *et al.*, 1982).

Another point is that a temperature increase during machining may act as an over ageing or annealing process, causing softening of the material (GITTING; NOUARI, 2009). Once machining simultaneously involves mechanical loads, a competing process takes places, but frequently the last one is more significant so that a work hardened surface is observed.

If during machining the temperature is sufficiently high, phase transformation may take place, with an associated volume change. As an example, in steels the martensitic transformation involves volume increase with respect to the ferritic-pearlitic structure, introducing highly compressive residual stresses (TOTTEN; HOWES; INOUE, 2002).

In summary, the final state of the surface is a balance of mechanical and thermal loads, as well as phase transformation effects. Depending on the material and the conditions of the manufacturing process, some of those effects may not take place.

The valuable study developed by SUN and GUO (2009) shed light on the behavior of the SI parameters that were cited before. Milling of Ti-6Al-4V, wet cut, was performed with a coated solid carbide tool, in the range of parameters normally used for titanium machining. The residual stress variation with the cutting speed achieves a minimum (most compressive) for an intermediate value of 80 m/min, this behavior being considered a result of interaction between thermal and mechanical effects. Increasing the feed led to slightly less compressive stresses in the cutting direction, while at the transversal direction there was little difference.

JACOBUS, DEVOR and KAPOOR (2000) established a model that is also based on orthogonal cut, in which the material was divided in three layers: the surface, the sub-surface, and the bulk material. The surface is subjected to thermal, plastic and elastic strains, and actually it is defined as the layer affected by the heat generated by the cutting process. In the sub-surface only plastic (always less than or equal to that of the surface) and elastic deformation persists, while the bulk material is only elastically deformed and residual stress magnitudes are negligible. From the balance of plastic strains at surface and sub-surface, and thermal strain the residual stress profile along the depth arises. According to this model, shown in Figure 3.21, three cases are possible:

- Case I: thermal strain is lower than subsurface plastic strain. Both surface and subsurface plastic strains lead to a condition with fully compressive residual stresses;
- Case II: thermal strain is higher than subsurface plastic strain, promoting tensile residual stresses at the surface layer;
- Case III: plastic strain at the subsurface (and also at the surface) is negative. Once the residual stresses counteract the plastic strains, their profile beneath surface will be fully tensile.

The experimental work is well correlated to simulations for AISI 4340 steel, and all the tested conditions fall into the Case II. For the Case I, however, the conditions that are imposed originate a conflicting situation regarding the plastic deformation of surface and sub-surface layers, thermal strain, and far field boundary condition. Thus, the algorithm may not be suitable for this situation. Anyway it provides an insight into the way thermal and mechanical loads interact, resulting in residual stresses.
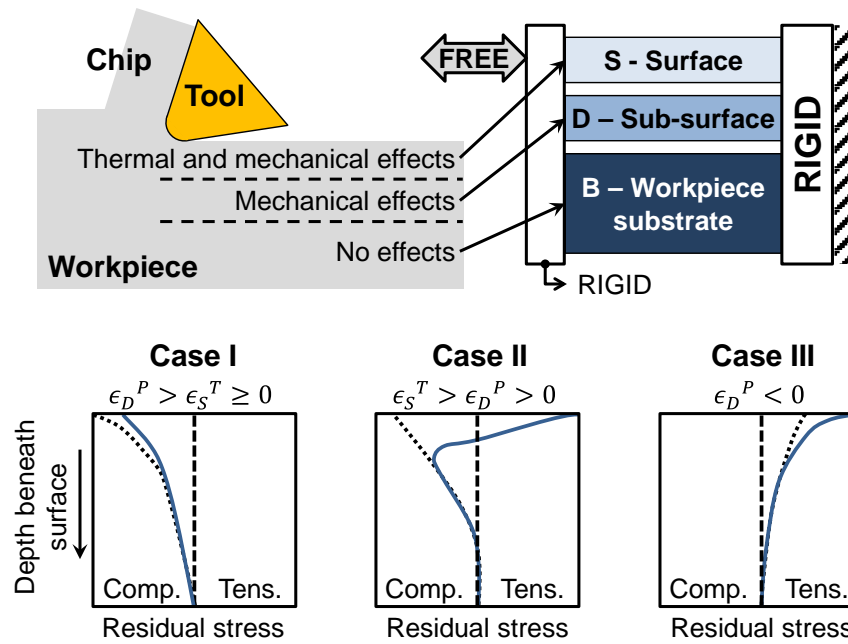
**Figure 3.21.** Residual stress model proposed by JACOBUS, DEVOR and KAPOOR (2000). The subscript S refers to the surface layer, D to the subsurface; the superscript P means plastic deformation and T deformation by thermal action. Adapted from the cited reference.

Titanium milling experiments performed by WYEN, JAEGER and WEGENER (2013) concluded that larger cutting edge radius promotes less compressive residual stresses. An intermediate cutting edge radius (20~40 μm) provided the most compressive surface residual stress, evaluated at cutting direction. A larger radius (50 μm) moved residual stresses towards tensile character. Hardness at the surface was virtually the same, in spite of the edge geometry or cutting direction. This indicates that plastic strain is very similar, and most of the difference in terms of residual stress can be attributed to the thermal load. In a finite element (FE) analysis of orthogonal machining, NARS, NG and ELBESTAWI (2007) came to similar conclusions. Increasing the cutting edge radius increases the amount of heat generated by friction, and at the same time the heat dissipation from the workpiece to the tool. Once residual stresses become more tensile, the first action prevails.

Tools with chamfered and honed cutting edges were highly successful in generating compressive residual stresses. This is credited to the increase of surface and subsurface deformation. Thermal load is not increased, once ploughing effects are associated to the cutting edge radius, which remains the same (MATSUMOTO; HASHIMOTO; LAHOTI, 1999).

CHEN, EL-WARDANY and HARRIS (2004) built a finite element model with mathematical criteria to consider the phenomenon of saw-tooth chip formation in orthogonal cutting of Ti-6Al-4V. Comparisons with experimental data have shown that results are significantly different when considering of not segmented chips, both in terms of cutting forces and residual stress profile. As shown in Figure 3.22, the chip formation mechanism is closely related to the residual stress profile that is developed. This indicates that the nature of forces involved in saw-tooth chip formation promotes significant changes in the residual stress profile after machining.
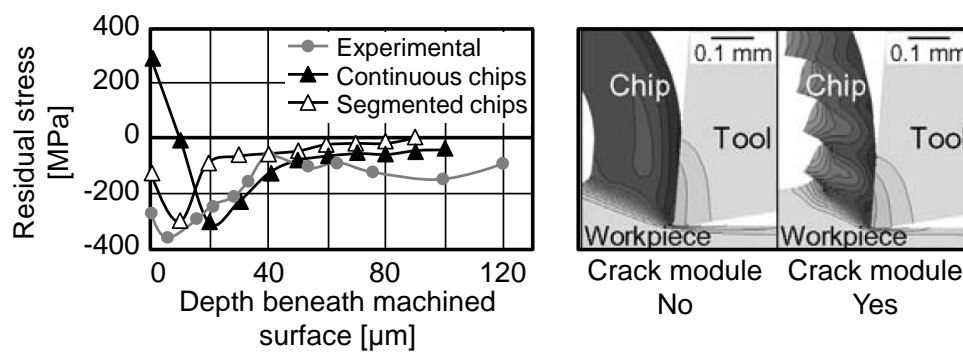
**Figure 3.22.** Finite element model of orthogonal cut including a mathematical proposition for considering the saw tooth chip formation. Adapted from: CHEN, EL-WARDANY and HARRIS (2004)

Compared to peripheral milling, face milling is an operation which creates a more compressive residual stress state. This can be seen in the results of KÖHLER *et al.* (2012) – surface residual stress in face milling is more than three times that from peripheral milling of Ti-6Al-4V. On the other hand, one should consider that it is not trivial to establish parameters for the sake of comparison of distinct machining operations. Once the way by which the cutting edge contacts the workpiece is distinct, so will be the forces, heat generation, and effects on the workpiece.

The more pronounced the cooling effect, the harder will be the surface layer. Once the thermal load is suppressed, the yield strength of the material is not reduced by temperature effects. Therefore cutting forces will be larger, as well as the level of cold work. Experiments demonstrate that, in terms of the lubri-cooling method, surface hardness increases in the following order: dry cutting; MQL; flood cut; high pressure coolant supply; cryogenic cooling

(LN2). The same trend may be true for residual stresses, but studies are needed for validation (CHE-HARON; JAWAID, 2005; KLOCKE *et al.*, 2013; ROTELLA *et al.*, 2014).

Despite this, EZUGWU et. al (2007) came to the conclusion that machining led to surface softening when applying high pressure coolant in turning. The hardness profiles along the depth, however, present significant fluctuation making the comparison rather unreliable. For both dry and MQL machining, some references also indicate surface softening and lower levels of hardness (GITTING; NOUARI, 2009; RAHIM, SASAHARA, 2011). It is possible that such results are associated to indentations very close to the surface and thus excessive yielding of the material (SUN; GUO, 2009).

Regarding the microstructural alterations, THIELE and MELKOTE (1999) reported that for large cutting edge radius there is an increased probability of producing a white transformed layer in steels. Grinding with abusive parameters introduces similar results, both cases because of the high thermal load. For titanium alloys, as discussed before, the development of new microstructures is not common during machining. Some authors reported a change in the volume fractions of α and β phases. Lower thermal dissipation resulted in higher final volume fraction of β phase: from 11% in the unprocessed state to 30% in dry machining, 25% for MQL, and 22% for cryogenic (SUN; GUO, 2009; ROTELLA *et al.*, 2014).

Several other references present the microstructure under the machined surface in order to give an insight into its deformation state. Nevertheless, retrieving quantitative and meaningful information is a challenge, and seldom discussed from a point of view of the functional performance. Even if this were the case, the correlation between microstructural alterations due to machining and fatigue strength of Ti-6Al-4V is not totally established (CHE-HARON, 2001; CHE-HARON; JAWAID, 2005; EZUGWU *et al.*, 2007; GITTING; NOUARI, 2009; RAHIM; SASAHARA, 2011b; SAFARI *et al.*, 2015).

The limited deformation modes of α titanium were shown to influence in the way by which surface grains absorb the plastic strain in machining. Enforcing what was previously exposed, this is likely to induce a heterogeneous residual stress state. This connection, its reflex on the fatigue strength, and the variance in fatigue life, are further gaps which were not studied yet (THOMAS; TURNER; JACKSON, 2010).

Few studies have explored the generation of residual stresses in titanium and heat resistant alloys by MQL. Even considering that cooling effect is almost absent, the improvement of lubrication is capable of reducing the temperatures to the same level of

conventional cooling. In theory, thus, the thermal load is not significantly increased in MQL conditions (RAHIM; SASAHARA, 2011; RAHIM; SASAHARA, 2011b).

## 3.4    Summary

Machining of titanium and its alloys represents many challenges in terms of process performance and final quality of the workpieces. In this context, several methods have been studied in search for a better balance of both factors. Cryogenic cooling, MQL (also termed near-dry machining), compressed air at low temperature and high pressure coolant supply are some examples. Literature references are mainly focused on turning operations, presenting results of tool life, roughness, hardness profile, microstructural alterations and, in some cases, residual stresses.

The impact of alternative lubri-cooling techniques in titanium milling presents some gaps. MQL milling with vegetable oils represents an opportunity because of the combination of reasonable results indicated by literature references and practical feasibility. The combination of reduction in coolant usage, satisfactory wear behavior, as well as machining loads comparable to conventional cooling are the motivations for studying MQL in machining of titanium alloys.

Machining of products for high performance and reliability levels, such as aeronautical structural parts, require further process knowledge. Assessment of workpiece quality must consider the factors that affect fatigue life – primarily residual stresses; also surface hardness – and roughness, because of the significance in terms of process control at the shop floor. Although many references present cross section images of machined surfaces, in most of the cases little information is extracted. Exceptions evaluate the depth of the affected layer, slip systems, and even the strain distribution among the surface grains. The correlation to fatigue strength, however, is not properly established.

The combination of reduction in coolant usage, satisfactory wear behavior, as well as machining loads comparable to conventional cooling are the motivations for studying MQL in machining of titanium alloys. Once the focus is on the potential gains in fatigue life, residual stress is the main surface property to be assessed. From the viewpoint of process control, roughness will also be evaluated, and hardness beneath the surface in order to obtain information on the level of cold work.

# 4 Experimental procedure

The main activities, experiments and methods applied are summarized in the Figure 4.1 as a workflow. Two phases with slightly distinctive objectives can be identified. At the first one, multiple machining experiments were performed for obtaining and comparing the differences in the cutting forces of flood cutting condition to MQL. Cutting parameters referring to finishing and semi-finishing milling conditions were used. This was because most of the final surfaces, even in the simpler parts, are produced by those types of operations. Besides, the cutting force map was used for comparison of the parameters selected for manufacturing the workpieces whose surfaces would be measured.
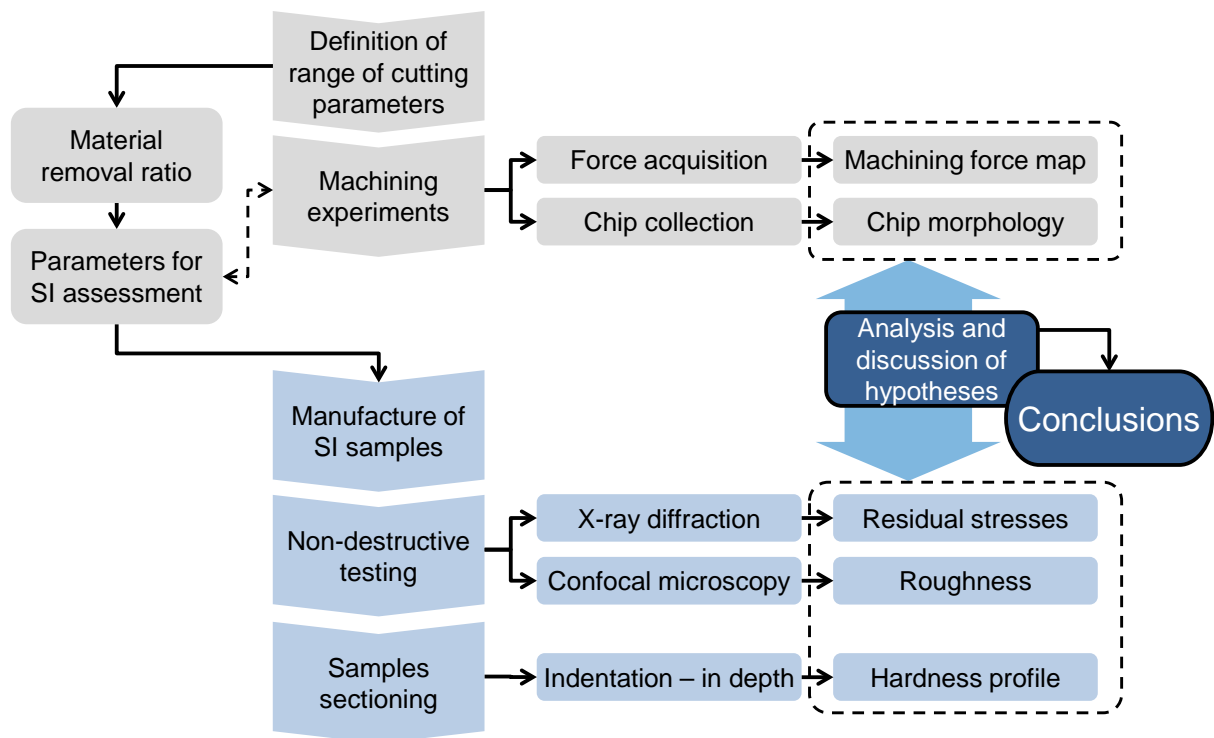


**Figure 4.1.** Workflow of the experiments that were performed.

The second phase is the surface integrity characterization itself, concerning surface residual stresses, hardness and topography / roughness. Fatigue life is mostly affected by residual stresses, while the other parameters give information about the machining process and general quality of the final surface. Besides, roughness is the most common index of surface quality due to the ease of measurement at the shop floor.

It must be highlighted that the present study has mainly conceptual intent and tries to establish guidelines that may be applied to demonstrative workpieces (mock ups based on structural parts) in the future. Therefore simple blocks of 35 x 35 x 50 mm were used both for collecting cutting data and as representative surfaces. They were cut from a Ti-6Al-4V bar of 190x70x50 mm by wire electrical discharge machining. Mechanical properties of the alloy are shown in Table 4.1, as well as the nominal chemical composition of the material. Proportions of the main elements, Ti, Al and V, were confirmed by an EDS (energy-dispersive X-ray spectroscopy) analysis.

**Table 4.1.** Properties and chemical composition of Ti-6Al-4V.

| 0.2% yield strength, MPa | Tensile strength, MPa | Composition, wt% | | | Impurity limits, wt% (max) | | | | |
|---|---|---|---|---|---|---|---|---|---|
| | | Ti | Al | V | N | C | H | Fe | O |
| 830 | 900 | 90.0 | 6.0 | 4.0 | 0.05 | 0.10 | 0.01 | 0.30 | 0.20 |

*Annealed condition; may be solution treated and aged to increase strength.*
Adapted from: (DONACHIE, 2000)

Metallographic analysis of the material in its initial state was done in the three directions to verify the microstructure, shown in Figure 4.2. Grinding and polishing was performed in automated equipment from Allied High Tech Inc. model MetPrep 3, up to 1 μm grit alumina. The microstructure was revealed by using Kroll's reagent (91% H2O, 6% HNO3, 3% HF; volume fractions), and observed in a Tescan scanning electron microscope (SEM), model Vega. A bimodal microstructure can be seen, with equiaxed primary α phase in a lamellar α+β matrix. As discussed in the literature review this microstructure provides balanced properties, so that material may be considered as an alternative for general use.

The microstructure of the base material allows the identification of directions along which the crystallographic planes favored the martensitic transformation. Even so, it is considered that no preferred orientation can be identified, such as what would arise from plastic deformation during cold work. Therefore it was inferred that the influence of prior mechanical processing in the results is limited. Grain size of the equiaxed α and lamellar secondary α phases is shown in Table 4.2. For equiaxed grains, the lengths along the vertical and horizontal were measured for 10 grains, and the average was taken for each direction. In the second case 5 colonies were taken along each direction, the mean length, width and number of intercepts being used to calculate the average size of lamellar grains.
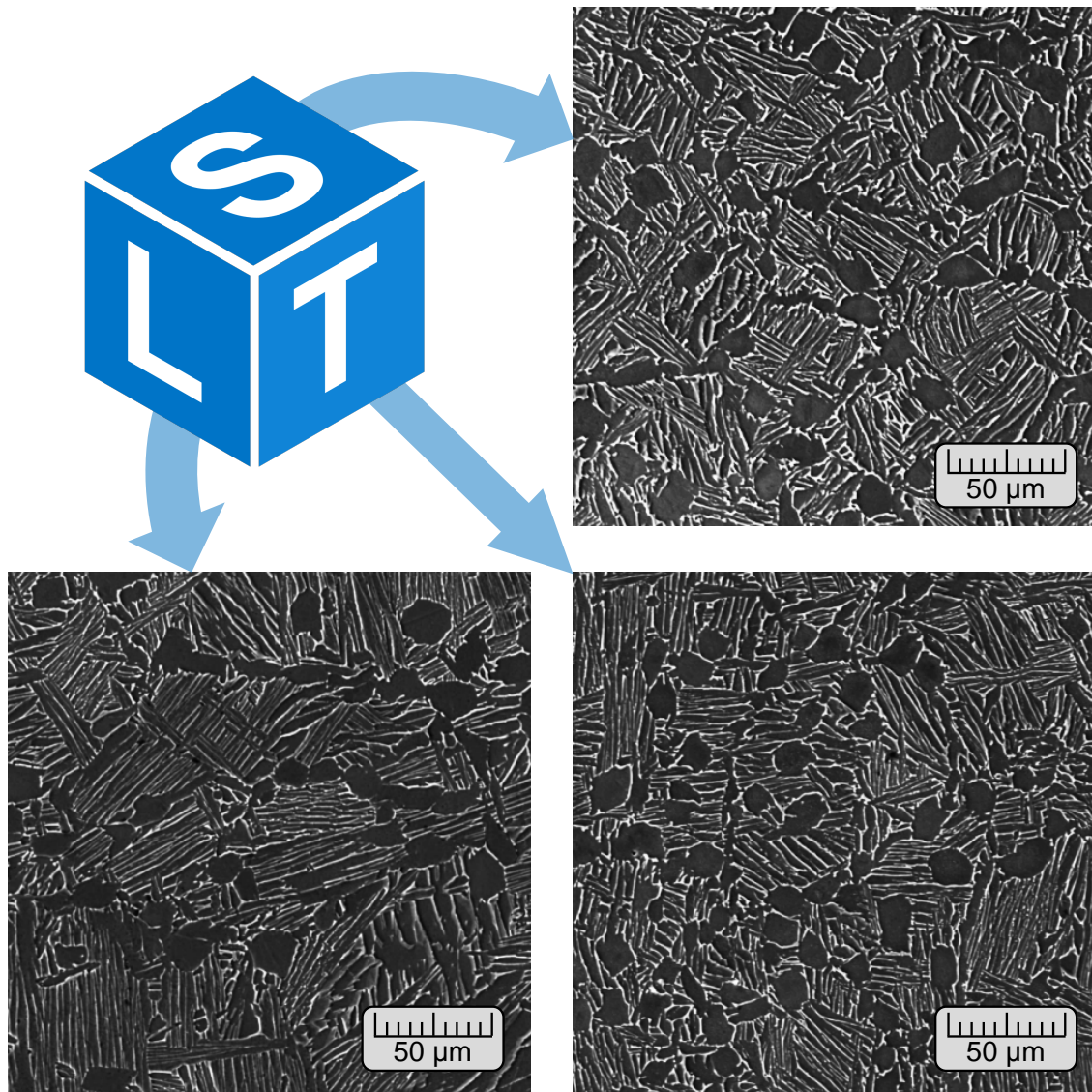
**Figure 4.2.** Microstructure of Ti-6Al-4V in its initial state along the longitudinal direction (L), transversal direction (T) and parallel to the top surface (S). Dark and white regions correspond to alfa and beta phases, respectively.

**Table 4.2.** Grain size of the equiaxed and lamellar phases, at three perpendicular directions.

| Grain morphology | | Grain size [µm] | | | Mean value [µm] | Standard dev. [µm] |
|---|---|---|---|---|---|---|
| | | Longit. | Transversal | Surface | | |
| Equiaxed | | 24.7 | 18.8 | 25.4 | 23.0 | 4.3 |
| Lamellar | Length | 46.6 | 36.2 | 39.0 | 40.6 | 7.81 |
| | Thickness | 2.7 | 2.4 | 2.9 | 2.7 | 0.5 |

Literature references indicate that in machining operations the effects on the surface are hardly perceptible over a distance of 400 μm below the surface (CHE-HARON, 2001; RAHIM; SASAHARA, 2011b; LI; GUO; GUO, 2013). The depth of cut of the current study, on the other side, was at least 625 μm. Therefore it was considered that all the effect generated by prior machining was subsequently removed, and the final surface is a product of the last operation alone.

## 4.1    Evaluation of the milling process of Ti-6Al-4V

At this stage of the experimental work, the titanium blocks were successively machined with distinct cutting parameters. Process forces were measured and chips collected to allow a general characterization of titanium machining. Once the cutting conditions refer to finishing and semi-finishing operations with relatively low material removal rates (MRR), it was possible to obtain a large amount of data with each block. This general idea is shown in Figure 4.3 below.
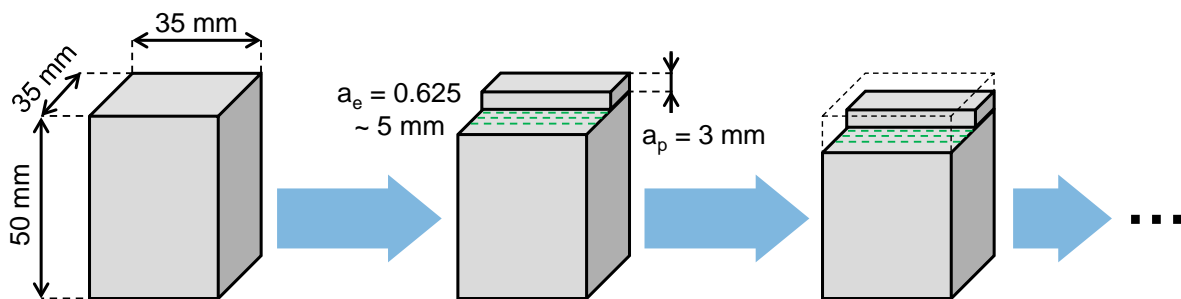


**Figure 4.3.** Representation of the cutting path for obtaining the process forces.

The machining experiments were performed on a Romi D-800 3-axis machining center, spindle power of 15 hp, 12000 RPM of maximum speed and ISO BT-40 tool holder. Peripheral (end) milling was executed with a Sandvik tool R390-025A25-11L, diameter of 25 mm, mounted with two S30T class inserts. This is the manufacturer's first recommendation for titanium milling for its improved toughness provided by the micrograin structure, as well as TiAlN coating applied by physical vapor deposition (PVD) (COROMANT, 2002; KLOCKE, 2011). Despite this recommendation, most of the coating at the cutting edge (and other regions in contact with the chip / workpiece) is quickly removed. Once the operations to

be performed would comprise both finishing and semi-finishing cut, an intermediate tip radius of 1.2 mm was selected. Additionally, a cutting wedge microgeometry for medium operations, in order to avoid excessive weakness. Figure 4.4 depicts the tool and the inserts that were used.



| D$_c$ [mm] | 25.0 |
|---|---|
| l$_2$ [mm] | 120.0 |
| l$_3$ [mm] | 32.0 |
| λ$_s$ [°] | 17.06 |

| R390-11 T3 12E-PM | |
|---|---|
| iW [mm] | 6.8 |
| l$_a$ [mm] | 11.0 |
| b$_s$ [mm] | 0.8 |
| r$_\varepsilon$ [mm] | 1.2 |
| s [mm] | 3.5 |
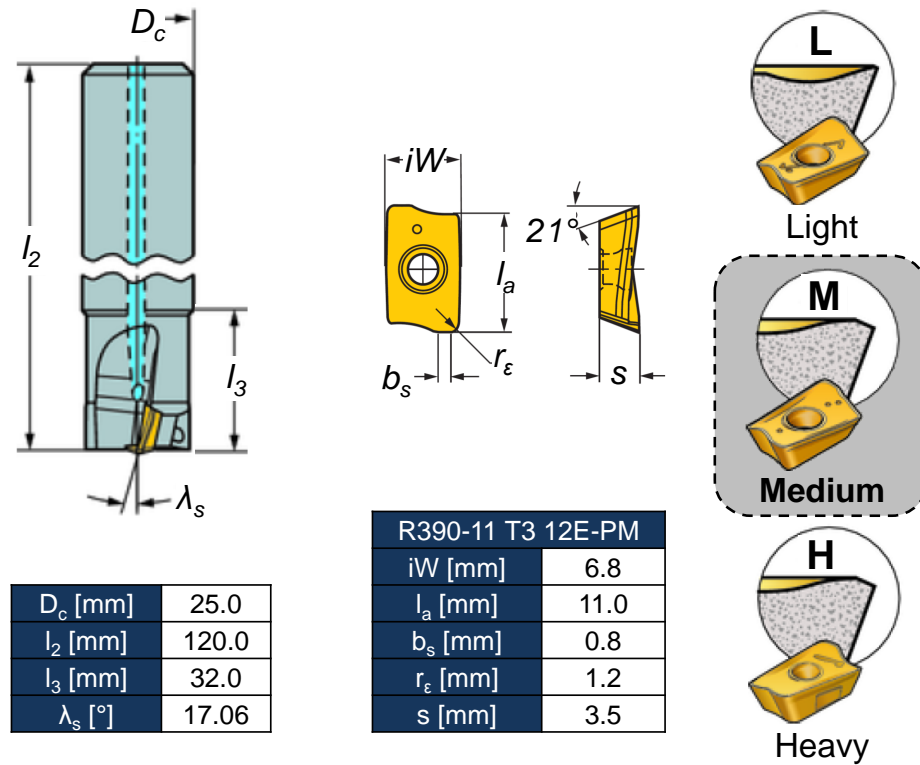
**Figure 4.4.** Details of the tool and inserts that were used in the experiments. Inserts are from S30T class, micrograin cemented carbide, PVD coated with TiAlN (COROMANT, 2002).

Two lubri-coolant techniques were compared: flood cut and MQL. In essence, each one represents a distinct methodology for improving the cutting process. While flood cut is primarily focused on removing the generated heat, MQL sustains that heat generation can be reduced by the strictly controlled application of lubricant. Thus, an emulsion of water-soluble oil and high lubricity vegetable oil were selected as metalworking fluids for the respective techniques.

For flood cut, the internal channels of the tool were used to supply the coolant flow. It is composed by water and semi-synthetic soluble oil Quakercool 7040 BF containing ester-based lubricity additives. The concentration of the emulsion is 8% in volume, and the flow rate of nearly 550 l/h (9.20 l/min).

Concerning MQL, the selected oil was an integral vegetable ester, Iorgalube MQL ESP 30. It was delivered by an external MQL system from Accu-Lube (model 02A0-DMO) that conduces oil and compressed air separately up to the nozzle, were the mixture is finally produced. This avoids the coalescence of large drops, which would have detrimental effects in regard of producing the lubricant layer over the cutting edge. A single nozzle was positioned at nearly 30 mm in front of the tool, thus the lubricant mist was applied mainly over the tool rake face and flank face. Lubricant flow was adjusted to 27 ml/h, pumped at approximately 100 cycles per minute. The compressed air was provided at 6 bar, its flow set up according to the recommendations of the manufacturer for milling operations.

An industrial exhauster 400HX, from the company Air Clean, was used together with the MQL device. It is required for removing and filtering the lubricant mist, reducing environmental and health hazard issues. The equipment is rated for a flow of 2250 $m^3$/min, and used an electric motor of 4 hp.

Force acquisition was done by means of a Kistler piezoelectric dynamometer, Type 9265B. A fixture system, shown in Figure 4.5, was manufactured to hold the workpieces over the base plate. It was composed by a cast iron support, which also provided references for the machine tool setup, and screws that held the workpieces in place. The sample frequency of the acquisition system was set up to 4000 Hz, considerably higher than the tooth passing frequency (29.7 Hz or 38.2 Hz, depending on the cutting condition). Measuring range was configured based on prior trials, respecting the maximum forces along each axis. The software for processing the acquired data was also from Kistler, Dynoware Type 2825D-02.
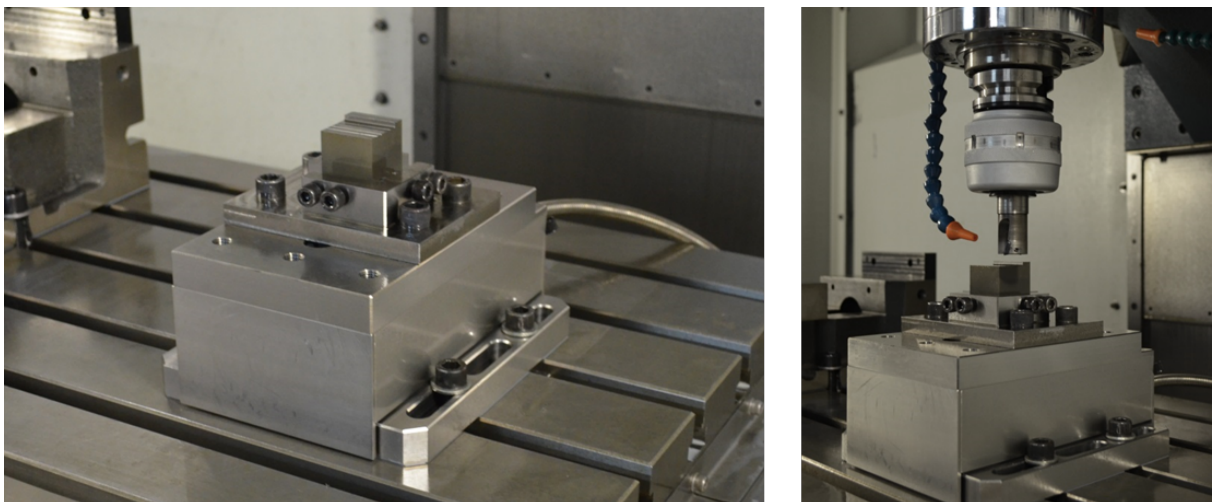


**Figure 4.5.** Dynamometer, cast iron support, and Ti-6Al-4V block mounted over it.

In accordance to what was described, the machining experimental setup is shown in Figure 4.6, with the MQL system.



**Figure 4.6.** Experimental setup for the machining experiments. (a) Accu-Lube MQL equipment; (b) machine tool with the MQL device and dynamometer installed; (c) close view of the tool, MQL nozzle, sample and its support over the dynamometer.

The cutting parameters were selected respecting the general practice for finishing and semi-finishing operations, as well as recommendations from the tool manufacturer. They are presented on Table 4.3, with the chosen levels (values). Radial depth of cut and feed were varied in four levels each one. The axial depth of cut, on the other side, was kept constant for all the tests. This decision is justified by the fact that its effect on cutting force is linear. Besides this, scallops and marks will be present on the surface in the direction of axial depth only when the workpiece is significantly tall, and several steps are necessary.

**Table 4.3.** Cutting parameters and levels that were selected for the machining experiments. $a_p$ - axial depth of cut; $a_e$ – radial depth of cut; $f_z$ – feed per tooth; $v_c$ – cutting speed.

| $a_p$ [mm] | $a_e$ [mm]; [% $D_{Tool}$] | $f_z$ [mm/tooth] | $v_c$ [m/min] | Lubri-cooling technique |
|---|---|---|---|---|
| 3.0 | 0.625; 2.5% | 0.075 | 70.0 | Flood cut |
| | 1.250; 5.0% | 0.100 | | |
| | 2.500; 10% | 0.125 | 90.0 | MQL |
| | 5.000; 20% | 0.150 | | |

Cutting speeds for titanium alloys are generally restricted by excessive tool wear. As pointed out before, this is a direct result of very large thermal loads and heat concentration at the cutting edge. Thus cutting speed was varied in just two levels: one recommendation from the manufacturer, and other slightly larger, similar to values that are found at other studies.

For statistical significance, all the experiments were repeated three times. Besides this, to reduce systematic errors, they were performed in random order. Tool wear was not considered a variable, but once it may have a large influence on cutting forces and chip formation mechanism, it was monitored. After a certain amount of material was removed, the primary and secondary cutting edges were observed on a Wild M3C stereoscope. Tool chipping, breakage and any other harsh damage led to immediate change of inserts; flank wear was considered acceptable up to VB = 0.4 mm.

The machining force was calculated as the vectorial sum of "x" and "y" components measured by the dynamometer. Then the moving average was obtained, in order to partially filter the measurement noise. Figure 4.7 shows a comparison of this method with the calculation considering also the "z" component. It can be seen that it does not introduce significant difference in the results, since its value is much smaller than the other components. Correlations with the cutting parameters and lubri-cooling method were made taking the average of ten subsequent force peaks, so that values presented in the results chapter are peak forces.
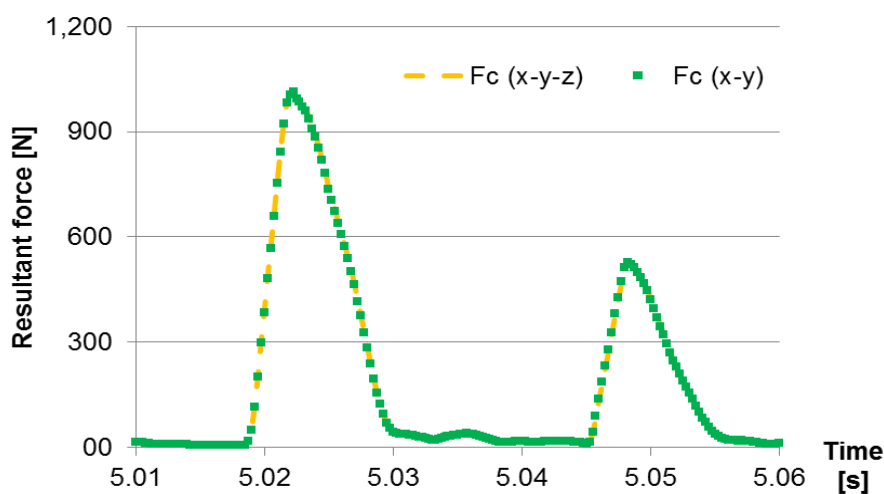


**Figure 4.7.** Comparison of machining force calculation considering x-y-z and only x-y components.

Chips of the limit conditions were collected and evaluated by SEM. Analysis and comparison of morphologies are capable of providing an insight into the differences of thermal loads and heat dissipation. The equipment is the same that was used to characterize the microstructure of the base material. Before obtaining the images, chips were cleaned in an ultrasonic device, Branson 5510, in order to remove oil and particles. Then they were positioned for SEM observation, trying to expose the lateral profile and the curved shape.

## 4.2 Surface integrity assessment

This stage of the experimental work corresponds to the manufacture of surface with selected parameters and measurement of their characteristics. As shown before, certain properties have strong influence on the functional requirements of titanium parts for aerospace structural applications. The main idea developed here was the evaluation of two conditions corresponding to finishing machining, and two semi-finishing operations. These categories of operations are distinguished by the radial depth of cut. Both the lubri-cooling conditions studied before were applied, namely flood cut and MQL, resulting in eight samples. Cutting parameters for the "testing pairs" were chosen among the ones that were tested in the first phase. The criteria were that both should have similar material removal rates, as calculated by Equation (4), and different cutting speeds. If significant differences are detected between those surfaces, then machining parameters can be defined to improve the general quality without decreasing the productivity. In Equation (4), Q is the material removal rate; $a_p$ the axial depth of cut; $a_e$ the radial depth of cut; $v_c$ the cutting speed; $f_z$ the feed per tooth; z the number of teeth of the tool; and $D_o$ the diameter of the tool.

$$Q = \frac{a_p \cdot a_e \cdot v_c \cdot f_z \cdot z}{\pi D_o} \tag{4}$$

Table 4.4 presents the identification code of the SI samples, their cutting conditions and machining forces obtained in the first phase. Each block was used for the analysis of two surfaces manufactured in opposite sides. The workpieces are thick enough so that when machining one of the surfaces, the other side is not affected.

**Table 4.4.** Samples for surface integrity assessment and respective manufacturing parameters.
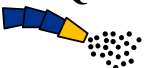
| Surface code | $v_c$ [m/min] | $a_e$ [mm] | $f_z$ [mm/tooth] | Q [cm³/min] | $F_c$ [N] | Lubri-cooling strategy |
|---|---|---|---|---|---|---|
| SI-01 | 70.0 | 0.625 | 0.150 | 0.501 | 496.4 | |
| SI-02 | 90.0 | 1.250 | 0.075 | 0.645 | 414.6 | **Flood cut** |
| SI-03 | 70.0 | 2.500 | 0.150 | 2.005 | 817.1 | |
| SI-04 | 90.0 | 5.000 | 0.075 | 2.578 | 692.7 | |
| SM-01 | 70.0 | 0.625 | 0.150 | 0.501 | 429.9 | |
| SM-02 | 90.0 | 1.250 | 0.075 | 0.645 | 374.8 | **MQL** |
| SM-03 | 70.0 | 2.500 | 0.150 | 2.005 | 728.2 | |
| SM-04 | 90.0 | 5.000 | 0.075 | 2.578 | 598.8 | |

Figure 4.8 presents a schematic view of the workpiece, main directions, and positioning for the subsequent surface measurements.
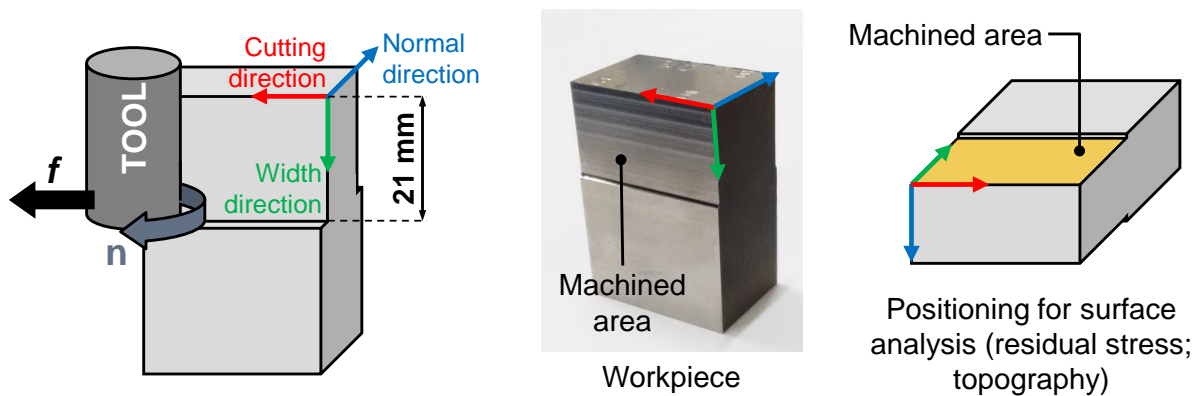


**Figure 4.8.** Schematic view of main directions and position for surface analysis.

Surface residual stresses were measured by the X-ray diffraction (XRD) $Sin^2\psi$ technique. The principle of residual stress measurement by XRD is Bragg's law (Equation 5), schematized in Figure 4.9, which correlates the wavelength ($\lambda$) of a radiation beam with the incidence angle ($\theta$) such that scattered rays manifest constructive interference. This angle is related to the distance between sets of densely packed planes ($d$), so that very specific angles result in diffraction.

$$\lambda = 2 \cdot d \cdot \sin\theta \tag{5}$$
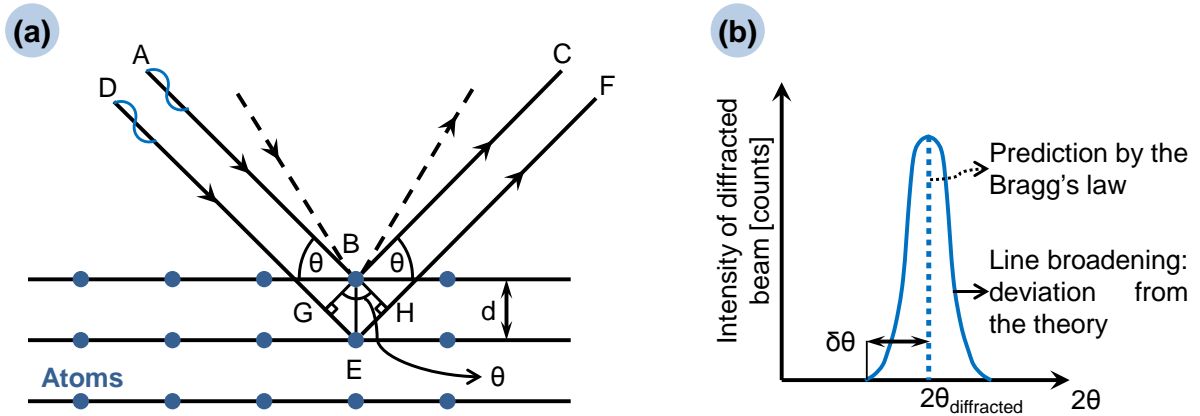
**Figure 4.9.** (a) Diffraction phenomena in crystallography: for a given wavelength, there are incidence angles corresponding to reflections (from different sets of planes) that will result in constructive interference. (b) In practice, diffracted signal is "broadened" because of deviations of the interplanar distance, defocusing etc. Adapted from: (NOYAN; COHEN, 1987).

When the material is subjected to elastic stress, the distance between the planes changes and this is related to the diffraction angle if a specific wavelength is used (in other words, monochromatic radiation). Therefore, by tracking this angular variation it is possible to obtain the residual stress by means of equations also considering the elastic properties of the material. More details are shown in Figure 4.10 and described below. Normally the term $2\theta$ is used in the equations; it is the angle between the extension of the incident beam and the diffracted beam (CULLITY, 1954; PREVEY, 1977; NOYAN; COHEN, 1987).
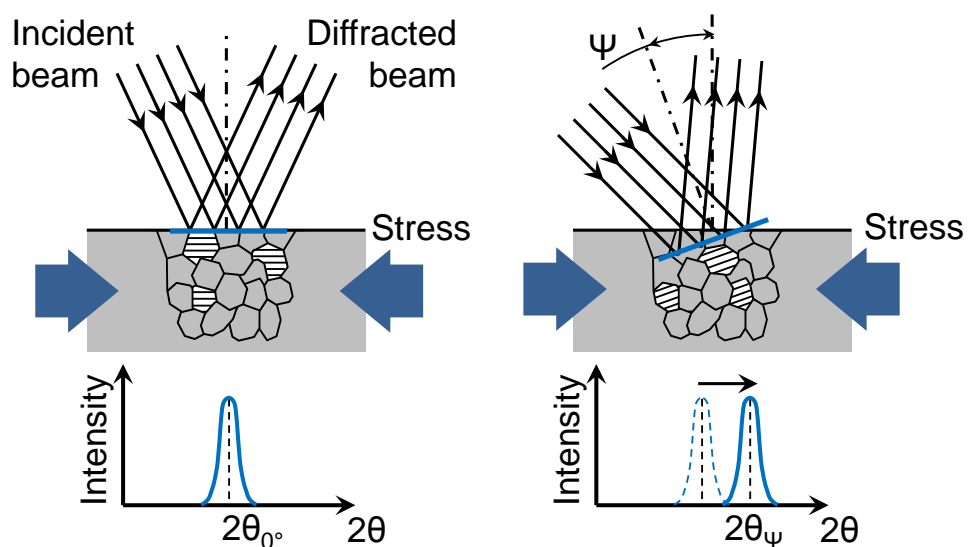


**Figure 4.10.** Residual stress measurement using X-ray diffraction. A specific set of planes is scanned, locating the $2\theta$ peak position along several tilt angles $\psi$. This change of peak position is then used in equations. Adapted from: (NOYAN; COHEN, 1987).

The incident beam is diffracted by the planes parallel to the sample's surface. If the material is in compression, these planes are further apart because of Poison's ratio. The interplanar distance is obtained from the peak intensity versus scattering angle 2θ and Bragg's law λ=2.d.sinθ. When the specimen is tilted (equivalent to tilting both the incident and diffracted beams), diffraction occurs from another grains, but from the same crystallographic planes. Once these are more nearly perpendicular to the stress, they are less separated than in the other case and at higher angles 2θ. The rate of change in 2θ with respect to the tilt angle ψ is used in the calculation of residual stresses.

In the present experiments residual stresses were measured in equipment from PANalytical, model Empyream. Cu Kα$_1$ radiation with wavelength of 0.15405 nm was used with a voltage of 45 kV, 40 mA current, and point focus mode. For titanium and its alloys, references recommend the {213} diffraction plane, at 2θ equal to 141° CULLITY, 1954; NOYAN; COHEN, 1987; HAUK, 1997). In the incident beam path, a crossed slits collimator (CSC) was mounted. It works as both a mask and a divergence slit, with variable apertures that can be set to irradiate a definite area. In the diffracted beam path, a parallel plate collimator (PPC) with 0.27° of equatorial acceptance and a V β-filter were applied. Thus the diffracted beam reaching the detector is conditioned and quasi-parallel. This makes the residual stress measurement less sensible to vertical displacements and sample height positioning.

For each surface, three areas were selected for measurement in the cutting direction, in order to evaluate the homogeneity of the residual stresses. As can be seen in Figure 4.11, they are shifted laterally by about 6.5 mm, but centered along the longitudinal tool path. The CSC mask was set with a 1.75 mm aperture, and the divergence slit, 0.35 mm. Irradiated area depends on the 2θ and the tilt angle (ψ), as show in the Figure 4.11. The values that were selected to the apertures ensure that measured areas are not superposed, and then the stress homogeneity at the surface can also be evaluated.

Both positive and negative values of tilt angles were considered, from ψ = 0° to ψ = ±45° and Sin$^2$ψ step size of 0.1. Measuring range was set equal to 7.2°, around three times the FWHM (full width half maximum), mostly because of measuring time; the 2θ step size is 0.18°, and exposure time 12.0 s.
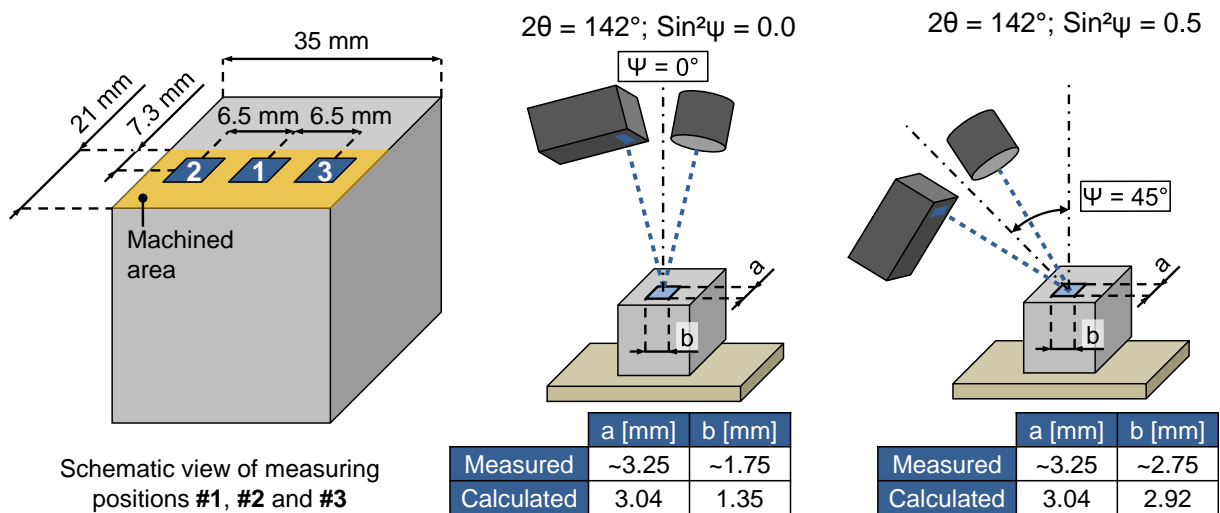
**Figure 4.11.** Residual stress measurement positions; incident area for tilt angle equal to zero; and incident area for limiting tilt angle.

Data was analyzed using PANalytical's software Stress. It makes possible to select among several techniques for peak location, to apply a background correction and Lorentz polarization factor, as well as removing a large part of the undesired Kα2 wavelength. Diffracted curves presented significant measurement noise, which adversely affected the analysis of the data. In order to mitigate this issue, a Pearson VII function was used for profile fitting. In some cases fitting was poor, what could be verified by the parameter "R", a percentage expressing the amount of error. Above 13%, the fitting was considered inadequate and the peak position was discarded from the analysis. No background correction was applied prior to curve fitting because this would make measurement noise even more evident when compared to the peak intensity. Instead, background level and slope were computed together with the profile fitting. Material properties for calculating the residual stress were retrieved from literature (PREVEY, 1977).

Topography of the surface was evaluated by means of a Cyber CT-100 non-contact profilometer - more specifically, a chromatic aberration confocal microscope. An area of 5.6 x 5.0 mm was analyzed for each surface. According to the calculation method of the equipment, this would be equivalent to a cutoff length of 0.8 mm, a value that is usually adopted in the context of machined surfaces. The measurement step was set as 5 μm, enabling quick acquisition while maintaining the precision. With the acquired data, it is possible to obtain the standard roughness parameters in the longitudinal and transversal directions to the tool path. Hybrid and area parameters can also be extracted, depending on the functional requirement

that is being studied. For the present work, Ra, Rz, Rq were selected once they are frequently used parameters for production control at the shop floor. Their values were taken as the average of 5 measurements, along several measurement lines as represented in Figure 4.12.

It is important to highlight that roughness results obtained here may not be directly comparable to values from standard rugosimeters. This is due the fact that the measurement principles are rather distinct: rugosimeters make use of a round probe in contact with the surface, while the equipment used here scans the surface by means of a light beam. Although prior experiments have shown that results are similar, in the strict sense the data obtained here cannot be referred as the roughness according to the standards.
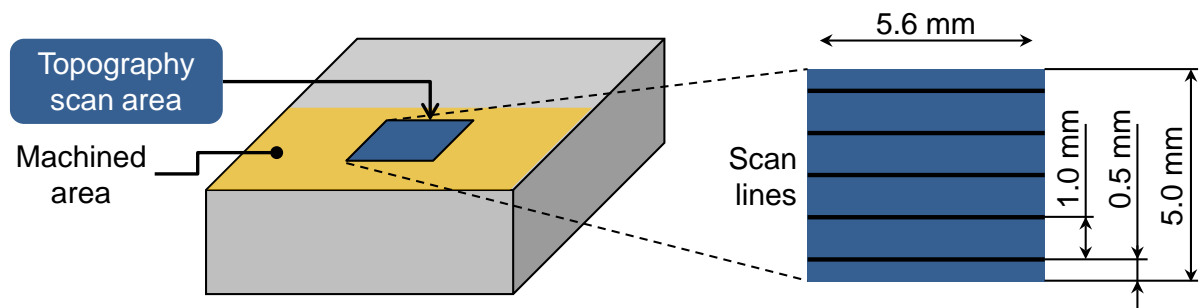


**Figure 4.12.** Area and profiles for roughness measurement.

As it was exposed in the literature review, from the viewpoint of fatigue life of titanium parts, the influence of roughness is seldom significant. In this study, roughness was measured because of two reasons: (1) in order to maintain coherence with literature references; (2) it is the most common process control parameter.

Further characterization of the material - analysis of hardness profile along the depth - required destructive procedures. This was made carefully to avoid any mechanical or microstructural modification induced by sample preparation. The workpieces were sectioned by abrasive disc cut, with abundant flow of coolant and light pressure, and mounted in Bakelite. Figure 4.13 describes the cutting steps used to expose the depth profile of the machined surface. Then grinding up to grit 400 abrasive was performed.
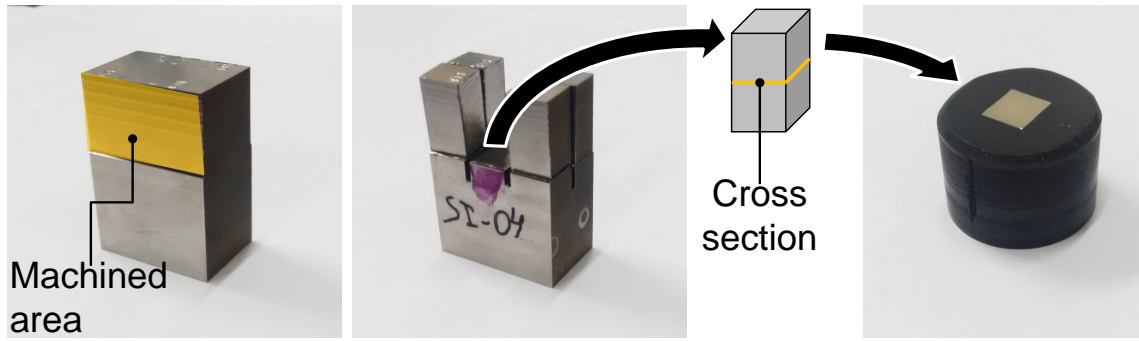
**Figure 4.13.** Sample sectioning for hardness measurement beneath the machined surface.

The micro indentations require a surface that is polished and free of risks. The procedure that was adopted here was an electrolytic polishing step, performed in Buehler ElectroMet 4 equipment. A solution composed of 95% of acetic acid and 5% of perchloric acid, volume fraction, was used (VANDER VOORT, 1999). In order to establish electrical contact the Bakelite mount of the samples was drilled, allowing a copper pin to be positioned right over the material. Polishing parameters were 40 V and 30 s. With this procedure most of the risks were removed, but it also etched the surface, so that a final mechanical polishing step was necessary. In the same equipment from Allied High Tech Inc., 1 μm grit alumina had been applied, polishing force of 13 N, for at least 15 min.

Hardness measurements were made with Vickers indenter and load of 50 g, in equipment from Emco-Test, DuraScan 70. In the finishing conditions, S*-01 and S*-02, data was collected at every 50 μm, up to a depth of 500 μm. For S*-03 and S*-04, it was necessary to measure up to 700 μm, where the hardness value was then stable and equal to the bulk material. For each depth, 9 indentations were made, and values that were different by more than 10% of the mean were discarded.

# 5   Results and discussion

Herein the results obtained by the experimental procedure described in the previous chapter will be exposed. Discussions, comments and remarks are going to be presented concomitantly with them. Surface integrity results will be presented for each parameter separately, with the appropriate comparisons to the cutting conditions.

## 5.1   Machining forces and chip morphology

For all the cutting conditions, chip formation with localized shear was observed. As discussed in the literature review, this phenomenon is typical especially considering titanium and its alloys. Figure 5.1 shows the saw-tooth form and details at two regions. Once at the borders of the chip there is less restriction to plastic deformation, they often become irregular. Segmented chips are undesired because they are usually associated with instability in the cutting process and cutting force oscillation. When machining titanium, however, this is almost inevitable (KOMANDURI; HOU, 2002).
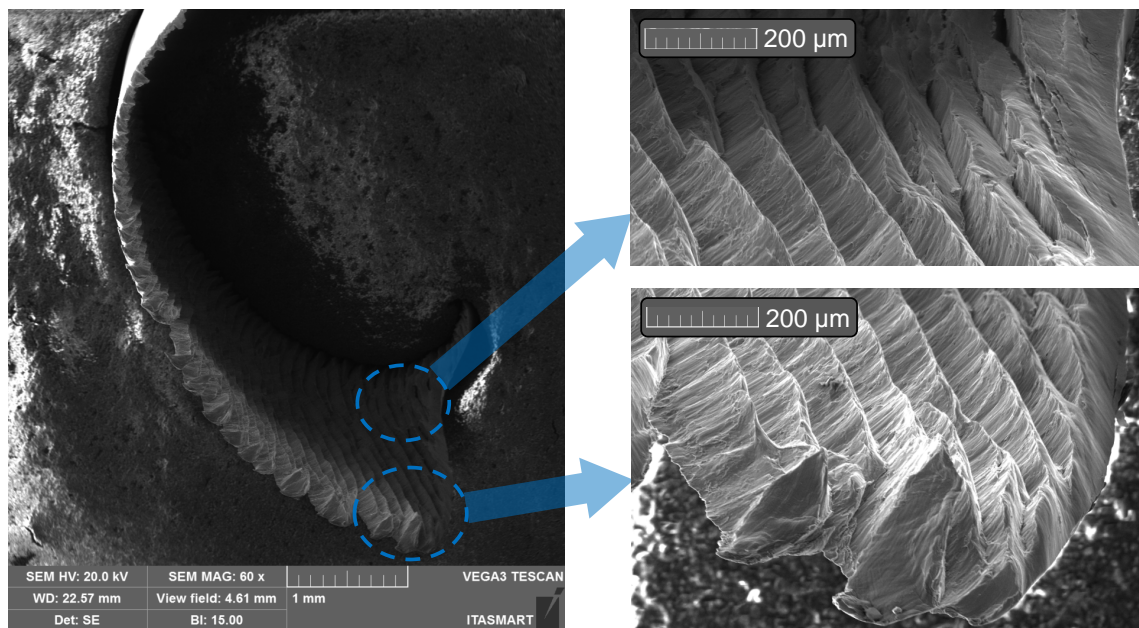


**Figure 5.1.** Aspect of a chip produced in machining of titanium. On the right side, with a greater magnification, the segments are clearly visible.

A further aspect of the saw-tooth chip formation can be noted by an observation from another angle, pointing towards the free surface. This allows a better visualization of the valleys that are formed in between the segments. From this upper angle gaps can be seen, as depicted in Figure 5.2 with several magnifications. This is evidence that the chip segments are not entirely connected, although it was not possible to measure the depth of such gaps. Two hypotheses may be associated with their formation:

- Crack propagation starting from the free surface of the chip (NAKAYAMA, 1974; VYAS and SHAW, 1999);

- Chip formation associated with a bending moment that curves the chip segment around the shear band that is active at the moment (KOMANDURI; VON TURKOVICH, 1981; KOMANDURI; HOU, 2002; ASTAKHOV, 2006).
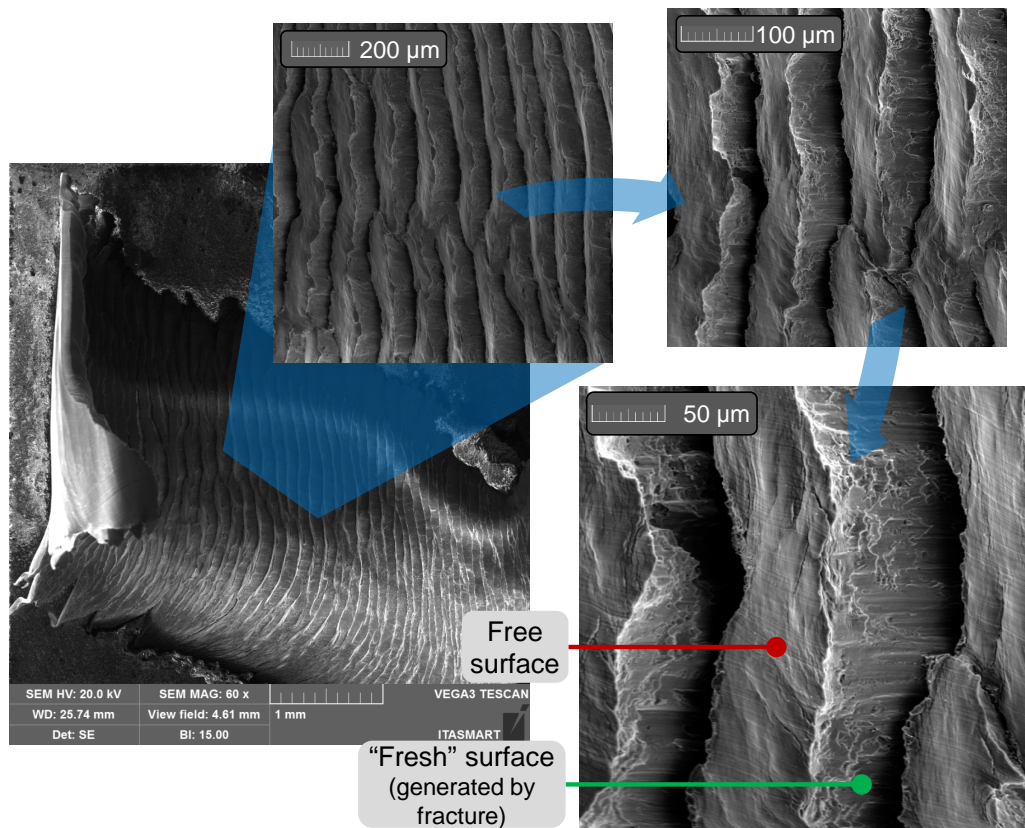


**Figure 5.2.** Free surface of a typical chip produced when machining titanium and titanium alloys. The subsequent magnifications show that in between the segments there is a gap.

Verification of cracks in between the chip segments would be further evidence to the theory developed by NAKAYAMA (1974), as described by ASTAKHOV (2006), and VYAS and SHAW (1999). The challenging issue is precisely the identification of whether or not

there is a crack propagation process starting from the free surface. The micrographs of both chips and shear zone obtained by interrupted cut presented by VYAS and SHAW (1999), for example, do not allow one to clearly identify such cracks. This statement is also supported by ASTAKHOV (2006).

ZHANG *et al.* (2013) observed chips with a free surface aspect similar to the ones shown here when machining Inconel 718. The theory of crack propagation was once again claimed, but cross section micrographs of the chips are rather inconclusive. GUO, COMPTON and CHANDRASEKAR (2015), on the other side, have shown images with visible cracks. Their conclusions might not be directly applicable to machining operations because of the very low cutting speeds and tool rake angles that were used. Finally, a recent study made by Shashikant JOSHI, TEWARI and Suhas JOSHI (2013) provided images of titanium chips suggesting that a discontinuities exist between the segments, but without discussing the mechanisms involved to originate them.

There are other remarkable details in the presented images of the chips, which are highlighted in the Figure 5.3. The sides of the segments corresponding to the free surface, generated by the previous cut, preserve both the machining marks and flat shapes. On the contrary, the opposite sides (named as "fresh" surface in the previous figure) have rough aspect, and their connections to the free surfaces form sharp edges. In some cases several other cracks can be observed in the boundaries, as in the right part of the figure.
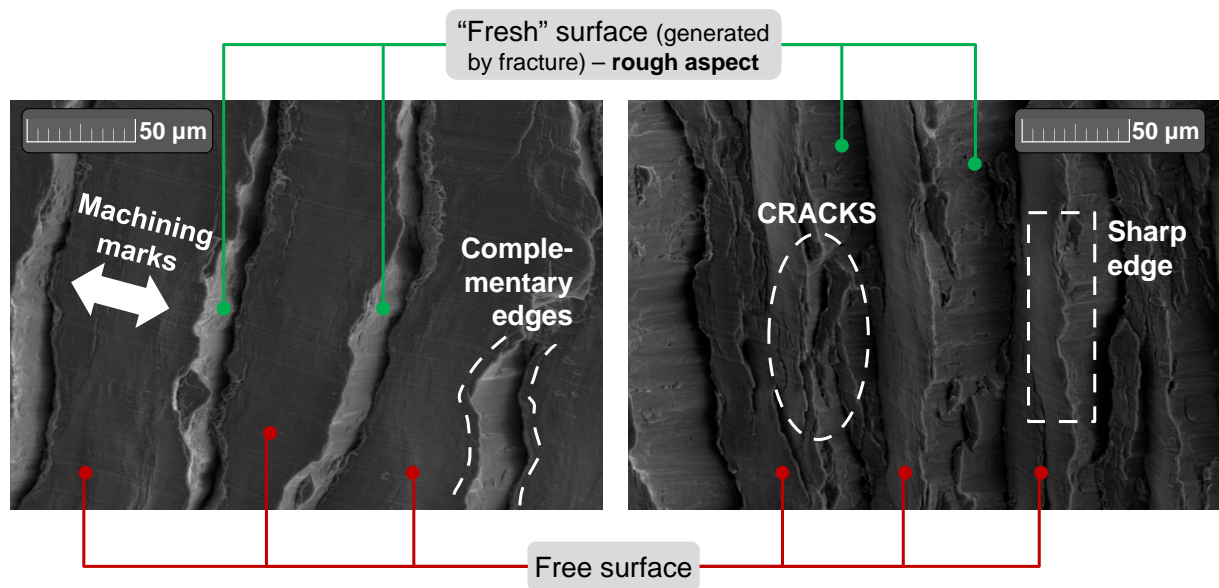


**Figure 5.3.** Aspects of the saw-tooth chip produced in machining titanium.

According to the mechanism described by NAKAYAMA (1974), as referred by VYAS and SHAW (1999), such feature results from the stress state when the resultant cutting force is parallel to the free surface, shown in Figure 5.4. This group of characteristics cannot be generated by a process involving uniquely unconstrained plastic deformation in the level that is required by the shear banding theory. If no fracture had occurred, then both sides of each segment should have precisely the same aspect. Thus crack generation and propagation must take place at some level. It is possible that both mechanisms act in order to produce segmented chips, the relative importance of each one depending on the properties of the material and the range of cutting parameters.
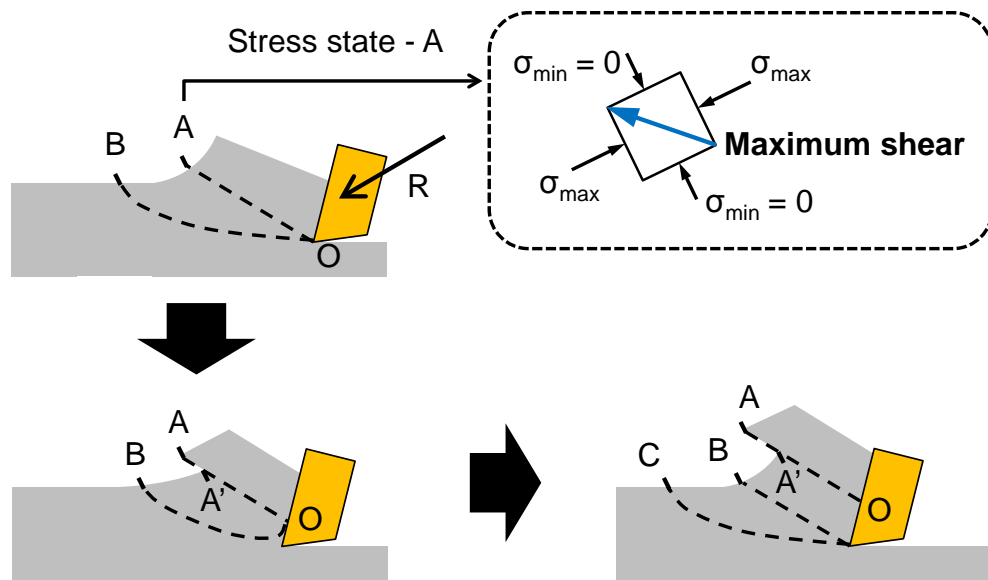


**Figure 5.4.** Mechanism of saw-tooth chip formation. When the cutting force is parallel to the free surface at point A, it is developed a stress state with maximum shear. This originates a crack, and the chip segment slides along AO. At the same time the tool tip further penetrates into the material, which slides over the rake face. When the segment A'B becomes parallel to the resultant cutting force, the cycle is restarted. Adapted from: (VYAS; SHAW, 1999).

To extract additional information, the cross section of the chips should be analyzed. A suggestion is to evaluate the texture of the material at two regions, each one located at one side of the zone where it is assumed that crack propagates. Because of the lack of restrictions imposed by the crack, it is possible that texture patterns would develop.

A first insight into the differences of the cutting process using large amounts of coolant and MQL is given by analyzing the produced chips. By observing the curvature of

chips produced by the same cutting conditions, it is possible to infer which lubri-cooling method led to higher temperatures. Figure 5.5 depicts the chips of the limit conditions that were tested, with the smaller value of radial depth of cut, and the respective cutting parameters.



| $a_e$ = 0.625 mm | | $f_z$ [mm/tooth] | |
|---|---|---|---|
| | | 0.075 | 0.150 |
| $V_c$ [m/min] | 70 | 1 | 7 |
| | 90 | 2 | 8 |
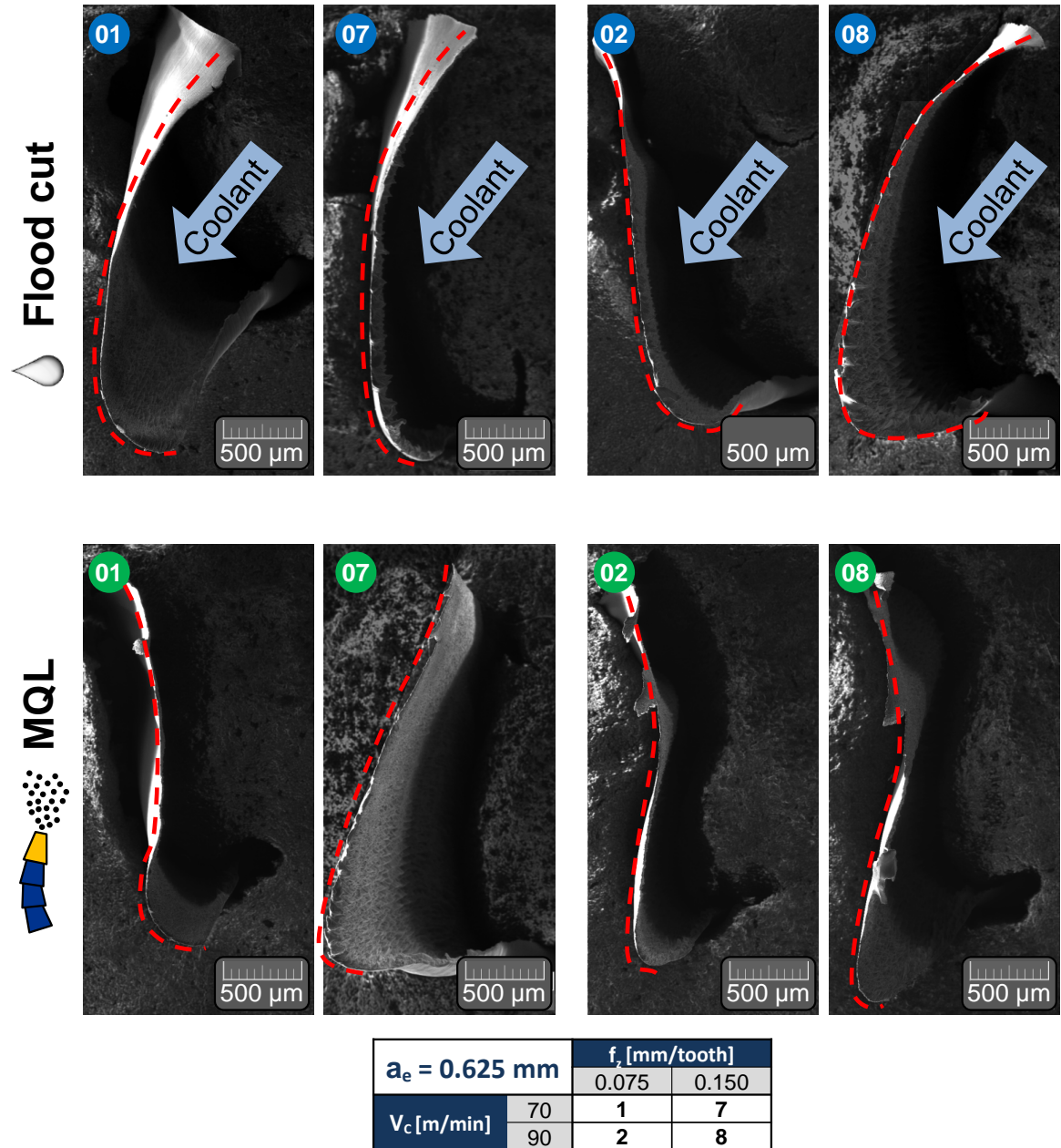
**Figure 5.5.** Chips produced in the limiting conditions, for the minimum radial depth of cut.

One trend is remarkable: chips produced in flood cut conditions are curved towards the free surface. When using MQL, they tend to assume a shape that is curved to the opposite side. The distinct curvatures can be associated with the way by which heat is removed from the cutting process.

In flood cut, the coolant is applied in the whole cutting zone, but it cannot penetrate in between the chip and the tool, as stated before. Heat that is generated in the process is transferred to the cutting fluid through the free surface, therefore establishing a thermal gradient along the thickness of the chip. Once the free surface is at a lower temperature, it contracts and causes the chip to bend.

The mist generated by MQL, in contrast, has very limited heat removal ability. Heat is transferred from the chip mostly to the tool, a process that also occurs in flood cut. In this case, the difference is that heat transfer through the free surface is only due to convection with air. The thermal gradient along the thickness presents a higher temperature at the free surface, and the bending action is the opposite that was described for flood cut.

With the largest radial depth of cut ($a_e$ = 5.0 mm), the same trend is observed. Chips produced in flood cut assume a more curved shape. This is shown in Figure 5.6.
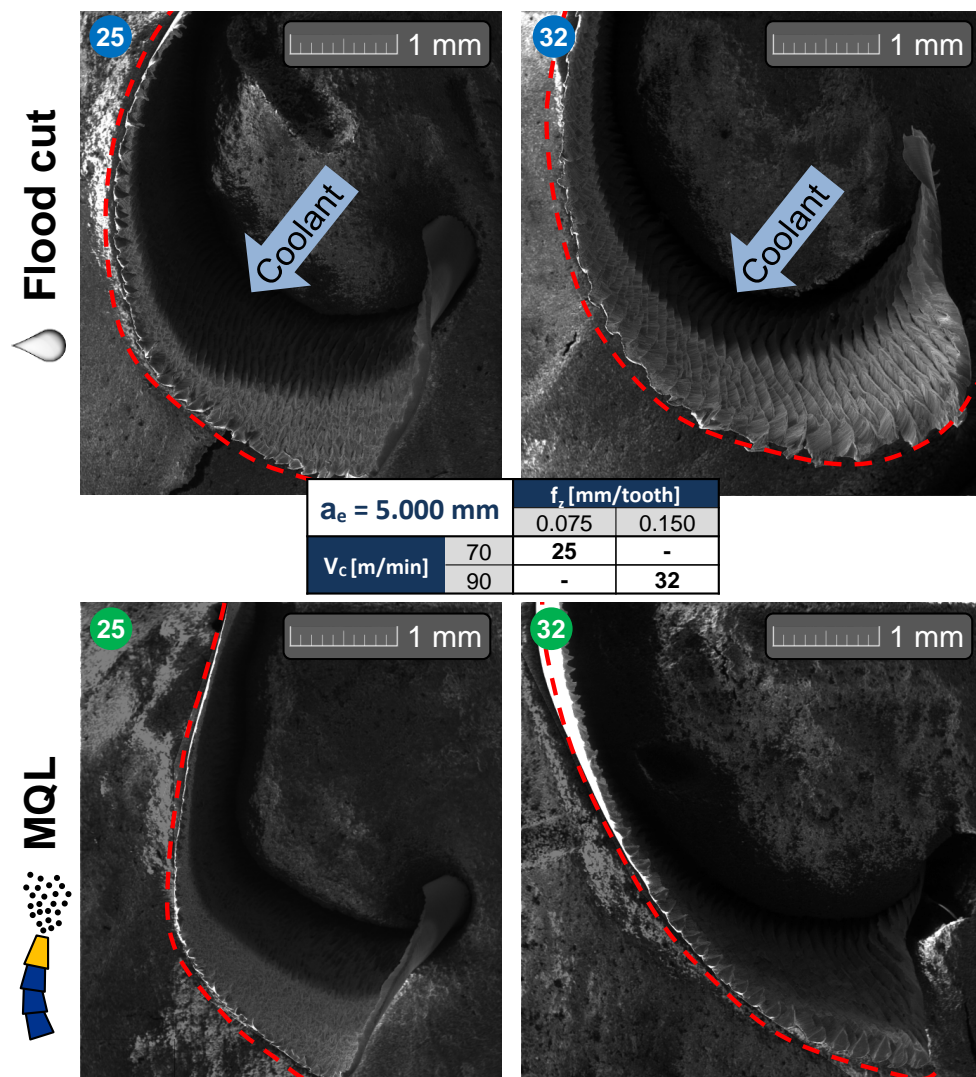


**Figure 5.6.** Chips produced by the conditions with the largest radial depth of cut.

Results of the machining experiments are exhibited in Figure 5.7, the means of the three trials, for each test condition. Standard deviation of the different trials was around 2% for flood cut conditions, and 5% for MQL. The forces that are measured by the dynamometer are not precisely the cutting force. This is because it acquires the sum of all loads acting on the workpiece: cutting force, friction force on the rake face and friction force on the flank face. Representation of the resultant along the three coordinate axes does not allow separation of these components, unless specific procedures for obtaining friction forces are applied. Even so, prediction of the friction force in the secondary shear zone usually is not precise. The term that will be adopted here is machining force, referring to the vectorial sum of the significant components measured by the dynamometer ("x" and "y" components).

**Machining force [N] - Flood cut**

| $v_c = 70$ m/min | | $f_z$ [mm/tooth] | | | |
|---|---|---|---|---|---|
| | | 0.075 | 0.100 | 0.125 | 0.150 |
| | 0.625 | 354 | 402 | 451 | 496 |
| $a_e$ | 1.250 | 452 | 532 | 594 | 626 |
| [mm] | 2.500 | 589 | 670 | 764 | 817 |
| | 5.000 | 683 | 834 | 932 | 1012 |

| $v_c = 90$ m/min | | $f_z$ [mm/tooth] | | | |
|---|---|---|---|---|---|
| | | 0.075 | 0.100 | 0.125 | 0.150 |
| | 0.625 | 313 | 352 | 402 | 446 |
| $a_e$ | 1.250 | 415 | 483 | 551 | 608 |
| [mm] | 2.500 | 552 | 636 | 717 | 775 |
| | 5.000 | 693 | 784 | 881 | 996 |

**Machining force [N] - MQL**

| $v_c = 70$ m/min | | $f_z$ [mm/tooth] | | | |
|---|---|---|---|---|---|
| | | 0.075 | 0.100 | 0.125 | 0.150 |
| | 0.625 | 322 | 368 | 393 | 430 |
| $a_e$ | 1.250 | 427 | 482 | 523 | 581 |
| [mm] | 2.500 | 487 | 610 | 669 | 728 |
| | 5.000 | 654 | 739 | 825 | 883 |

| $v_c = 90$ m/min | | $f_z$ [mm/tooth] | | | |
|---|---|---|---|---|---|
| | | 0.075 | 0.100 | 0.125 | 0.150 |
| | 0.625 | 281 | 323 | 351 | 399 |
| $a_e$ | 1.250 | 375 | 437 | 478 | 539 |
| [mm] | 2.500 | 477 | 563 | 629 | 717 |
| | 5.000 | 599 | 733 | 813 | 835 |

**Figure 5.7.** Mean values of the machining forces for all the tested conditions.

Evaluating absolute values, it is stated that peak forces in MQL machining are 11% lower than in flood cut, on average. Once again, two hypotheses may be stated to clarify this difference:

- Thermal softening due to heat generation and consequent temperature increase in the primary shear zone;
- Superior lubricating action of the mist applied by MQL substantially reduced the friction forces at the sliding interfaces.

It can be inferred, based on the previous discussion on the chip shape, that thermal softening is the responsible for lower machining forces. It does not mean that MQL is not

significant in reducing friction, but chip curvature points out to the development of higher temperatures as compared to machining with flood of coolant.

Influence of each cutting parameter on the machining force becomes clearer with a plot of the main influences. It is displayed in Figure 5.8, obtained from a factorial analysis. All the cutting parameters have the expected influence: both the feed and the radial depth of cut are related to chip thickness, and thus affect directly the machining force. The cutting speed is directly related to heat generation. Because of the reduction of mechanical strength with temperature, cutting speed is inversely related to the machining force.
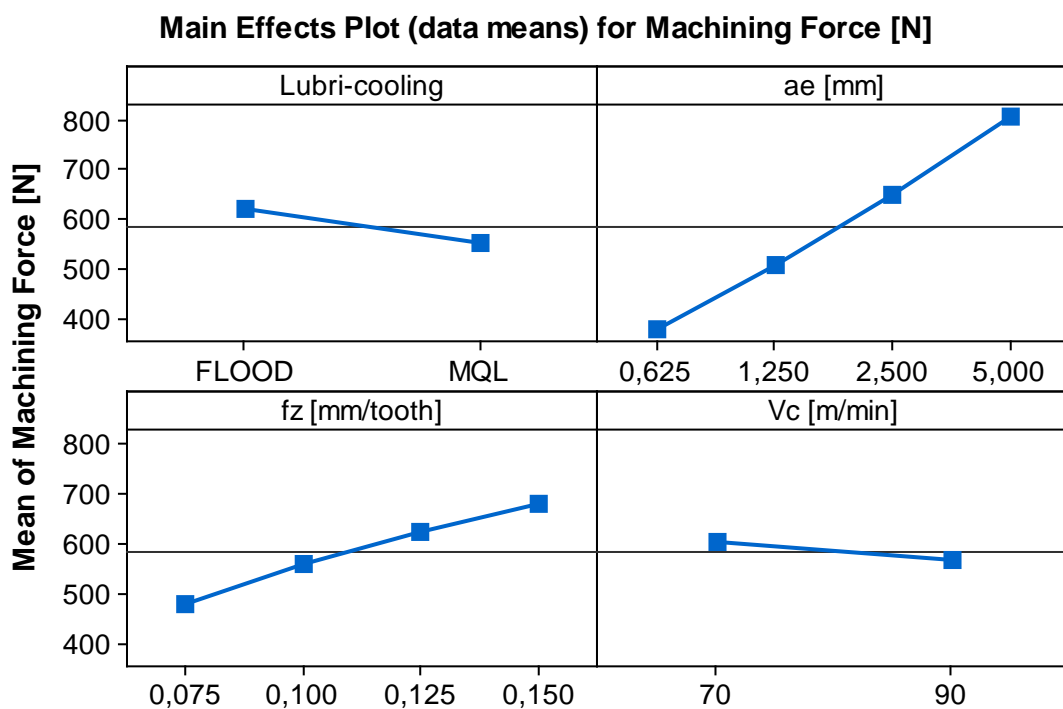


**Figure 5.8.** Factorial analysis of the machining force, considering the lubri-cooling technique, radial depth of cut, feed per tooth and cutting speed as the factors.

Several features have influence on the machining forces and originate deviations from values predicted by theoretical models, such as the microgeometry of the cutting edge. Classical machining theory model assumes that it is a sharp wedge. Real tools, on the other side, have round cutting edges and geometrical features to favor chip breakage and flow. Furthermore the nose radius of the tool gives rise to a vertical component that may be significant. This was not the case in the present study, as shown in the last chapter.

Even empirical models, such as Kienzle equations, are valid for a specific combination of tool geometry, workpiece material and lubri-cooling method. Changing one of these parameters requires new experiments to define the mathematical coefficients.

Especially in the case of tools with indexable inserts, the run out often achieves large values. This causes a significant variation of the machining force from one tooth to the others. In Figure 5.9 this is visible, and for all the cutting conditions this was a recurring fact. Once the thickness of material to be cut is directly related to the process forces, any geometrical inaccuracy of the tool will affect it. Due to the greater number of interfaces, indexable tools generally are more likely to have larger runout.
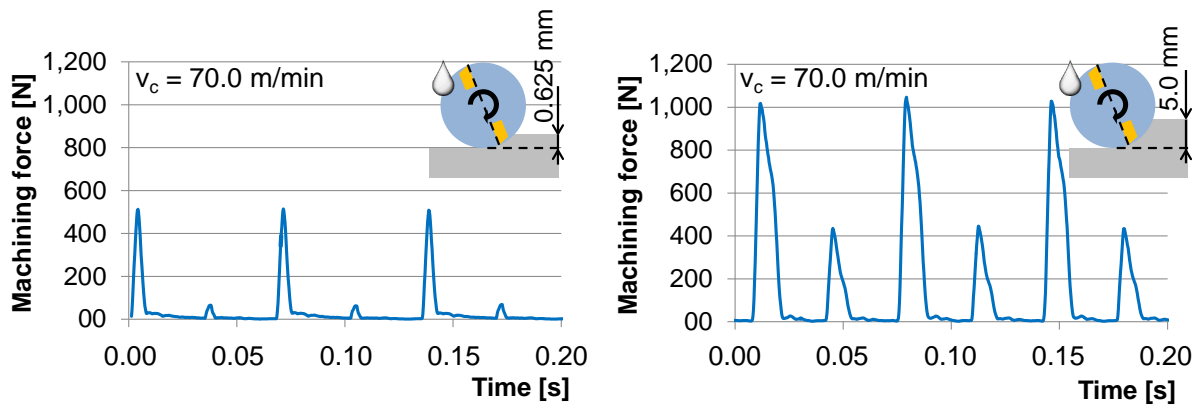


**Figure 5.9.** Machining forces of two test conditions. The difference in the peak force corresponding to each insert of the tool is remarkable. It means that the mechanical load input in the workpiece is constantly changing along the tool path. $v_c = 70.0$ m/min; $f_z = 0.150$ mm / tooth; flood cut.

## 5.2    Residual stresses

Observation of the absolute and average values of surface residual stress reveals some remarkable aspects. Figure 5.10 shows the results of all measurements, and the column on the right side of the stress values is what the software (PANalytical Stress) considers as the standard deviation, STD.DV, of the measurement. This parameter is calculated taking into account instrument errors and the goodness of fit of the peak values to a line (or a set of lines, in the case of $\mathrm{Sin}^2\psi$ split) in the d x $\mathrm{Sin}^2\psi$ graph. Hence the method of peak location also influences this calculation. With this in mind, the referred parameter can be understood as the measurement uncertainty from the angular positioning of the equipment, the detection of the

diffracted signal, and the peak identification. In order to avoid confusion, it will be referred as method error.

Mean values of the measurements are also shown below the results. On the right side, it is presented the true standard deviation referring to the residual stress values that were measured at the three different areas. Method error was around 10 % for most of the cases, with a few exceptions. The highest value is 19%, for the measurement of the SI-03 workpiece, at the position 1.



**Flood cut**

| Sample | Area | $\sigma_{\varphi = 0°}$ [MPa] | STD.DV [MPa] |
|--------|------|------|------|
| SI-01 | 1 | -234.8 | 26.9 |
| | 2 | -286.1 | 5.0 |
| | 3 | -259.5 | 25.4 |
| | MEAN | **-260.1** | **25.7** |
| SI-02 | 1 | -343.3 | 13.4 |
| | 2 | -332.4 | 25.8 |
| | 3 | -326.8 | 17.7 |
| | MEAN | **-334.2** | **8.4** |
| SI-03 | 1 | -302.8 | 56.6 |
| | 2 | -212.8 | 20.3 |
| | 3 | -255.4 | 33.8 |
| | MEAN | **-257.0** | **45.0** |
| SI-04 | 1 | -334.9 | 19.0 |
| | 2 | -302.4 | 16.5 |
| | 3 | -317.6 | 29.4 |
| | MEAN | **-318.3** | **16.3** |

**MQL**

| Sample | Area | $\sigma_{\varphi = 0°}$ [MPa] | STD.DV [MPa] |
|--------|------|------|------|
| SM-01 | 1 | -258.5 | 30.1 |
| | 2 | -224.3 | 15.2 |
| | 3 | -250.3 | 33.5 |
| | MEAN | **-244.4** | **17.9** |
| SM-02 | 1 | -278.7 | 15.2 |
| | 2 | -262.2 | 18.3 |
| | 3 | -252.3 | 28.6 |
| | MEAN | **-264.4** | **13.3** |
| SM-03 | 1 | -256.4 | 33.1 |
| | 2 | -172.7 | 25.4 |
| | 3 | -258.0 | 23.1 |
| | MEAN | **-229.0** | **48.8** |
| SM-04 | 1 | -275.2 | 24.4 |
| | 2 | -262.2 | 11.3 |
| | 3 | -280.9 | 22.7 |
| | MEAN | **-272.8** | **9.6** |

Measurement positions

2   1   3

Machined area

**Figure 5.10.** Residual stress values measured at three different areas, as shown in the lower picture. Error related to the measuring method is shown in the column STD.DV. Means are below the values corresponding to the three areas, standard deviation on the right side.

The first point worth noting is the influence of the radial depth of cut. Essentially, the difference between the finishing and semi-finishing conditions performed here is this cutting parameter. Comparing the workpieces SI-01 and SI-03, as well as SI-02 and SI-04, one may state that the residual stresses present similar values (difference of 2% and 5%, respectively).

The same is valid for the SM workpieces, the ones manufactured by using the MQL technique (SM-01 and SM-03 are different by 6%; SM-02 and SM-04, 3%). An analysis of variance was performed, and comparing S*-01 to S*-03, the P-value for the influence of $a_e$ was 0.883, and for S*-02 and S*-04, 0.253. Considered factors were $a_e$ and the cooling condition. Hence the influence of radial depth of cut on residual stresses is concluded to be very limited. Once it is directly related to the chip thickness and thus the cutting force, the mechanical load also becomes larger. One may infer that it should have resulted in more compressive residual stresses, but this was not the case.

Physically, this fact can be explained by observing the course of action of two subsequent teeth. Figure 5.11 shows schematically the system behavior in these two steps, considering its section view (tool and workpiece). First pass removes a volume of material and induces both thermal and mechanical loads, yielding residual stresses along the course of action. The residual stress field is represented as a gradient, taking into account that it tends to stabilize along the depth. Once the cutting force is higher at the beginning of cut, where chip thickness achieves its maximum, the residual stress is also more compressive at this region, represented by point A. However the next tooth removes most of the material in which higher compressive stresses were induced. The volume delimited by ACD becomes the next chip so that only a small portion of the surface generated by the last tooth becomes the final surface.
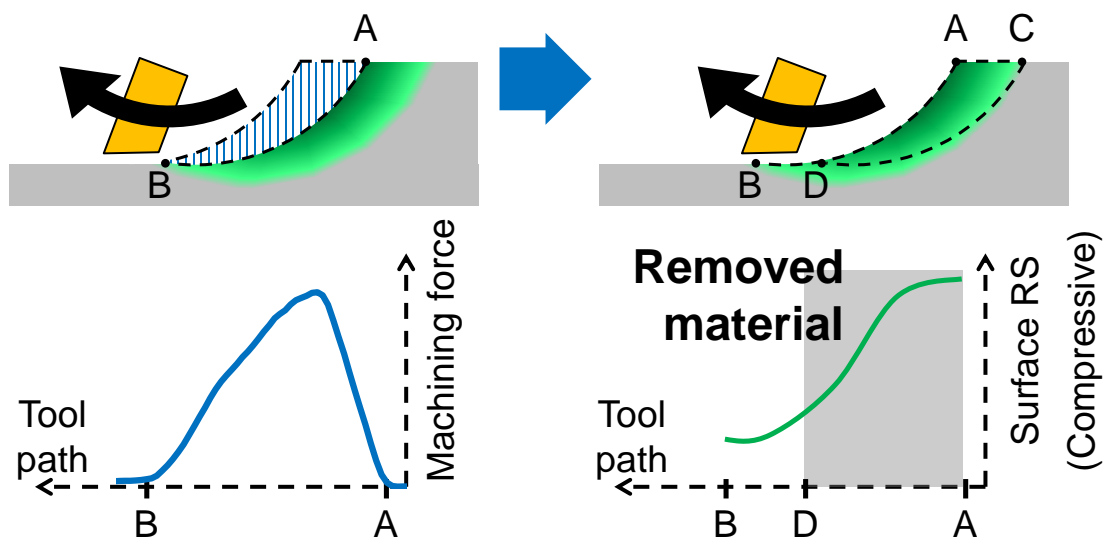


**Figure 5.11.** Physical reasoning for the lack of influence of radial depth of cut on the surface residual stress state.

Another point may be inferred from the same analysis. The distance between points B and D is affected by the feed. From the Figure 5.11, a larger distance BD means that a greater portion of the surface RS generated by a single tooth will be part of the final state. From another viewpoint, the difference in the RS value at points B and D will also increase with the distance between them. Therefore a more heterogeneous state of residual stresses will be developed. Evidence for this hypothesis comes from the results obtained in the present experiments. The conditions with the feed per tooth of 0.150 mm (SI-01, SI-03) present a larger standard deviation than those ones using a feed of 0.075 mm (SI-01, SI-03). This fact is also recurrent in MQL conditions.

Perhaps a larger measurement area would not have been able to detect such differences directly. It is probable that the heterogeneous stress state would result in peak broadening because differences in residual stresses lead to distinct diffraction angles. A suggestion for future development is the analysis of the heterogeneous state by means of mathematical methods extracting information from peak shape, rather than just evaluating the full width at half maximum (FWHM). The evaluation of the heterogeneity state is important because even if the mean value is considerably compressive, there might be positions in which the residual stress moves toward tension values.

YANG, LIU and GRANDT (2002) confirm the heterogeneity hypothesis by measuring Ti-6Al-4V samples at four different areas. They found standard deviations larger than 30% of the mean value for milled samples. Besides, measurement of a larger area provided significantly different values than in smaller areas and distinct positions. In other words, the average state of residual stress overlooks local information. Finally, fatigue testing verified a positive correlation between dispersion of residual stress and variation of the obtained endurance limit. This motivates further studies on the topic of residual stress heterogeneity on a surface, as well as the correlations to crack propagation and fatigue life.

A factorial analysis was performed in order to statistically verify the influence of both cutting parameters and lubri-cooling technique on residual stresses. Figure 5.12 shows the main effects plot, and Figure 5.13, the interactions plot.

| | f$_z$ [mm/tooth] | v$_c$ [m/min] |
|---|---|---|
| 1 | 0.150 | 70 |
| 2 | 0.075 | 90 |
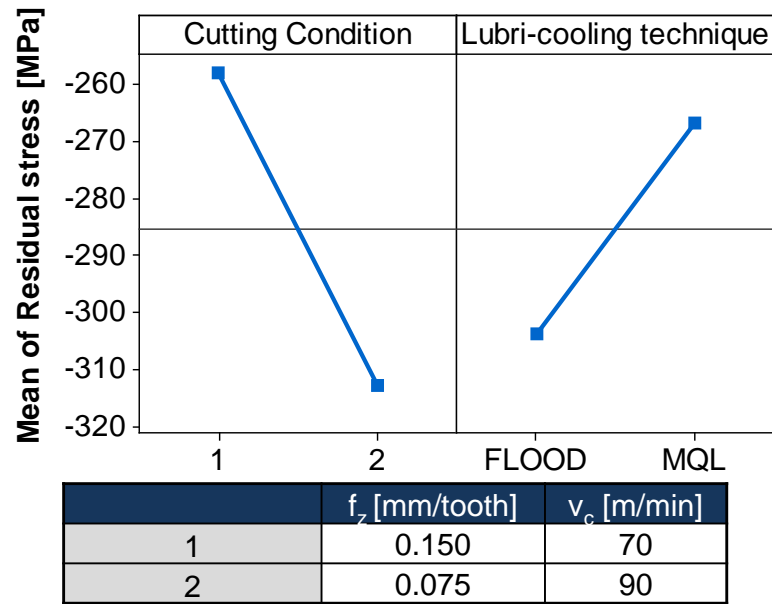
**Figure 5.12.** Main effects plot for residual stresses, taking the cutting condition (combination of feed and cutting speed) and the lubri-cooling technique.

Interaction Plot (data means) for Residual stress [MPa]



| | f$_z$ [mm/tooth] | v$_c$ [m/min] |
|---|---|---|
| 1 | 0.150 | 70 |
| 2 | 0.075 | 90 |
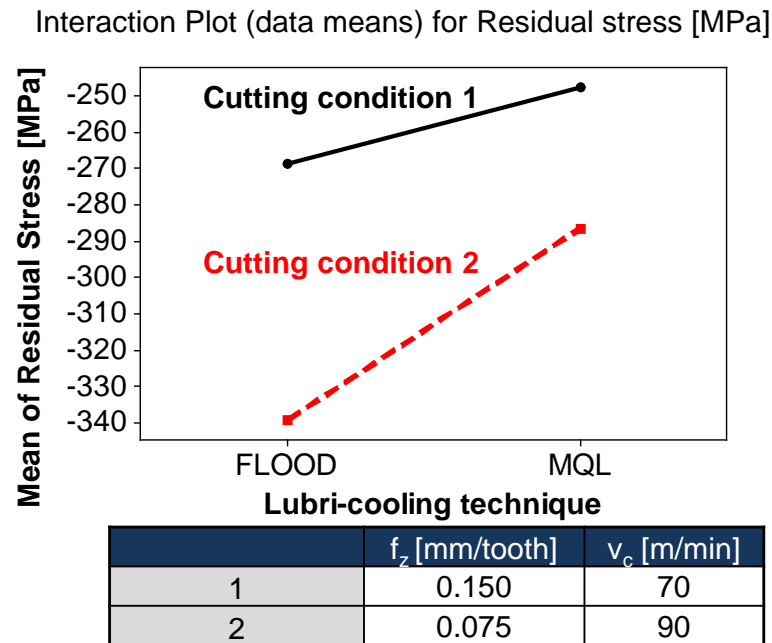
**Figure 5.13.** Interaction plot for the residual stress.

The main effects plot confirms what could be inferred from Figure 5.10. Residual stresses become less compressive by the use of MQL, in comparison to flood cut. For all the machining conditions this behavior was observed, although in conditions 01 (SI-01, SM-01)

and 03 (SI-03, SM-03) the standard deviation was so large that in practice the results are equal for both flood cut and MQL).

It is deduced that the less compressive residual stresses generated in machining with MQL result from a combination of higher thermal load, and lower mechanical load in comparison to flood cut. Both the effects have been discussed in the last section, namely:

- The oil mist is much less capable of removing heat than the emulsion in flood cut, which is also applied in much greater volumes;
- Thermal softening reduces the strength of the material.

The second factor is related to the temperature increase, and thus the primary cause of the decrease in the value of compressive residual stresses is the higher thermal load.

Comparison of the effect of the cutting condition, representing the two combinations of feed and cutting speed that were used, reveals a peculiar trend. On a first moment, expected results on the workpieces were as follow: the conditions S*-01, with larger feed, should produce higher cutting force and introduce a larger mechanical load. The lower cutting speed (70 m/min) contributes to lower temperatures due to friction, reducing the thermal load. Differences in radial depth of cut are very limited, as demonstrated and discussed before. Thus residual stresses should be more compressive than that on the workpieces S*-02.

This was not the case, though. It can be seen that, in fact, the development of residual stresses followed the opposite trend. Taking note of values of the machining forces, the main effects of each parameter correspond to what was expected. In other words, the larger feed in conditions S*-01 did resulted in larger machining force, introducing a higher mechanical load than S*-02. Therefore the only physical explanation to the less compressive residual stress measured on S*-01 is that those conditions also develop a very high thermal load.

A temperature increase in machining is related to the energy that is dissipated as heat when deformation work is done on the workpiece / chip, as well as friction on the interfaces. If the thickness of the uncut material is larger, more energy will be required for cutting it, and part of this will be transferred to the workpiece. It seems that in the high feed conditions the heat produced in the plastic deformation of the material was so extreme that it compensated a considerable amount of the mechanical load, in terms of residual stress generation. In order to confirm this hypothesis, experiments with temperature measurement are fundamental to obtain evidence about the heat generation and thus the thermal load.

SUN and GUO (2009) found a similar trend for the influence of the feed in the residual stress measured at the cutting direction in milling. Increase of the feed led to decrease in the compressive residual stress. Experiments were conducted with a single cutting speed of

65 m/min and radial depth of cut of 4 mm. When evaluating the influence of cutting speed, results indicate that compressive residual stresses increase with cutting speed, achieve a maximum value at 80-100 m/min, and then start decreasing. Their suggestion is that there is a strong interaction of mechanical and thermal effects, but no rationale is proposed.

The same trend is supported by LI, Y. GUO and C. GUO (2013), in milling experiments of H13 steel with a similar tool to the one use in the present study. At the surface, increasing the feed was noted to decrease the residual stress. However this was not the case at the subsurface, where an intermediate feed produced a profile with higher values to the compressive side. Unfortunately no hypotheses are presented to explain these differences. Several other references are also focused on the results alone, while the reasons why variations occur are not entirely explored (GUO; LI; JAWAHIR, 2009; ULUTAN; OZEL, 2011).

A challenging issue in the measurement of the residual stresses was that diffracted signal presented significant noise. Together with the low relative intensity of titanium peaks in the high angle range, identification of peak positions becomes less certain. The poor signal to noise ratio is mainly accounted to the low representativeness of the irradiated area. The amount of grains satisfying Bragg's law is not sufficient to produce an intense diffracted beam. An example of a typical diffracted curve that was obtained in the experiments is shown in Figure 5.14, in the interface of the software Stress.

GROVE, KÖHLER and DENKENA (2014) also present diffracted curves with the same characteristics, claiming that a larger irradiated area should be considered to achieve better results. Sometimes it is not possible, and even if this is not the case, it becomes harder to assess the homogeneity of the residual stresses on the surface. As stated in the previous results, there may be a wide variation (up to 50%). Another option that is pointed is the use of synchrotron radiation. Due to the much higher power source, the peak shape is improved and allows much more precise identification of its position (CRISTO; ALVES; VIEIRA, 2013).
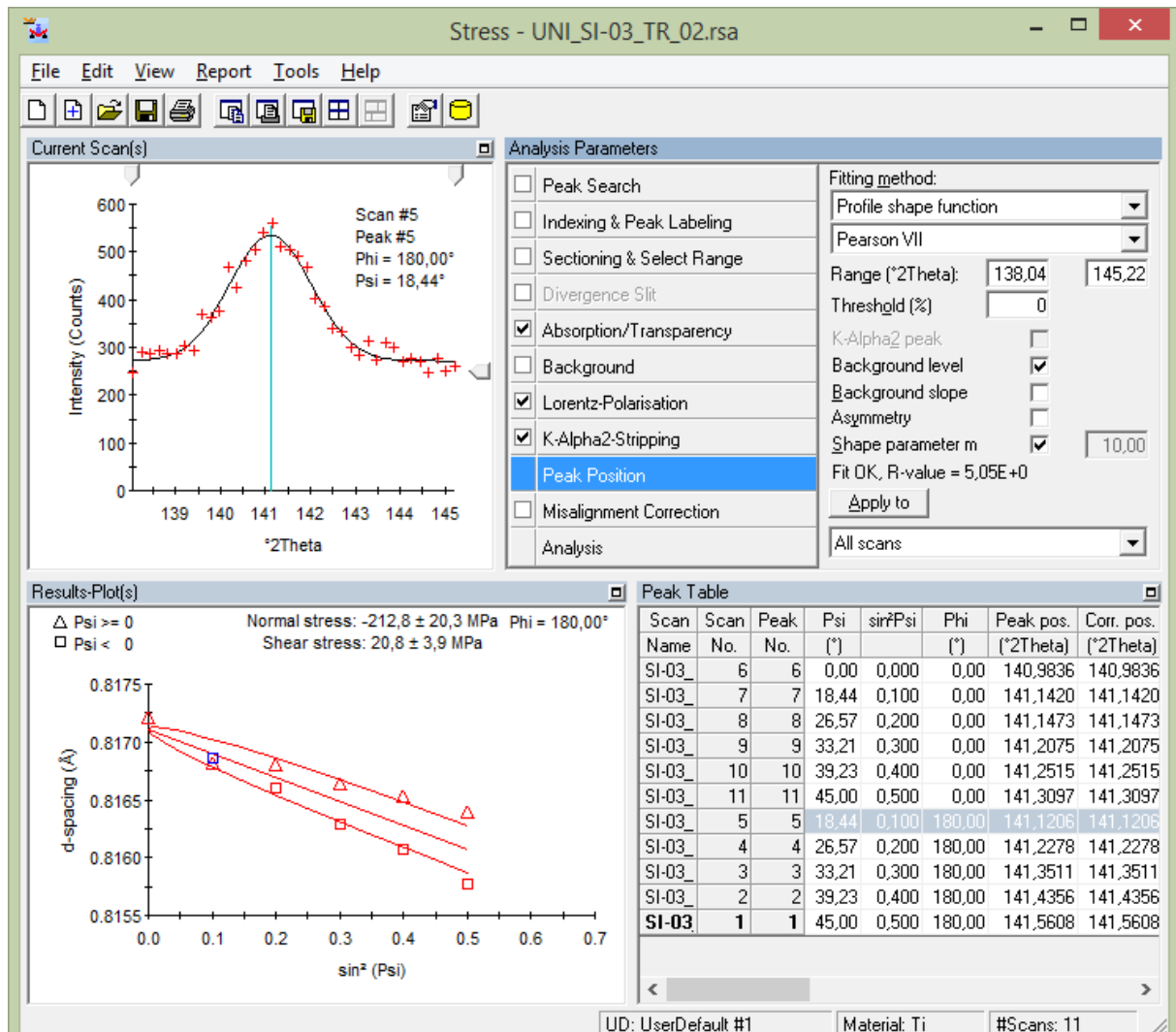
**Figure 5.14.** Typical diffracted curve, in the upper left. On the right side, the properties panel displays the filters and possible corrections.

## 5.3    Topography and roughness

Surface roughness is mostly influenced by the feed, if only geometrical aspects and a sharp tool are taken into account. As it was exposed in the literature review, predictive models often fail because most of them consider only geometrical parameters. Friction between the tool and the workpiece and adhesion are some examples of additional phenomena affecting the roughness of the samples.

Collected data is shown in Figure 5.15, according to the procedure described earlier. The scanned area is shown partially to allow a better level of details, and vertical axis is maximized 10 times for the same reason. Machining marks are more perceptible in the conditions with larger feed rate, which seems natural once the tool moves further between

each tooth cutting pass. Once again, it must be highlighted that values of roughness parameters are comparative, since the measurement principle that was used is different from the standard method.
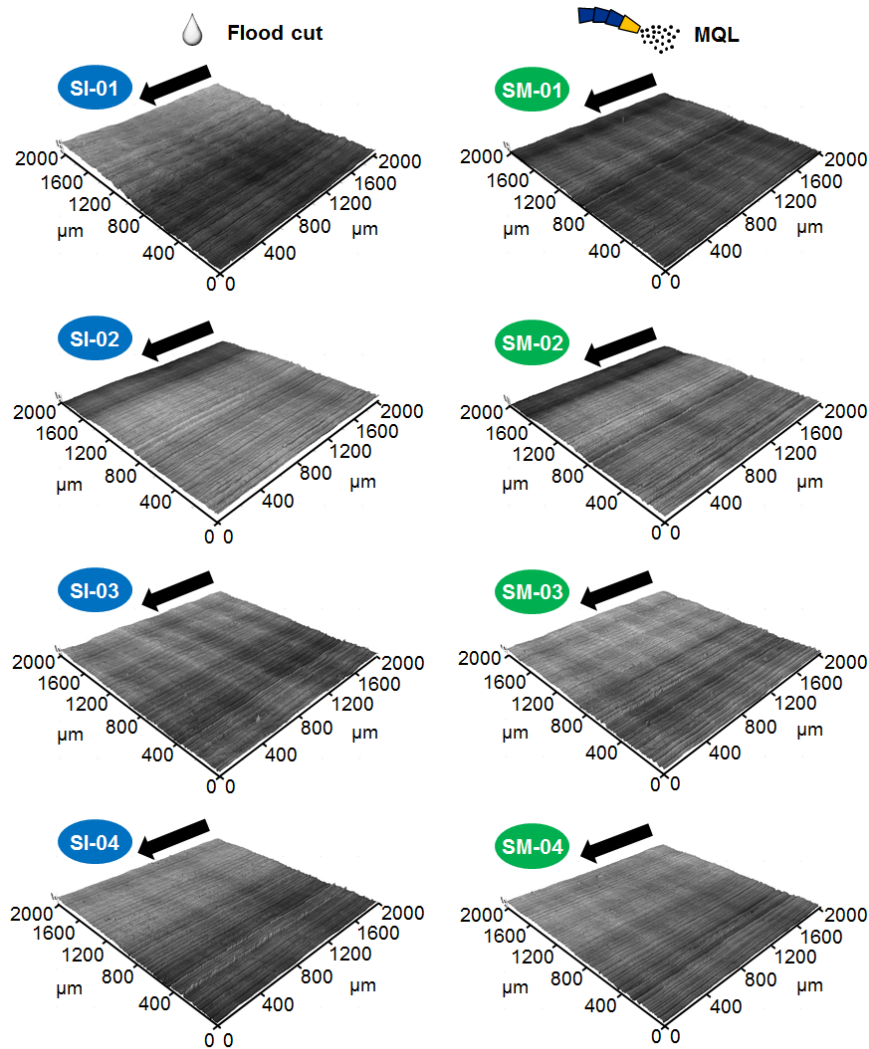


**Figure 5.15.** Scan of the manufactured surfaces, feed direction indicated by the arrow. Feed marks are mostly visible in S*-01 and S*-03.

Comparing to the results that were obtained, shown in Figure 5.16, the lubri-cooling method had no influence on the surface roughness. Both the mean value and the standard deviation are similar for MQL and flood cut. The same is also valid in regard of the radial depth of cut. Only the cutting condition (combination of cutting speed and feed) had effect, and this is believed to be related mainly to the feed rate. Geometrically, the cutting speed has no impact on the marks left on the surface. In practice, it can lead to higher temperatures and adhesion phenomena, and this may generate higher surface roughness.
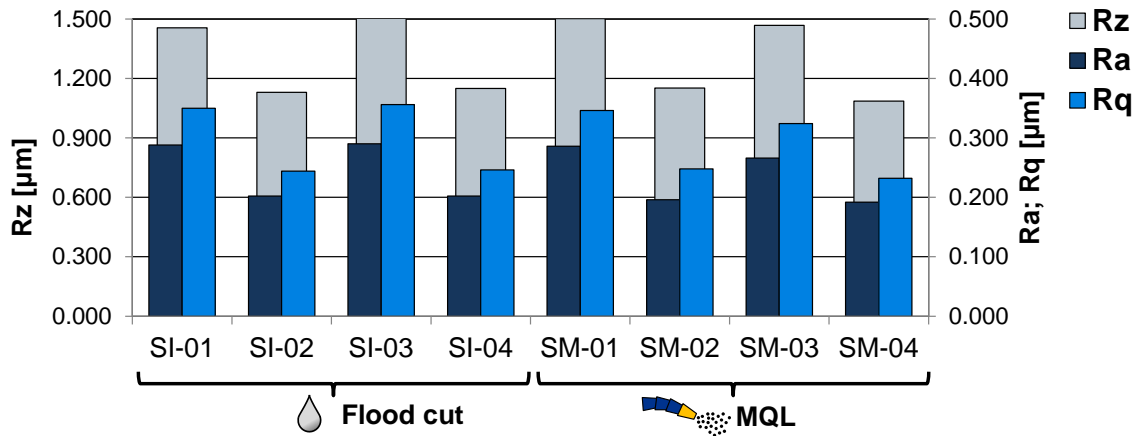
**Figure 5.16.** Roughness data; measurements made at de same direction of tool movement.

It is suggested that results can be explained by the same reasoning that was developed when discussing residual stresses. The values that were obtained here are similar to the ones reported by SAFARI *et al.* (2015), in which a similar tool was used for peripheral milling.

Besides the feed marks, transversal direction also has a characteristic pattern. It was verified that the roughness in this direction presented higher values than on the feed direction. In order to clarify the origin of such marks, the wedge of the tool was measured in the same equipment. The roughness was then obtained, considering the same cutoff length, and compared to measurements of the workpieces in the transversal direction, according to Figure 5.17. Results are presented in Table 5.1, which compares tool and workpiece data.
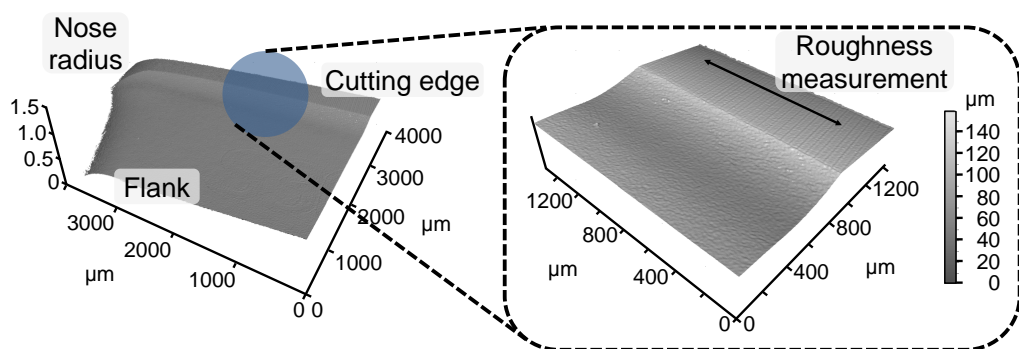


**Figure 5.17.** Surface scan of the main cutting edge of the inserts, in order to obtain the roughness and correlate to that one from the workpiece, at the transversal direction.

For all the cutting conditions and lubri-cooling method, roughness results in the transversal direction were the same and similar to the value measured at the tool. In the case of the average maximum height of the profile - $R_z$ – a significant difference was found. It is

possible that ploughing and adhesion between the flank face and the machined surface are responsible for this difference.

**Table 5.1.** Comparison of workpiece roughness at transversal direction and tool cutting edge.

|  | $R_a$ [μm] | $R_z$ [μm] | $R_q$ [μm] |
|---|---|---|---|
| Workpieces – transversal direction | 0.55 | 4.26 | 0.69 |
| Cutting edge of the inserts | 0.50 | 2.70 | 0.62 |
| Difference ($R^{Tool}$ / $R^{Workpiece}$) | 10.3% | 57.7% | 12.2% |

## 5.4    Surface hardness

Hardness was measured along the depth of the material in order to provide an insight about the level of work hardening. Results for the finishing conditions, S*-01 and S*-02, are shown in Figure 5.18. The mean hardness of the bulk material is 348 HV0.05 with standard deviation equal to 12.5 HV0.05, obtained from 15 indentations. The limit values of hardness are shown in the picture as well. At the different depths, the standard deviation of the hardness was similar to that of the bulk material.
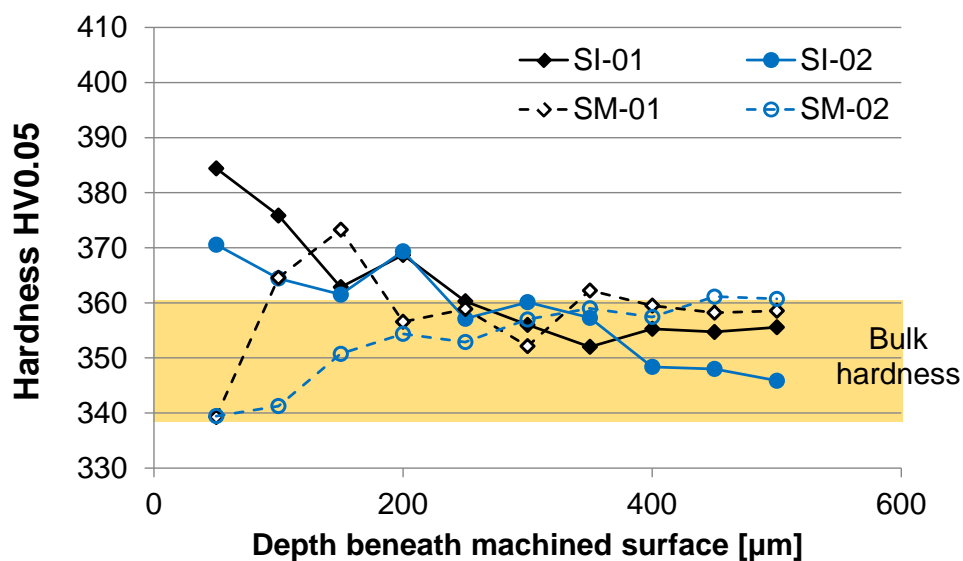


**Figure 5.18.** Hardness profile beneath the surface of the workpieces manufactured with conditions of finishing operation.

It can be observed that workpieces manufactured with flood of coolant present higher values of hardness close to the surface. The fact that both SI-01 and SM-01 present higher hardness up to 150-200 μm than SI-02 and SM-02 agrees with the higher cutting forces that were observed, thus inducing more cold work of the material.

In the case of MQL, results indicate a tendency of surface softening, although in a statistical sense the values are nearly the same as in the bulk material. At a depth of 100-150 μm the hardness of condition SM-01 increases, and thus it can be inferred that thermal softening effects are restricted to the layer between the surface and this depth.

In regard of SM-02, such hardness peak is not observed. Once this sample was manufactured with a higher cutting speed (90 m/min) and lower feed rate (0.075 mm/tooth), it seems natural that a higher thermal load is developed. On the other side, the residual stress results indicate an opposite result, because in SM-02 the value is more compressive than that of SM-01. This contradiction suggests that the balance of thermal and mechanical loads that originate residual stresses and cold work of the surface layer is different for each case. Anyhow, it also points the need of measuring the temperature developed in cutting for a better understanding.

Results for the semi-finishing conditions, S*-03 and S*-04, are shown in Figure 5.19. Such operations revealed trends those are totally distinct from the ones shown before, for finishing conditions.



**Figure 5.19.** Hardness profile beneath the surface of the workpieces manufactured with conditions of semi-finishing operation.
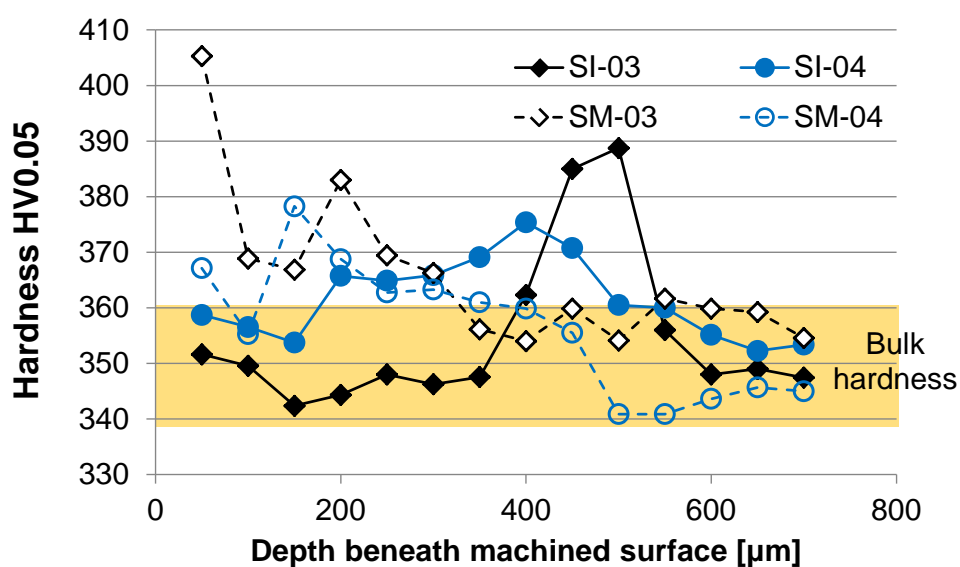
Workpieces manufactured by MQL milling show higher hardness up to a depth of 300-400 μm, differently from the finishing conditions. However, the standard deviation in this region (from the surface up to 300 μm) is also higher especially for SM-03, from 20 to 26 HV0.05. In the depth of 350-400 μm the values are inside the limits of the bulk material, and despite the variations that occur after this depth, the hardness can be considered stable.

Both the workpieces from flood cut conditions present a subsurface hardness peak. Those higher values are followed by larger standard deviation, in the range of 15 to 33 HV0.05 for SI-03, and 14 to 23 HV0.05 for SI-04. It is probable that mechanical effects act up to a depth of 600 μm, while thermal softening occurs from the surface until around 350 μm below. Therefore, the plastic strain is compensated by temperature effects.

Once again, the lack of agreement with the residual stress data demands further analyses and experiments, especially temperature measurements. Furthermore, a complete comparison between hardness data with residual stresses requires that both should be evaluated along the depth.

# 6 Conclusions and suggestions for future developments

Analysis of the data retrieved from experiments supports several conclusions, which are summarized in this section and follow the order of appearance in the text. Some statements have already been mentioned when discussing the results.

**Cutting forces and chip morphology:**

- Serrated chips were observed irrespective of the cutting condition and lubri-cooling method;

- The segments of the chips are originated by the action of cracks, according to evidences that were observed by SEM: gaps between segments, surfaces on the opposite sides of the segments present a distinct morphology and their interception forms a sharp edge, complementary geometry between one segment and the other, cracks near the edges of the saw-tooth;

- As shown in other studies, the adiabatic shearing mechanism takes place at some level. Hence there must be a balance of effects, which depends on the cutting conditions;

- Chips produced when cutting with flood of coolant are more curved towards the free surface than in MQL machining because of the better cooling effect. Therefore heat dissipation is more significant in flood cut conditions;

- Cutting parameters influenced the machining force according to theory predictions: increasing the feed rate and the radial depth of cut also increased machining force, and increasing the cutting speed slightly reduced the forces;

- Machining with MQL results in 10% lower forces because of thermal softening of the material, as compared to flood cut;

**Residual stresses:**

- Surface residual stress was insensitive to the radial depth of cut, despite the direct influence of this parameter on the cutting force and thus in the mechanical load. The fact is that the volume which is affected by the higher mechanical load is removed in the subsequent cut by the next tooth;

- A larger feed rate leads to a larger variation among the residual stress measurements at the different areas (S*-01 and S*-03). This variation ranges from 15% to 49%, while in the conditions with lower feed rate (S*-02 and S*-04) it ranges from 5% to 11%;

- Besides the higher machining forces for conditions with lower cutting speed and higher feed rate (S*-01 and S*-03), the amount of heat that is produced leads to residual stresses that are less compressive than in the opposite case (S*-02 and S*-04);

- The lower heat removing capacity of MQL results in residual stresses that are less compressive than in flood cut. This is valid for all the cutting conditions, although for S*-01 and S*-03 the lubri-cooling method is less remarkable;

- The small measurement areas allow the assessment of heterogeneity of the residual stresses in a specified surface. On the other side, it punishes the quality of the diffracted signal because of the poor representativeness in terms of quantity of grains that are exposed to the X-ray beam. Once residual stress variation reflects on fatigue life variation, it is fundamental to develop a method for its assessment (of residual stress) with improved signal quality;

**Roughness and topography:**

- Roughness of the surface was insensitive to the radial depth of cut and lubri-cooling condition;

- The main factor of influence on the roughness is the feed rate, so that the conditions with lower feed rate produced smoother surfaces;

- In the perpendicular direction in respect to the tool movement, a larger value of roughness was obtained. This is caused by the wedge of the tool, and comparison has shown that roughness values are similar;

**Hardness beneath the machined surface:**

- A direct correlation between hardness values and residual stresses could not be obtained. Samples with the same surface residual stress had different hardness profiles;

- For the finishing conditions (S*-01 and S*-03), flood of coolant produced an increase in hardness up to a depth of nearly 300 μm, where the bulk value was

achieved. The use of MQL results in a tendency of surface softening, although the mean value remains in the limits of the bulk hardness. It is inferred that surface softening is a result of the increased thermal load;

- In regard of the semi-finishing conditions, MQL resulted in increased surface hardness. Surfaces manufactured with the use of flood of coolant present a subsurface hardness peak (from 300 to 600 μm, approximately), while the near surface layer presents basically the same values than the bulk material. This is a result of thermal softening, which acts up to a depth of nearly 300 μm, compensating the mechanical effect.

**Further challenges to be overcome and opportunities for future research include:**
- Investigation of tool wear behavior in milling with MQL, as compared to flood cut, and measurement of temperatures during cutting;
- Analysis of the consumption of energy and other resources, evaluating both MQL and machining with flood of coolant;
- Development of a method for assessing the residual stress heterogeneity on the surface and correlations to fatigue life, as well as fatigue life variance;
- In-depth analysis of residual stresses and comparison to the hardness data;
- Development of a mock up geometry, representing an aeronautical structural component, and analysis of the potential fatigue life variation in respect to the residual stresses produced by different cutting conditions.

# References

ALTINTAS, Y. **Manufacturing automation**: metal cutting mechanics, machine tool vibrations, and CNC design. 2$^{nd}$ ed. New York: Cambridge University Press, 2012, 380 p.

ASTAKHOV, V. P. Ecological machining: near-dry machining. In: DAVIM, J. P. (Ed.) **Machining**: fundamentals and recent advances. Springer London, 2008. cap. 7. p. 195-223.

ASTAKHOV, V. P. On the inadequacy of the single-shear plane model of chip formation. **International Journal of Mechanical Sciences**, v. 47, n. 11, p. 1649-1672, Nov. 2005.

ASTAKHOV, V. P. Surface integrity–definition and importance in functional performance. In: DAVIM, J. P. (Ed.). **Surface integrity in machining**. New York: Springer London, 2010. cap. 1. p. 1-35.

ASTAKHOV, V. P. **Tribology of metal cutting**. 1$^{st}$ ed. Oxford: Elsevier, 2006, 454 p.

ASTAKHOV, V. P.; SHVETS, S. The assessment of plastic deformation in metal cutting. **Journal of Materials Processing Technology**, v. 146, n. 2, p. 193-202, Feb. 2004.

ASTAKHOV, V. P.; SHVETS, S. V. A system concept in metal cutting. **Journal of Materials Processing Technology**, v. 79, n. 1-3, p. 189-199, July 1998.

BOYER, R. R. An overview on the use of titanium in the aerospace industry. **Materials Science and Engineering: A**, v. 213, n. 1, p. 103-114, Aug. 1996.

BOYER, R. R. Attributes, characteristics, and applications of titanium and its alloys. **JOM**, v. 62, n. 5, p. 21-24, May 2010.

BRINKSMEIER, E.; CAMMETT, J. T.; KÖNIG, W.; LESKOVAR, P.; PETERS, J.; TÖNSHOFF, H. K. Residual stresses - measurement and causes in machining processes. **CIRP Annals - Manufacturing Technology**, v. 31, n. 2, p. 491-510, 1982.

BRINKSMEIER, E.; WALTER, A.; JANSSEN, R.; DIERSEN, P. Aspects of cooling lubrication reduction in machining advanced materials. **Proceedings of the Institution of Mechanical Engineers, Part B: Journal of Engineering Manufacture**, v. 213, n. 8, p. 769-778, Aug. 1999.

BROOKS, C. R.; CHOUDHURY, A. **Failure analysis of engineering materials**. 1$^{st}$ ed. New York: McGraw-Hill Professional, 2002, 700p.

BUSSU, G.; IRVING, P. E. The role of residual stress and heat affected zone properties on fatigue crack propagation in friction stir welded 2024-T351 aluminium joints. **International Journal of Fatigue**, v. 25, n. 1, p. 77-88, Jan. 2003.

CAMPBELL, G. S.; LAHEY, R. A survey of serious aircraft accidents involving fatigue fracture. **International Journal of Fatigue**, v. 6, n. 1, p. 25-30, Jan. 1984.

CHE-HARON, C. H. Tool life and surface integrity in turning titanium alloy. **Journal of Materials Processing Technology**, v. 118, n. 1, p. 231-237, Dec. 2001.

CHE-HARON, C. H.; JAWAID, A. The effect of machining on surface integrity of titanium alloy Ti-6% Al-4% V. **Journal of Materials Processing Technology**, v. 166, n. 2, p. 188-192, Aug. 2005.

CHEN, L.; EL-WARDANY, T. I.; HARRIS, W. C. Modelling the effects of flank wear land and chip formation on residual stresses. **CIRP Annals - Manufacturing Technology**, v. 53, n. 1, p. 95-98, 2004.

COROMANT, Sandvik. **Application guide**: gas turbines. Sandvik Coromant, Aug. 2009, p. 43-74. (C-2920:18)

CULITY, B. D. **Elements of X-ray diffraction**. Reading: Addison-Wesley, 1954.

DA SILVA, R. B.; MACHADO, A. R.; EZUGWU, E. O.; BONNEY, J.; SALES, W. F. Tool life and wear mechanisms in high speed machining of Ti–6Al–4V alloy with PCD tools under various coolant pressures. **Journal of Materials Processing Technology**, v. 213, n. 8, p. 1459-1464, Aug. 2013.

DEARNLEY, P. A.; GREARSON, A. N. Evaluation of principal wear mechanisms of cemented carbides and ceramics used for machining titanium alloy IMI 318. **Materials Science and Technology**, v. 2, n. 1, p. 47-58, Jan. 1986.

DONACHIE, M. J. **Titanium**: a technical guide. 2nd ed. Materials Park: ASM international, 2000, 367 p.

EL-HELIEBY, S. O. A.; ROWE, G. W. Influences of surface roughness and residual stress on fatigue life of ground steel components. **Metals Technology**, v. 7, n. 1, p. 221-225, Jan. 1980.

EZUGWU, E. O. Key improvements in the machining of difficult-to-cut aerospace superalloys. **International Journal of Machine Tools and Manufacture**, v. 45, n. 12-13, p. 1353-1367, Oct. 2005.

EZUGWU, E. O.; BONNEY, J.; DA SILVA, R. B.; ÇAKIR, O. Surface integrity of finished turned Ti–6Al–4V alloy with PCD tools using conventional and high pressure coolant supplies. **International Journal of Machine Tools and Manufacture**, v. 47, n. 6, p. 884-891, May 2007.

EZUGWU, E. O.; WANG, Z. M. Titanium alloys and their machinability - a review. **Journal of materials processing technology**, v. 68, n. 3, p. 262-274, Aug. 1997.

FIELD, M.; KAHLES, J. F. **The surface integrity of machined and ground high strength steels**. DMIC Report 210, 1964, p. 54–77.

FINDLAY, S. J.; HARRISON, N. D. Why aircraft fail. **Materials today**, v. 5, n. 11, p. 18-25, Nov. 2002.

GHANEM, F.; SIDHOM, H.; BRAHAM, C.; FITZPATRICK, M. E. Effect of near-surface residual stress and microstructure modification from machining on the fatigue endurance of a tool steel. **Journal of Materials Engineering and Performance**, v. 11, n. 6, p. 631-639, Dec. 2002.

GHANI, J. A.; CHE HARON, C. H.; HAMDAN, S. H.; SAID, A. Y. M.; TOMADI, S. H. Failure mode analysis of carbide cutting tools used for machining titanium alloy. **Ceramics International**, v. 39, n. 4, p. 4449-4456, May 2013.

GINTING, A.; NOUARI, M. Surface integrity of dry machined titanium alloys. **International Journal of Machine Tools and Manufacture**, v. 49, n. 3, p. 325-332, Mar. 2009.

GOMES, J. O. **Fabricação de superfícies de forma livre por fresamento no aço temperado ABNT 420, na liga de alumínio AMP8000 e na liga de cobre Cu-Be**. 2001. 180f. Tese (Doutorado em Engenharia Mecânica) – Universidade Federal de Santa Catarina, Florianópolis.

GROVE, T.; KÖHLER, J.; DENKENA, B. Residual Stresses in Milled β-Annealed Ti6Al4V. **Procedia CIRP**, v. 13, p. 320-326, 2014.

GRZESIK, W.; KRUSZYNSKI, B.; RUSZAJ, A. Surface integrity of machined surfaces. In: DAVIM, J. P. (Ed.). **Surface integrity in machining**. New York: Springer London, 2010. cap. 5. p. 143-179.

GUO, Y. B.; LI, W.; JAWAHIR, I. S. Surface integrity characterization and prediction in machining of hardened and difficult-to-machine alloys: a state-of-art research review and analysis. **Machining Science and Technology**, v. 13, n. 4, p. 437-470, 2009.

GUO, Y.; COMPTON, W. D.; CHANDRASEKAR, S. In situ analysis of flow dynamics and deformation fields in cutting and sliding of metals. In: **Proceedings of the Royal Society of London A**: Mathematical, Physical and Engineering Sciences. The Royal Society, June 2015.

HALE, J. Boeing 787 from the ground up. **Aero**, v. 4, p. 17-24, 2006.

HAUK, V. **Structural and residual stress analysis by nondestructive methods**. Amsterdam: Elsevier, 1997, 640 p.

JACOBUS, K.; DEVOR, R. E.; KAPOOR, S. G. Machining-induced residual stress: experimentation and modeling. **Journal of Manufacturing Science and Engineering**, v. 122, n. 1, p. 20-31, Feb. 2000.

JAWAID, A.; SHARIF, S.; KOKSAL, S. Evaluation of wear mechanisms of coated carbide tools when face milling titanium alloy. **Journal of Materials Processing Technology**, v. 99, n. 1-3, p. 266-274, Mar. 2000.

JOSHI, Shashikant; TEWARI, A.; JOSHI, Suhas. Influence of preheating on chip segmentation and microstructure in orthogonal machining of Ti6Al4V. **Journal of Manufacturing Science and Engineering**, v. 135, n. 6, paper nº. 061017, Nov. 2013.

KAHLES, J. F.; FIELD, M.; EYLON, D.; FROES, F. H. Machining of titanium alloys. **JOM**, v. 37, n. 4, p. 27-35, April 1985.

KIENZLE, O. Bestimmung von Kräften und Leistungen an Spanenden Werkzeugen und

KLOCKE, F. **Manufacturing processes 1**: cutting. 1$^{st}$ ed. Berlin: Springer, 2011, 504 p.

KLOCKE, F.; EISENBLÄTTER, G. Dry cutting. **CIRP Annals - Manufacturing Technology**, v. 46, n. 2, p. 519-526, 1997.

KLOCKE, F.; KRÄMER, A.; SANGERMANN, H.; LUNG, D. Thermo-mechanical tool load during high performance cutting of hard-to-cut materials. **Procedia CIRP**, v. 1, p. 295-300, 2012.

KLOCKE, F.; SETTINERI, L.; LUNG, D.; PRIARONE, P. C; ARFT, M. High performance cutting of gamma titanium aluminides: Influence of lubricoolant strategy on tool wear and surface integrity. **Wear**, v. 302, n. 1-2, p. 1136-1144, April-May 2013.

KÖHLER, J.; GROVE, T.; MAISS, O.; DENKENA, B. Residual stresses in milled titanium parts. **Procedia CIRP**, v. 2, p. 79-82, 2012.

KOMANDURI, R.; HOU, Z.-B. On thermoplastic shear instability in the machining of a titanium alloy (Ti-6Al-4V). **Metallurgical and Materials Transactions A**, v. 33, n. 9, p. 2995-3010, Sept. 2002.

KOMANDURI, R.; VON TURKOVICH, B. F. New observations on the mechanism of chip formation when machining titanium alloys. **Wear**, v. 69, n. 2, p. 179-188, June 1981.

KOSTER, W. P.; FIELD, M.; KAHLES, J. F.; FRITZ, L. J. **Surface integrity of machined structural components**. Cincinnati, OH: METCUT RESEARCH ASSOCIATES INC., 1970. 362 p. (AD0870146).

KRUPP, U. **Fatigue crack propagation in metals and alloys**: microstructural aspects and modelling concepts. 1$^{st}$ ed. Weinheim: Wiley-VCH, 2007. 311 p.

LEVERANT, G. R.; LANGER, B. S.; YUEN, A.; HOPKINS, S. W. Surface residual stresses, surface topography and the fatigue behavior of Ti-6AI-4V. **Metallurgical Transactions A**, v. 10, n. 2, p. 251-257, Feb. 1979.

LEYENS, C.; PETERS, M (Ed.). **Titanium and titanium alloys**: fundamentals and applications. 1$^{st}$ ed. Weinheim: Wiley-VCH, 2003, 513 p.

LI, W.; GUO, Y.; GUO, C. Superior surface integrity by sustainable dry hard milling and impact on fatigue. **CIRP Annals - Manufacturing Technology**, v. 62, n. 1, p. 567-570, 2013.

LI, W.; GUO, Y.; GUO, C. Superior surface integrity by sustainable dry hard milling and impact on fatigue. **CIRP Annals - Manufacturing Technology**, v. 62, n. 1, p. 567-570, 2013.

LÜTJERING, G.; WILLIAMS, J. C. **Titanium**. 2$^{nd}$ ed. Berlin: Springer, 2007, 442 p.

MATSUMOTO, Y.; HASHIMOTO, F.; LAHOTI, G. Surface integrity generated by precision hard turning. **CIRP Annals - Manufacturing Technology**, v. 48, n. 1, p. 59-62, 1999.

MITSUBAYASHI, M.; MIYATA, T.; AIHARA, H. Phenomenal analysis of shot peening: analysis of fatique strength by fracture mechanics for shot-peened steel. **JSAE Review**, v. 15, n. 1, p. 67-71, Jan 1994.

MOISEYEV, V. N. **Titanium alloys**: Russian aircraft and aerospace applications. 1$^{st}$ ed. Boca Raton: CRC press, 2005, 216p.

MOLINARI, A.; MUSQUAR, C.; SUTTER, G. Adiabatic shear banding in high speed machining of Ti–6Al–4V: experiments and modeling. **International Journal of Plasticity**, v. 18, n. 4, p. 443-459, April 2002.

M'SAOUBI, R; OUTEIRO, J. P.; CHANDRASEKARAN, H.; DILLON, O. W.; JAWAHIR, I. S. A review of surface integrity in machining and its impact on functional performance and life of machined products. **International Journal of Sustainable Manufacturing**, v. 1, n. 1-2, p. 203-236, 2008.

NAKAYAMA, K. Formation of saw tooth chips. In: International Conference on Production Engineering, 1974, Tokyo. **Procedings…**

NASIR, A.. General comments on ecological and dry machining. In: First International Seminar of Ecofrim, 1998, Sobotin-Sumperk. **Procedings…**, p. 10-14.

NASR, M. N. A.; NG, E.-G.; ELBESTAWI, M. A. Modelling the effects of tool-edge radius on residual stresses when orthogonal cutting AISI 316L. **International Journal of Machine Tools and Manufacture**, v. 47, n. 2, p. 401-411, Feb. 2007.

NOVOVIC, D.; DEWES, R. C.; ASPINWALL, D. K.; VOICE, W.; BOWEN, P. The effect of machined topography and integrity on fatigue life. **International Journal of Machine Tools and Manufacture**, v. 44, n. 2, p. 125-134, Feb. 2004.

NOYAN, I. C.; COHEN, J. B. **Residual stress**: measurement by diffraction and interpretation. 1st ed. New York: Springer, 1987, 276 p.

OUTEIRO, J. C.; UMBRELLO, D.; M'SAOUBI, R. Experimental and numerical modelling of the residual stresses induced in orthogonal cutting of AISI 316L steel. **International Journal of Machine Tools and Manufacture**, v. 46, n. 14, p. 1786-1794, Nov. 2006.

PETERS, M.; KUMPFERT, J.; WARD., C. H.; LEYENS, C. Titanium alloys for aerospace applications. **Advanced Engineering Materials**, v. 5, n. 6, p. 419-427, Jul. 2003.

PETROPOULOS, G. P.; PANDAZARAS, G. N.; DAVIM, J. P. Surface texture characterization and evaluation related to machining. In: DAVIM, J. P. (Ed.). **Surface integrity in machining**. New York: Springer London, 2010. cap. 2. p. 36-66.

PIPPAN, R. Threshold and effective threshold of fatigue crack propagation in ARMCO iron I: the influence of grain size and cold working. **Materials Science and Engineering: A**, v. 138, n. 1, p. 1-13, May 1991.

PREVEY, P. S. A method of determining the elastic properties of alloys in selected crystallographic directions for X-ray diffraction residual stress measurement. **Advances in X-ray Analysis**, v. 20, p. 345-354, 1977.

PUSAVEC, F.; KRAMAR, D.; KRAJNIK, P.; KOPAC, J. Transitioning to sustainable production - part II: evaluation of sustainable machining technologies. **Journal of Cleaner Production**, v. 18, n. 12, p. 1211-1221, Aug. 2010.

RAHIM, E. A.; SASAHARA, H. A study of the effect of palm oil as MQL lubricant on high speed drilling of titanium alloys. **Tribology International**, v. 44, n. 3, p. 309-317, Mar. 2011.

RAHIM, E. A.; SASAHARA, H. Investigation of tool wear and surface integrity on MQL machining of Ti-6AL-4V using biodegradable oil. **Proceedings of the Institution of Mechanical Engineers, Part B: Journal of Engineering Manufacture**, v. 225, n. 9, p. 1505-1511, Sept. 2011.

RECH, J.; HAMDI, H.; VALETTE, S. Workpiece surface integrity. In: DAVIM, J. P. (Ed.) **Machining**: fundamentals and recent advances. Springer London, 2008. cap. 3. p. 59-96.

REISSIG, L.; VÖLKL, R.; MILLS, M. J.; GLATZEL, U. Investigation of near surface structure in order to determine process-temperatures during different machining processes of Ti6Al4V. **Scripta Materialia**, v. 50, n. 1, p. 121-126, Jan. 2004.

ROTELLA, G.; DILLON, O. W.; UMBRELLO, D.; SETTINERI, L.; JAWAHIR, I.S. The effects of cooling conditions on surface integrity in machining of Ti6Al4V alloy. **The**

**International Journal of Advanced Manufacturing Technology**, v. 71, n. 1, p. 47-55, Mar. 2014.

SAFARI, H; SHARIF, S.; IZMAN, S.; JAFARI, H. Surface integrity characterization in high-speed dry end milling of Ti-6Al-4V titanium alloy. **The International Journal of Advanced Manufacturing Technology**, v. 78, n. 1-4, p. 651-657, April 2015.

SASAHARA, H. The effect on fatigue life of residual stress and surface hardness resulting from different cutting conditions of 0.45% C steel. **International Journal of Machine Tools and Manufacture**, v. 45, n. 2, p. 131-136, Feb. 2005.

SCHWACH, D. W.; GUO, Y. B. A fundamental study on the impact of surface integrity by hard turning on rolling contact fatigue. **International Journal of Fatigue**, v. 28, n. 12, p. 1838-1844, Dec. 2006.

SHARIF, S.; RAHIM, E. A. Performance of coated-and uncoated-carbide tools when drilling titanium alloy – Ti-6Al4V. **Journal of Materials Processing Technology**, v. 185, n. 1-3, p. 72-76, April 2007.

SHOKRANI, A.; DHOKIA, V.; NEWMAN, S. T. Environmentally conscious machining of difficult-to-machine materials with regard to cutting fluids. **International Journal of Machine Tools and Manufacture**, v. 57, p. 83-101, June 2012.

SIPOS, K.; LÓPEZ, M.; TRUCCO, M. Surface martensite white layer produced by adhesive sliding wear-friction in AISI 1065 steel. **Revista Latinoamericana de Metalurgia y Materiales**, v. 28, n. 1, p. 46-50, June 2008.

SOUZA, G. O. **Fresamento em 5-eixos silmultâneos de pás de compressores de turbinas a gás em TiAI6V4**. 2006. 144f. Dissertação (Mestrado em Engenharia Mecânica) – Universidade Federal de Santa Catarina, Florianópolis.

SOUZA, M. C. **Avaliação das dimensões técnico-econômica, social e ambiental para processo de fresamento em ferro fundido vermicular**. 2014. 163 f. Dissertação (Mestrado em Engenharia Aeronáutica e Mecânica) – Instituto Tecnológico de Aeronáutica, São José dos Campos.

STACHOWIAK, G.; BATCHELOR, A. W. **Engineering tribology**. 2nd ed. Butterworth-Heinemann, 2000, 750 p.

SUN, J.; GUO, Y. B. A comprehensive experimental study on surface integrity by end milling Ti–6Al–4V. **Journal of Materials Processing Technology**, v. 209, n. 8, p. 4036-4042, April 2009.

TAI, B. L.; STEPHENSON, D. A.; FURNESS, R. J.; SHIH, A. J. Minimum quantity lubrication (MQL) in automotive powertrain machining. **Procedia CIRP**, v. 14, p. 523-528, 2014.

TAYLOR, D.; CLANCY, O. M. The fatigue performance of machined surfaces. **Fatigue and Fracture of Engineering Materials and Structures**, v. 14, n. 2-3, p. 329-336, Feb. 1991.

THIELE, J. D.; MELKOTE, S. N. Effect of cutting edge geometry and workpiece hardness on surface generation in the finish hard turning of AISI 52100 steel**. Journal of Materials Processing Technology**, v. 94, n. 2-3, p. 216-226, Sept. 1999.

THOMAS, M.; TURNER, S.; JACKSON, M. Microstructural damage during high-speed milling of titanium alloys. **Scripta Materialia**, v. 62, n. 5, p. 250-253, Mar. 2010.

TOTTEN, G.; HOWES, M.; INOUE, T. (Ed.). **Handbook of residual stress and deformation of steel**. 1$^{st}$ ed. Materials Park: ASM International, 2002, 550 p.

TRETYACHENKO, L. Aluminium–Titanium–Vanadium. In: **Ternary alloy systems:** phase diagrams, crystallographic and thermodynamic data. Berlin: Springer, 2006. p. 26-53.

ULUTAN, D.; OZEL, T. Machining induced surface integrity in titanium and nickel alloys: a review. **International Journal of Machine Tools and Manufacture**, v. 51, n. 3, p. 250-280, Mar. 2011.

VANDER VOORT, G. F. **Metallography** - principles and practice. New York: McGraw-Hill, 1999, 773 p.

VYAS, A.; SHAW, M. C. Mechanics of saw-tooth chip formation in metal cutting. **Journal of Manufacturing Science and Engineering**, v. 121, n. 2, p. 163-172, May 1999.

WAGNER, L. Mechanical surface treatments on titanium, aluminum and magnesium alloys. **Materials Science and Engineering: A**, v. 263, n. 2, p. 210-216, May 1999.

WAGNER, L.; BIGONEY, J. K. Fatigue of titanium alloys. In: LEYENS, C.; PETERS, M (Ed.). **Titanium and titanium alloys**: fundamentals and applications. 1$^{st}$ ed. Weinheim: Wiley-VCH, 2003. cap. 5. p. 153-185.

WEBER, J. H.; HERTZBERG, R. W. Effect of thermomechanical processing on fatigue crack propagation. **Metallurgical and Materials Transactions B**, v. 4, n. 2, p. 595-601, Feb. 1973.

KIENZLE, O. Bestimmung von kräften und leistungen an spanenden werkzeugen und werkzeugmaschinen. **Verein Deutsche Ingenieure**, 94, pg. 299-305, 1952.

WYEN, C.-F.; JAEGER, D.; WEGENER, K.. Influence of cutting edge radius on surface integrity and burr formation in milling titanium. **The International Journal of Advanced Manufacturing Technology**, v. 67, n. 1, p. 589-599, July 2013.

YANG, X.; LIU, C. R.; GRANDT, A. F. An experimental study on fatigue life variance, residual stress variance, and their correlation of face-turned and ground Ti 6Al-4V samples. **Journal of Manufacturing Science and Engineering**, v. 124, n. 4, p. 809-819, Oct. 2002.

YUAN, S. M.; YAN, L. T.; LIU, W. D.; LIU, Q. Effects of cooling air temperature on cryogenic machining of Ti–6Al–4V alloy. **Journal of Materials Processing Technology**, v. 211, n. 3, p. 356-362, Mar. 2011.

ZANIN, E. **Airbus perspective on titanium sourcing**. Atlanta: International Titanium Association, 2012. Available at: http://c.ymcdn.com/sites/www.titanium.org/resource/resmgr/2010_2014_papers/ZaninEric_2012.pdf

ZHANG, S.; LI, J. F.; SUN, J.; JIANG, F. Tool wear and cutting forces variation in high-speed end-milling Ti-6Al-4V alloy. **The International Journal of Advanced Manufacturing Technology**, v. 46, n. 1, p. 69-78, May 2010.

ZHANG, S.; LI, J.; ZHU, X.; LV, H. Saw-tooth chip formation and its effect on cutting force fluctuation in turning of Inconel 718. **International Journal of Precision Engineering and Manufacturing**, v. 14, n. 6, p. 957-963, June 2013.
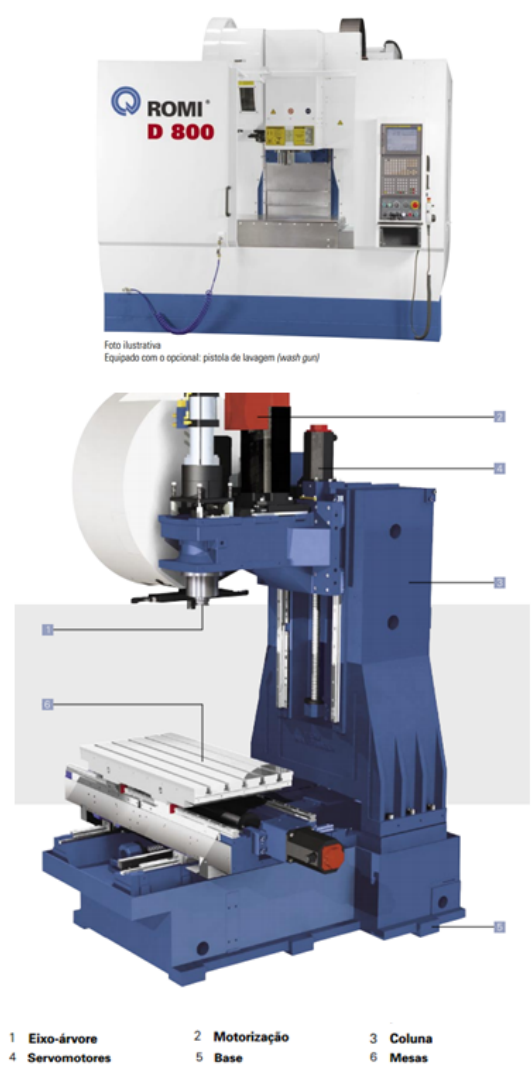
CRISTO, B.; ALVES, M. V.; VIEIRA, M. **Otimização do processo de fresamento e análise de tensões residuais na liga Ti6Al4V**. 2013. 78 f. Monografia (Bacharelado em Engenharia Mecânica) – Universidade São Francisco, Campinas.

# 7 Attachments

## Equipment data

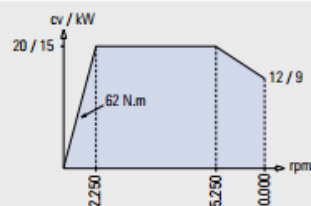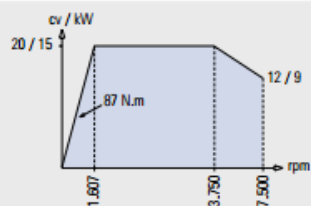This section provides information about the equipments that were used in the experimental phase.

**Machine tool: Romi D800**



| Especificações Técnicas | | Romi D 800 Alta Performance |
|---|---|---|
| **Cabeçote Vertical** | | |
| Cone do eixo-árvore | ISO | 40 |
| Faixa de velocidades (versão 7.500 rpm) | rpm | 7 a 7.500 |
| Faixa de velocidades (versão 10.000 rpm) | rpm | 10 a 10.000 |
| Faixa de velocidades (versão 12.000 rpm) | rpm | 12 a 12.000 |
| **Avanços** | | |
| Avanço rápido (eixos X / Y) | m / min | 40 |
| Avanço rápido (eixo Z) | m / min | 40 |
| Avanço de corte programável | m / min | 20 |
| **Cursos** | | |
| Curso da mesa superior (eixo X) | mm | 800 |
| Curso da mesa inferior (eixo Y) | mm | 530 |
| Curso do cabeçote (eixo Z) | mm | 580 |
| Distância entre nariz do eixo-árvore e mesa | mm | 115 a 695 |
| **Mesa** | | |
| Superfície da mesa | mm | 914 x 500 |
| Largura das ranhuras x distância | mm | 18 x 89 |
| Número de ranhuras (rasgos T) | - | 5 |
| Peso admissível (uniformemente distribuído) | kg | 900 |
| **Potência instalada** | | |
| Motor principal ca | cv / kW | 20 / 15 (regime 30 min) |
| Potência total instalada | kVA | 35 |
| **Dimensões e peso (aproximado)** | | |
| Altura | mm | 2.700 |
| Área ocupada (frente x lateral) (*) | mm | 2.600 x 2.680 |
| Peso líquido | kg | 5.500 |

1 Eixo-árvore    2 Motorização    3 Coluna
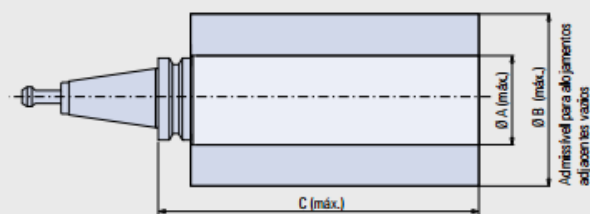4 Servomotores   5 Base           6 Mesas

## Gráficos de potência

### Romi D 600 / Romi D 800 (Standard) - Regime 15 min



### Romi D 800 (Alta Performance) - Regime 30 min
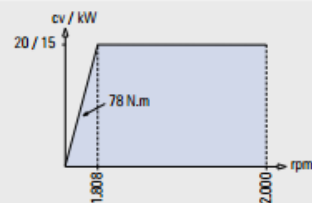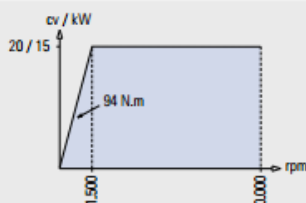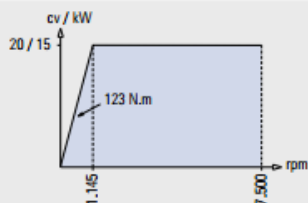


## Mandris * - Dimensões em mm



* Para máquinas com sistema de refrigeração pelo centro do eixo-árvore, os mandris porta-barras e pinos de fixação deverão ter furo de passagem para fluído refrigerante

| | | Trocador para 20 ferramentas BT 40 | Trocador para 30 ferramentas BT 40 |
|---|---|---|---|
| A | mm | 80 | 80 |
| B | mm | 160 | 150 |
| C | mm | 254 | 300 |
| Peso máximo | kg | 6 | 8 |

## Dimensões das mesas - Dimensões em mm
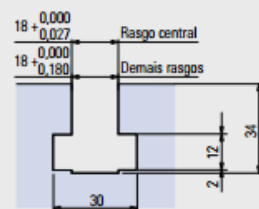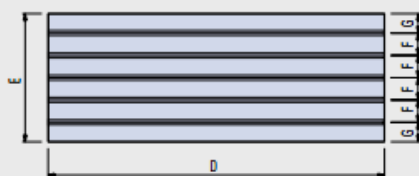


Detalhe do rasgo T

| | | D | E | F | G |
|---|---|---|---|---|---|
| Romi D 600 | mm | 840 | 500 | 89 | 72 |
| Romi D 800 | mm | 914 | 500 | 89 | 72 |

## Layout de trabalho - Dimensões em mm
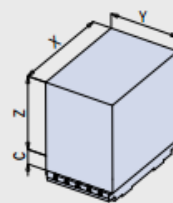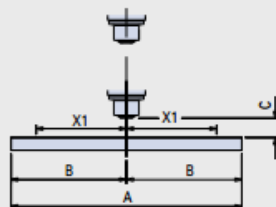


| | | A | B | C | X | X1 | Y | Z |
|---|---|---|---|---|---|---|---|---|
| Romi D 600 | mm | 840 | 420 | 115 | 600 | 300 | 530 | 580 |
| Romi D 800 | mm | 914 | 457 | 115 | 800 | 400 | 530 | 580 |

## Dynamometer: Kistler 9265B (with 9443B – mounting plate for clamping workpieces)

### Multi-Component Dynamometer with Tool Holder or Clamping Plate up to 30 kN
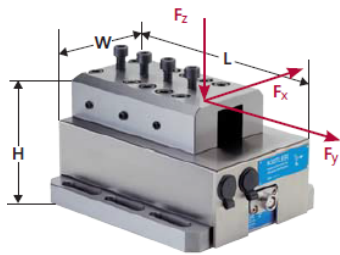


Type 9265B & 9441B

| Specifications | | | Type 9265B with 9441B | Type 9265B with 9443B |
|---|---|---|---|---|
| Measuring range | $F_x$, $F_y$ | kN | –15 ... 15 | –15 ... 15 |
| | $F_z$ | kN | 0 ... 30 | –10 ... 30 |
| Calibrated measuring ranges | $F_x$, $F_y$ | kN | 0 ... 15 | 0 ... 15 |
| | | kN | 0 ... 1,5 | 0 ... 1,5 |
| | $F_z$ | kN | 0 ... 30 | 0 ... 30 |
| | | kN | 0 ... 3 | 0 ... 3 |
| Sensitivity | $F_x$, $F_y$ | pC/N | ≈–8 | ≈–8 |
| | $F_z$ | pC/N | ≈–3,7 | ≈–3,7 |
| Natural frequency | $f_nx$, $f_ny$ | kHz | ≈1,5 | ≈1,7 |
| | $f_nz$ | kHz | ≈2,5 | ≈2,7 |
| Operating temperature range | | °C | 0 ... 70 | 0 ... 70 |
| LxWxH | | mm | 175x100x126 | 203x135x100 |
| Weight | | kg | 20 | 19,8 |
| Degree of Protection IEC/EN 60529 | | | IP67 with connected cable | |
| Connection | | | Fischer Flange 9-pole neg. | |

➡ *This sensor is calibrated and ready for measurement.*

**Characteristics**
The cutting force dynamometer with integral cooling channels for temperature-stable measurement. The basic unit must only be used in conjunction with the steel holder Type 9441B (for turning) or with the clamping plate Type 9443B (for milling or grinding).
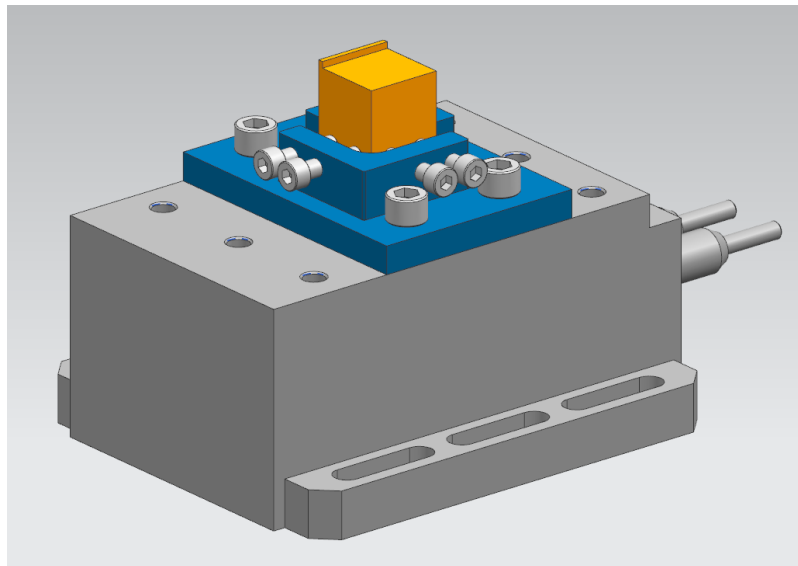
**Application**
Cutting forces during turning, milling or grinding.

**Accessories**
• Connecting cable
  - Type 1687B5/1689B5 (3-comp.)
  - Type 1677A5/1679A5 (6-comp.)
• Tool holder Type 9441B for cutting tools max. 32x32 mm
• Clamping plate Type 9443B

**Data sheet** 9265B_000-152

## Fixture system mounted on the dynamometer

## Charge amplifier: Kistler Type 5070A

**Multi-Channel Charge Amplifier for Multi-component Force Measurement**



*Type 5070A...*

| Technical data | | 5070Ax0xxx | 5070Ax1xxx | 5070Ax2xxx |
|---|---|---|---|---|
| Number of channels | | 4 | 8 | 8 with 6-component summing calculator |

| General technical data | | | |
|---|---|---|---|
| Measuring ranges  FS | pC | optional | ±200 ... 200 000 ±600 ... 600 000 |
| Measuring range adjustment | | continous | |
| Frequency range (–3 dB)  kHz | | ≈0 ... 45 | |
| Output signal | V | ±10 | |
| Supply voltage | VAC | 100 ... 240 | |
| Input signal | Type/connector | piezoelectric, optional with • BNC neg. • Fischer 9-pole neg. | |
| Degree of Protection to IEC/EN 60529 | | IP40 | |
| Interface | | optional | • RS-232C • RS-232C and IEEE-488 |
| Case | | optional | • 19" cassette for rack mounting • Desktop unit with support bracket • 19" cassette with panel mounting set |

| Other features | |
|---|---|
| | • Display of peak values • Display of mechanical measurands |

→ *The parameters of this charge amplifier can be quickly and easily configured with the DynoWare software package for the PC.*

**Characteristics**
This amplifier is ideal for multicomponent force-torque measurement with piezoelectric dynamometers or force plates for cutting force measurement.

**Application**
The 4-channel amplifier is effective for measuring cutting forces with Kistler dynamometers. The 8-channel amplifier is suitable for 6-component force-torque measurement in laboratories, research and development.

**Accessories**
• RS-232C null modem cable, l = 5 m, D-Sub 9-pole pos. / D-Sub 9-pole neg. Type 1200A27
• Connecting cable for signal outputs from charge amp to data acquisition card, l = 2 m, D-Sub 15-pole pos./D-Sub 37-pole neg. Type 1500B15
• Connecting cable for signal outputs from 6-component summing calculator to data acquisition card, l = 2 m, D-Sub 15-pole pos. / D-Sub 37-pole neg. Type 1500A7
• Inductive proximity swith Type 2233B

## Highly insulation cable: Kistler Type 1677A5

**Cables, High Insulation, Temperature Range –5 ... 70 °C**



*Type 1677A5*

| Specifications | | Type 1677A5 |
|---|---|---|
| Connection | | Fischer 9-pole pos. Fischer 9-pole pos. |
| Length | m | 5 |
| Diameter | mm | 12,3 (metal sheath) |
| Number of conductors | | 8 |
| Used for | | 6-component measurement |

## X-ray diffractometer: PANalytical Empyrean

PANalytical Empyrean X-ray diffractometer

Incident beam optics

X-ray tube (Cu)

Crossed slits collimator

Diffracted beam optics

Detector

Parallel plate collimator (PPC)

β filter (Ni)
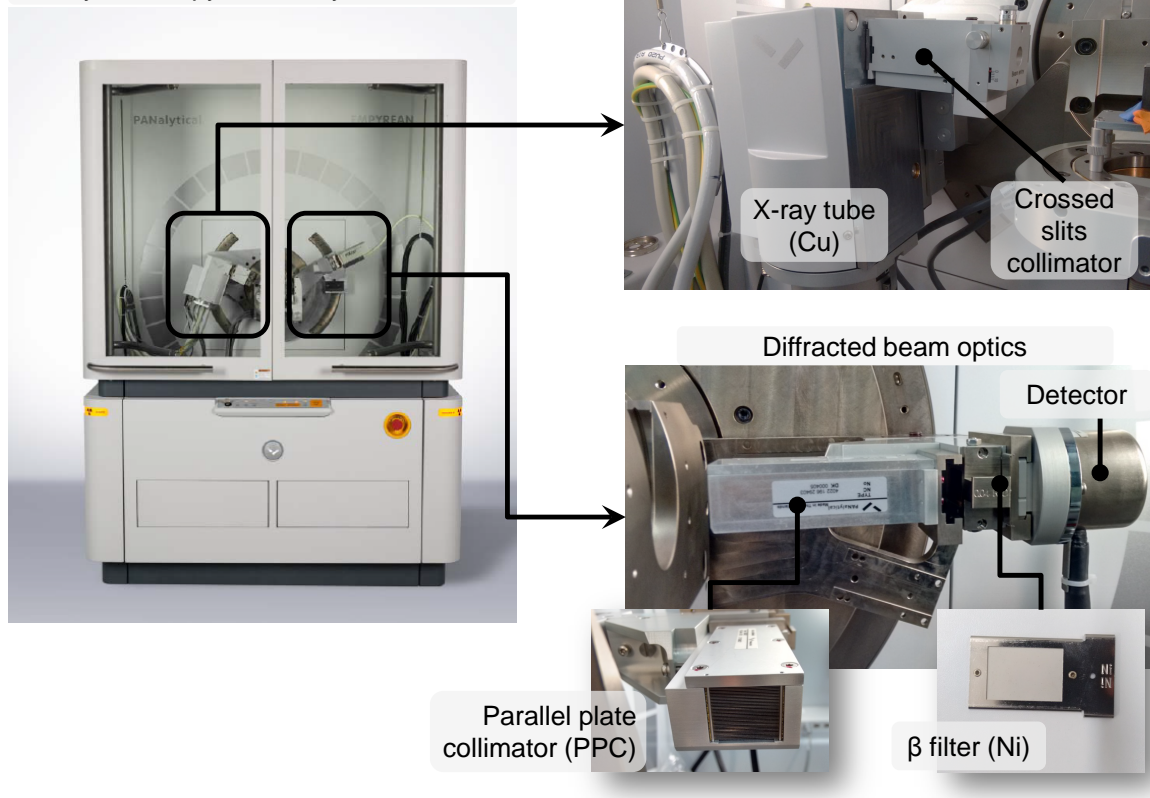
## X-ray diffractometer accessory: crossed slits collimator

Attenuation Foil or Beta-filter

Shutter Lever

Adjustment Knob for Beam Width

Adjustment Knob for Beam Height

Axial Width Mask Scale (not visible)

Crossed Slits Assembly

Equatorial Divergence Slit Scale
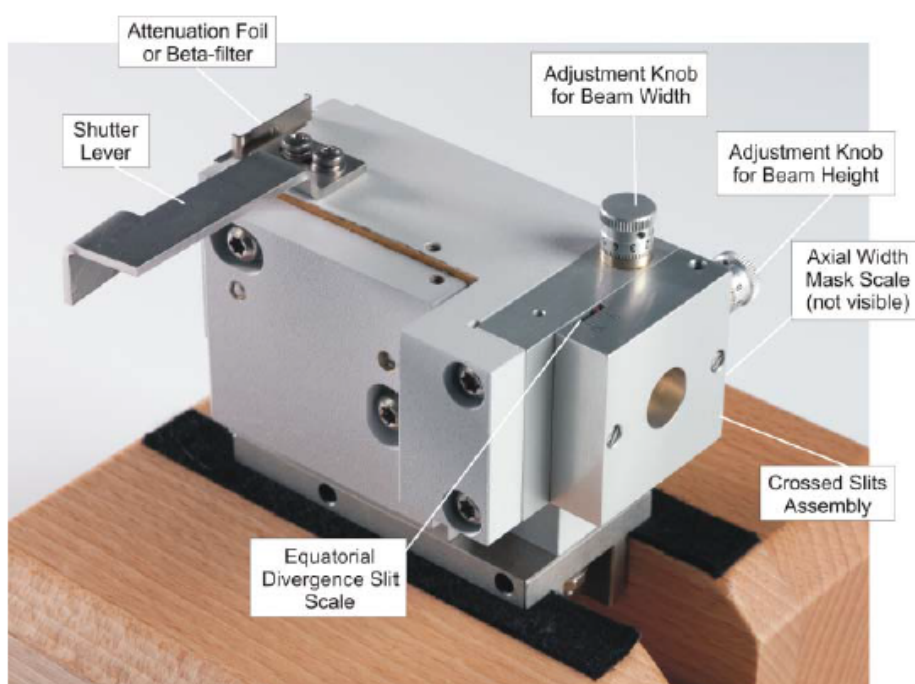
**Non-contact profilometer: cyberSCAN CT 100**



# SPECIFICATIONS

| | |
|---|---|
| DIMENSIONS (L X W X H) | 450 x 350 x 450 [mm] (17 x 14 x 16 [in]) |
| WEIGHT | 44 kg (97 lbs) |
| SYSTEM CONTROLLER | Includes Motion Control, Sensor Controller (2 kHz), Power Supplies, USB Interface to Workstation |
| WORKSTATION PC | Inquire about current specifications, 22" widescreen monitor |
| CONNECTIONS | Ethernet, DVD Drive, USB (front and back side), Parallel Port, Keyboard, Mouse, DVI and Analog Video Output |
| POWER REQUIREMENTS | 100-240 V AC, 50-60 Hz, 2 amps (240 V), 5 amps (100 V) |
| OPERATING TEMPERATURE | 20°-30° C (68-86 F) |
| MEASUREMENT SURFACE SIZE | 230 x 230 [mm] 9 x 9 [in] |
| LINEAR ENCODER RESOLUTION | 0.05 µm 2 µin |
| MINIMUM LATERAL RESOLUTION | 1 micron |
| TRAVEL LIMITS IN X AND Y (MOTORIZED) | 150 x 150 [mm] 6 x 6 [in] |
| TRAVEL LIMIT IN Z (MANUAL) | 40 mm 4 in (adjustable height levels and micrometer fine adjustment) |
| MAXIMUM LOAD ON PLATFORM | 10 kg |
| AVAILABLE SENSORS | Confocal White Light Sensors Confocal Laser Sensors |

**Hardness tester: EMCO-TEST DuraScan 70**

|  | DuraScan 70 |
|---|---|
| Cross slide [mm] | 200 x 120 |
| Traverse path [mm] | 140 x 140 |
| Turret | DC motor |
| Max. workpiece weight | 10 kg |
| Dimensions (WxHxD) [mm] | 680 x 690 x 450 |
| Footprint (WxD) [mm] | 1100 x 800 |
| Monitor [inches] | 19" |
| Weight of basic unit | 92 kg |
| Base plate | Granite |
| Positioning accuracy [mm] | ± 0,0035 |
| Overview camera [mm] | 40 x 52 |

**Ambient conditions**

Room temperature (as per ISO/ASTM) [°C]          23 (±5)°C

Rel. humidity (non-condensing) [%]          40 – 70 %

Please take note of the information about the ambient temperature in chapter Manufacturer's notes [→ 1-2].

| General technical data |  |
|---|---|
| Test loads | 0.098 – 98 N (0.01 – 10 kgf) |
| Test area height | 260 mm |
| Resolution of test unit: |  |
| Z-axis | 5 nm |
| Feed speed of test unit | 0.03 nm/s to 2mm/s |
| Measuring and overview camera | CMOS, 1.3 mpix, USB 2.0 |

# FOLHA DE REGISTRO DO DOCUMENTO

| [1.] CLASSIFICAÇÃO/TIPO | [2.] DATA | [3.] REGISTRO N° | [4.] N° DE PÁGINAS |
|---|---|---|---|
| DM | 15 de dezembro de 2015 | DCTA/ITA/DM-097/2015 | 120 |

[5.] TÍTULO E SUBTÍTULO:

Impacts on the surface integrity of titanium milling with minimum quantity lubrication and flood of coolant.

[6.] AUTOR(ES):

**André Hemerly Maia**

7. INSTITUIÇÃO(ÕES)/ÓRGÃO(S) INTERNO(S)/DIVISÃO(ÕES):

Instituto Tecnológico de Aeronáutica - ITA

[8.] PALAVRAS-CHAVE SUGERIDAS PELO AUTOR:

1. Titanium machining. 2. End milling. 3. Surface integrity

9.PALAVRAS-CHAVE RESULTANTES DE INDEXAÇÃO:

Fresagem (usinagem); Ligas de titânio; Corte de metal; Usinagem; Ferramentas de cortes; Óleos lubrificantes; Fadiga; Engenharia mecânica.

[10.] APRESENTAÇÃO: **X Nacional Internacional**

ITA, São José dos Campos. Curso de Mestrado. Programa de Pós-Graduação em Engenharia Mecânica e Aeronáutica. Área de Materiais e Processos de Fabricação. Orientador: Prof. Dr. Jefferson de Oliveira Gomes. Defesa em 08/12/2015. Publicada em 2015.

[11.] RESUMO:

Titanium and its alloys are considered high performance materials because of the combination of properties such as mechanical strength, low density and strength up to high temperatures. The same properties also result in poor machinability and high temperatures that may produce tensile residual stresses and surface damage. These characteristics, in special residual stresses, impact directly on fatigue life, the main failure mode in aeronautical industry and corresponding to 60% of failures. Thus large amounts of coolant are required in machining operations to avoid surface damage, which may represent up to 30% of the total machining costs. Among the alternatives for reducing the coolant consumption, minimum quantity lubrication (MQL) has been evaluated for drilling and turning both in terms of tool wear and surface integrity. However there is a gap in regard of milling operations and the impacts on surface integrity parameters, and this is the focus of the present study. On a first phase, the machining forces were investigated, as well as chip morphology and characteristics related to its formation mechanism. Then the workpiece quality was evaluated in terms of surface residual stresses, roughness and hardness beneath the machined surface, comparing the MQL method to conventional cooling with flood of coolant. Machining forces were found to be lower for MQL conditions (10% lower as compared to flood cut), and this is believed to be a result of thermal softening of the material. Segmented chips were observed for all the cutting conditions. The aspect of the free surface of the chip, discontinuous segments, and cracks are evidence that a crack propagation mechanism is involved in chip formation. In terms of surface integrity parameters, results indicate that MQL does not affect the surface roughness, but residual stresses are less compressive than when using flood of coolant. Considering the range of parameters that were tested, radial depth of cut had no influence on residual stresses. Conditions which developed higher machining forces and consequently mechanical load resulted in less compressive residual stresses caused by the increased thermal load due to plastic strain. The hardness beneath the surface was affected by the lubri-cooling method in the finishing operations. Flood cut induced higher levels of cold work, while in MQL machining the thermal softening compensates the increase in surface hardness, and the final state is rather similar to the bulk value. In the case of semi-finishing conditions, machining with MQL increased the surface hardness. Flood cut, on the other side, produced a subsurface hardness peak (from 300 to 600 μm beneath surface, approximately).

[12.] GRAU DE SIGILO:

**(X ) OSTENSIVO ( ) RESERVADO ( ) SECRETO**